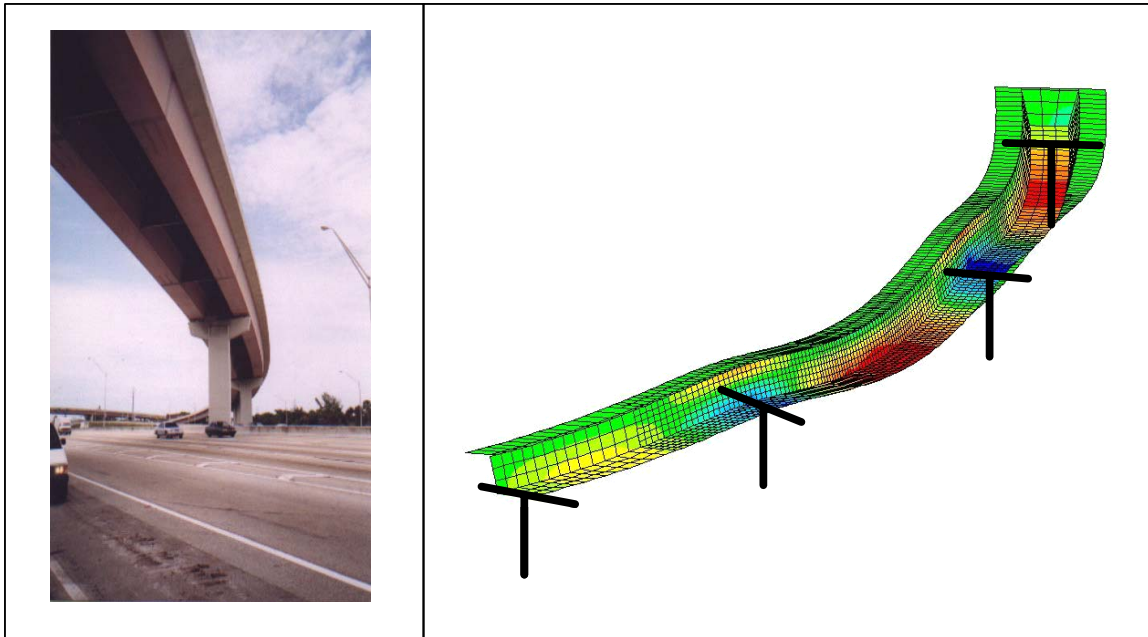


BEHAVIOR AND DESIGN OF CURVED COMPOSITE BOX GIRDER BRIDGES



FINAL REPORT

- October 2002 -

Sherif El-Tawil, PhD, PE and Ayman M. Okeil, PhD, PE

Department of Civil and Environmental Engineering
University of Central Florida, Orlando, FL 32816-2450

This report was prepared in cooperation with the State of Florida Department of Transportation and the U.S. Department of Transportation. The report does not constitute a design standard, specification, or regulation. The opinions, findings, and conclusions expressed in this publication are those of the authors in the course and scope of employment by the University of Central Florida and not necessarily those of the Florida Department of Transportation or the U.S. Department of Transportation.

ACKNOWLEDGEMENT

This project was funded in part by the Florida Department of Transportation (Contract BC-421) and the Department of Civil and Environmental Engineering at the University of Central Florida. Special thanks are due to former UCF graduate student Bibo Zhang, who worked as a research assistant on this project.

TABLE OF CONTENTS

1	Introduction.....	1
1.1	Background.....	1
1.2	Motivation and Research Objectives	3
1.3	Report Organization.....	4
2	Analysis of Curved Composite Box Girder Bridges	5
2.1	Introduction.....	5
2.2	Choice of Analysis Strategy.....	5
2.3	Program Structure	6
2.4	Graphical User Interface	6
2.5	Elements Library.....	10
2.5.1	Six DOF Implementation.....	10
2.5.2	Seven DOF Implementation	14
2.6	Special Features	17
2.6.1	Shear Deformations	17
2.6.2	Eccentricity between Shear Center and Centroid	23
2.6.3	Support Boundary Conditions.....	24
2.6.4	Implementation using Sparse Matrices.....	26
2.7	Program Verification	27
2.7.1	Comparison with closed-form solution.....	28

2.7.2	Comparison with beam element models (ABAQUS).....	29
2.7.3	Comparison with full shell element models (SAP2000).....	29
3	Warping Stresses In Composite Curved Box Girder Bridges.....	38
3.1	Background.....	38
3.2	Non-uniform Torsion.....	38
3.3	Analysis of Existing Bridges	41
3.3.1	Geometric properties of closed cross sections.....	41
3.3.2	Bridge models.....	46
3.3.3	Bridge loading and resulting forces.....	46
3.3.4	Stress Calculations.....	49
3.4	Warping Stress Ratio	50
3.5	Results.....	52
3.5.1	Normal stresses.....	52
3.5.2	Shear stresses	52
3.5.3	Effect of κ	52
3.6	Design Implications	53
3.7	Summary and Conclusions	58
4	Live Load Distribution Factors For Composite Curved Box Girders.....	59
4.1	Introduction.....	59
4.2	Concept of Distribution Factor	60

4.3	Analysis Procedure and Model Verification.....	60
4.3.1	Shell Models vs. Grillage Models.....	61
4.3.2	Determination of Distribution Factors.....	62
4.4	Parametric Study.....	66
4.5	Results and Conclusions.....	67
5	Access Hatches in Continuous Curved Composite Box Girder Bridges.....	71
5.1	Introduction.....	71
5.2	Practical Constraints for Choosing Access Hole Location.....	71
5.2.1	Strength.....	71
5.2.2	Feasibility.....	72
5.2.3	Accessibility.....	72
5.2.4	Water Leakage.....	73
5.2.5	Impact on Traffic.....	73
5.2.6	Unauthorized Access.....	73
5.3	Stresses in Curved Box Girder Bridges.....	74
5.4	Low Stress Regions.....	75
5.4.1	Results for Idealized Bridge.....	75
5.4.2	Study of Existing Bridges.....	78
5.5	Effect of Hole Location on Strength of an Existing Bridge.....	79
5.6	Summary and Conclusions.....	81

6	Summary and Conclusions	82
7	REFERENCES	84
8	APPENDIX A: Summary of Expressions used in Computing Geometric Properties	87
9	APPENDIX B: Research Dissemination	90
9.1	Papers Accepted for Publication.....	90
9.2	Papers Submitted for Publication.....	90

LIST OF FIGURES

Figure 1.1: View showing diaphragms connecting two box girders in an interchange.....	2
Figure 1.2: Interior of a box girder. Note the vertical cross-frames (comprised of sloping truss members), web stiffeners, bottom flange stiffeners, and top bracing.....	3
Figure 2.1: Flow chart of computer program (part I).....	7
Figure 2.2: Flow chart of computer program (part II).....	8
Figure 2.3: Plan view of the grid model.....	9
Figure 2.4: Setting 3-D viewing parameters.....	9
Figure 2.5: Isometric 3-D view of deformed shape.....	10
Figure 2.6: Local coordinate system for 6-DOF element.....	11
Figure 2.7: Local coordinate system for 7-DOF element.....	15
Figure 2.8: Warping of a closed thin-walled cross-section.....	15
Figure 2.9: A general element showing non-coincident shear center and centroid.....	23
Figure 2.10: Local and global CS for handling of restrained DOFs.....	25
Figure 2.11: Normal stress distribution under warping for a I-section beam.....	25
Figure 2.12: Bimoment distribution along the entire length of Bridge 521 (program results).....	30
Figure 2.13: Bimoment distribution along the entire length of Bridge 521 (ABAQUS results).....	30
Figure 2.14: Dimensions of the cross section for verification example (in inches).....	31
Figure 2.15: Loading of verification example.....	31
Figure 2.16: 3D-view of Model A in SAP 2000.....	32

Figure 2.17: Layout of diaphragms.....	33
Figure 2.18: Comparison of vertical displacement.....	35
Figure 2.19: Comparison of twisting angle.....	35
Figure 2.20: Maximum normal stress comparison along entire beam length.....	37
Figure 2.21: Maximum normal stress comparison in the vicinity of fixed end.....	37
Figure 3.1: Geometric properties of quasi-closed cross section (Dimensions in mm, ω in mm^2 , S_x , S_y in mm^3 , S_ω in mm^4).....	42
Figure 3.2: Geometric properties of closed cross section (Dimensions in mm, ω in mm^2 , S_x , S_y in mm^3 , S_ω in mm^4).....	43
Figure 3.3: Geometric properties of closed cross section (Dimensions in mm, ω in mm^2 , S_x , S_y in mm^3 , S_ω in mm^4).....	45
Figure 3.4: Positioning of live loads for a single lane bridge (dimension in mm)	47
Figure 3.5: Envelope of warping-related straining actions due to live loads for idealized bridge	48
Figure 3.6: Keypoints considered for stress calculations.....	50
Figure 3.7: Normal Warping Stress Ratios vs. L/R	54
Figure 3.8: Shear Warping Stress Ratios vs. L/R	55
Figure 3.9: Normal Warping Stress Ratios vs. κ	56
Figure 3.10: Shear Warping Stress Ratios vs. κ	57
Figure 4.1: Grillage modeling and its effect on deck span length	61
Figure 4.2: Schematic of single girder models used in determining the distribution factor...	62
Figure 4.3: Schematic of grillage models used in determining the distribution factor.....	63

Figure 4.4: Dimensions for calculation of total torsional constant based on BEF	63
Figure 4.5: Verification results for proposed grillage model.....	65
Figure 5.1: Alternative access hole locations	72
Figure 5.2: Low stress regions for idealized bridge (a - Approach I, b - Approach II).....	76
Figure 5.3: (a) Distribution of fatigue stresses. Empty regions are areas in compression and therefore not affected by fatigue. (b) Regions not critical for fatigue considerations (entire bridge).....	77
Figure 5.4: Regions that satisfy both normal stress criteria (<33% regions in Figure 5.2-a and fatigue stress criteria in Fig. 5.3-b). Shaded regions are suitable for access hole placement.....	78
Figure 5.5: General view of finite element mesh.....	80
Figure 5.6: Idealized stress-strain relationships for steel and concrete.	80
Figure 5.7: Bottom view of bridge model showing hole location in a minimally stressed region.	81
Figure 8.1: A general closed thin-walled cross-section.....	89
Figure 8.2: ω diagrams of closed and open section parts	89

LIST OF TABLES

Table 2.1: M_w verification results – Program vs. closed form solutions	29
Table 2.2: Summary of SAP2000 shell models	33
Table 2.3: Maximum normal stress from program and Models A, B, and C	36
Table 3.1: Summary data for analyzed existing bridges	40
Table 3.2: Definitions of Warping Stress Ratio (WSR)	51
Table 4.1: Details of variables considered in parametric study	67
Table 4.2: Comparison of distribution factor results (L=25 m).....	68
Table 4.3: Comparison of distribution factor results (L=50 m).....	69
Table 4.4: Comparison of distribution factor results (L=100 m).....	70
Table 5.1: Summary of advantages and disadvantages of access hole alternatives.....	74

EXECUTIVE SUMMARY

Problem Statement

Composite steel-concrete box girders are commonly used in curved bridges, interchanges, and ramps. Curved composite box girders have a number of unique qualities that make them suitable for such applications including: 1) their structural efficiency allows designers to build long slender bridges that have an aesthetically pleasing appearance, and 2) composite box girders are particularly strong in torsion and efficiently resist the large torsional demands created by horizontal bridge curvature and vehicle centrifugal forces.

Analysis and design of curved composite box bridges is complicated by many factors including: composite interaction between the concrete deck and steel U-girder, local buckling of the thin steel walls making up the box, torsional warping, distortional warping, interaction between different kinds of cross-sectional forces, and the effect of horizontal bridge curvature on both local and global behavior.

Current codes pertaining to analysis and design of curved composite girders are mostly based on experimental and analytical research conducted over 30 years ago as part of project CURT (Consortium of University Research Teams) funded by the Federal Highway Administration (FHWA). A new Curved Steel Bridge Research (CSBR) project is currently being conducted under the auspices of the FHWA. Although the CSBR project is expected to provide much needed information on behavior, analysis and design of curved composite bridges, it focuses more on I-girders than on box girders.

Objectives

The overall objective of the research reported herein is to provide information that complements existing data and that will be useful for formulating comprehensive design guidelines for composite curved box girders. Specific objectives include:

- Investigate and quantify the effect of nonuniform torsion on the behavior and design of existing curved box girders.
- Study the adequacy of existing distribution factors for curved box girder bridges.
- Provide information that is helpful in identifying suitable locations for placement of access hatches in the steel box. Access holes are needed so that maintenance crews can periodically inspect the interior of box girders.

Summary of Work

A computer program for simulating the behavior of curved box girders is developed. The program is graphically interactive and features a general purpose beam-column element that can account for the effect of warping. The developed program is used to conduct a detailed investigation of warping related stresses in eighteen existing box girder bridges chosen from the Florida Department of Transportation inventory. The bridges are carefully selected to cover a wide range of design parameters including horizontal curvature, cross sectional properties, and number of spans. They were designed by different firms and were constructed at different times and are considered to be representative of current design practice. Forces are evaluated from analyses that account for the construction sequence and the effect of warping. Loading is considered following the 1998 AASHTO-LRFD provisions. The differences between stresses obtained taking into account warping and those calculated by ignoring warping are used to evaluate the effect of warping.

Another study was undertaken to investigate load distribution factors promoted by current specifications. Single girder and detailed grillage models were created for a variety of bridges and analyzed using the developed program. The parameters investigated are the number of girders, roadway width expressed by number of lanes, girder spacing, span length, and radius of horizontal curvature. The distribution factor results were compared with those obtained using the equations recommended by AASTHO in the commentary of the guide specification for horizontally curved bridges. Results show that the recommended equation overestimates the distribution factor by as much as 25% with an average of about 15%. In some cases, AASHTO's equation yielded unconservative results.

Access hatches (holes) in curved box girder bridges are usually provided in the bottom flange immediately before or after an expansion joint. If additional access hatches are required after the bridge is built, they must be placed in such a way that 1) they satisfy important practical constraints such as feasibility, accessibility, water leakage, traffic impact, and unauthorized access; 2) they do not adversely affect the structural behavior of the bridge, i.e. their installation should not impair serviceability nor decrease ultimate strength or fatigue life. Both issues are discussed and approaches that are suitable for identifying appropriate locations for access hole placement are identified.

Main Findings and Conclusions

Following are the most important findings and conclusions from this work:

- By considering differences between stresses obtained taking into account warping and those calculated by ignoring warping, it is shown that warping has little effect on both shear and normal stresses in the limited sample of bridges considered. These results should not be construed to imply that warping is not important. Rather, this work points out that there could be a large subset of bridges where the warping effect is small enough to be ignored in structural calculations. This is particularly useful to designers because warping calculations

are complicated and time consuming. Additional work is needed to define relevant parameters that can be used to identify bridges where warping calculations are warranted. The authors also believe that there is a need for a validated approximate design method that accounts for the effect of warping, without which it is hard to envision designers performing detailed analyses such as those presented here.

- Existing distribution factor equations are in need of substantial improvement. More variables should be considered in developing the new expressions including torsional rigidity of the box.
- Access hatches can be installed without additional strengthening in low stress regions in the bottom steel flange. Low stress regions can be found using the program developed in this research.

1 INTRODUCTION

1.1 Background

Composite steel-concrete box girders are commonly used in curved bridges, interchanges, and ramps (Fig. 1.1). Curved composite box girders have a number of unique qualities that make them suitable for such applications including: 1) their structural efficiency allows designers to build long slender bridges that have an aesthetically pleasing appearance, and 2) composite box girders are particularly strong in torsion and can be easily designed to resist the large torsional demands created by horizontal bridge curvature and vehicle centrifugal forces.

Curved composite box girder bridges are generally comprised of one or more steel U-girders attached to a concrete deck through shear connectors. Diaphragms connect individual steel U-girders periodically along the length to ensure that the bridge system behaves as a unit (Fig. 1.1). The cross-section of a steel box is flexible (i.e. can distort) in the cross-wise direction and must be stiffened with cross-frames that are installed in between the diaphragms to prevent distortion (Fig. 1.2). Web and bottom plate stiffeners are required to improve stability of the relatively thin steel plates that make up the steel box. During construction, overall stability and torsional rigidity of the girder are enhanced by using top bracing members. These bracing members become unimportant once the concrete decks hardens, but are usually left in place anyway (Fig. 1.2).

Analysis and design of curved composite box bridges is complicated by many factors including: composite interaction between the concrete deck and steel U-girder, local buckling of the thin steel walls making up the box, torsional warping, distortional warping, interaction between different kinds of cross-sectional forces, and the effect of horizontal bridge curvature on both local and global behavior. Existing literature contains extensive information about the analysis, behavior, and design of horizontally curved composite box girder bridges. General theories can be found in textbooks (e.g. Guohao 1987 and Nakai and Yoo 1988) and a comprehensive survey of experimental and analytical work on curved steel girders (including box girders) can be found in Zureick et al (1994) and Sennah and Kennedy (2001 and 2002).

Current codes pertaining to analysis and design of curved composite girders include AASHTO's LRFD Bridge Design Specifications (1998) and Guide Specifications for Horizontally Curved Highway Bridges (1997). Provisions in these specifications are mostly based on experimental and analytical research conducted over 30 years ago as part of project CURT (Consortium of University Research Teams) funded by the Federal Highway Administration (FHWA). A new Curved Steel Bridge Research (CSBR) project is currently

being conducted under the auspices of the FHWA with the following objectives (Zureik et al 2000): 1) gain a better understanding of the behavior of curved steel girders through large scale tests and numerical modeling, and 2) update existing design provisions. Although the CSBR project is expected to provide much needed information on behavior, analysis and design of curved composite bridges, it focuses more on I-girders than on box girders.

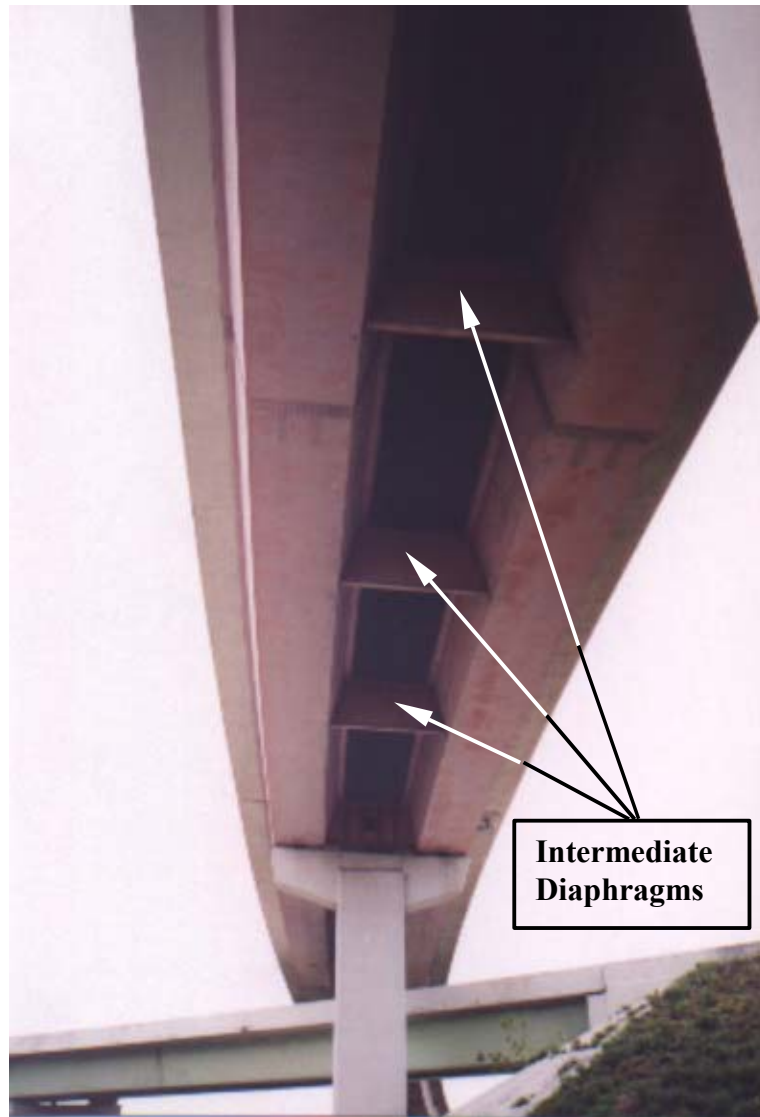


Figure 1.1: View showing diaphragms connecting two box girders in an interchange

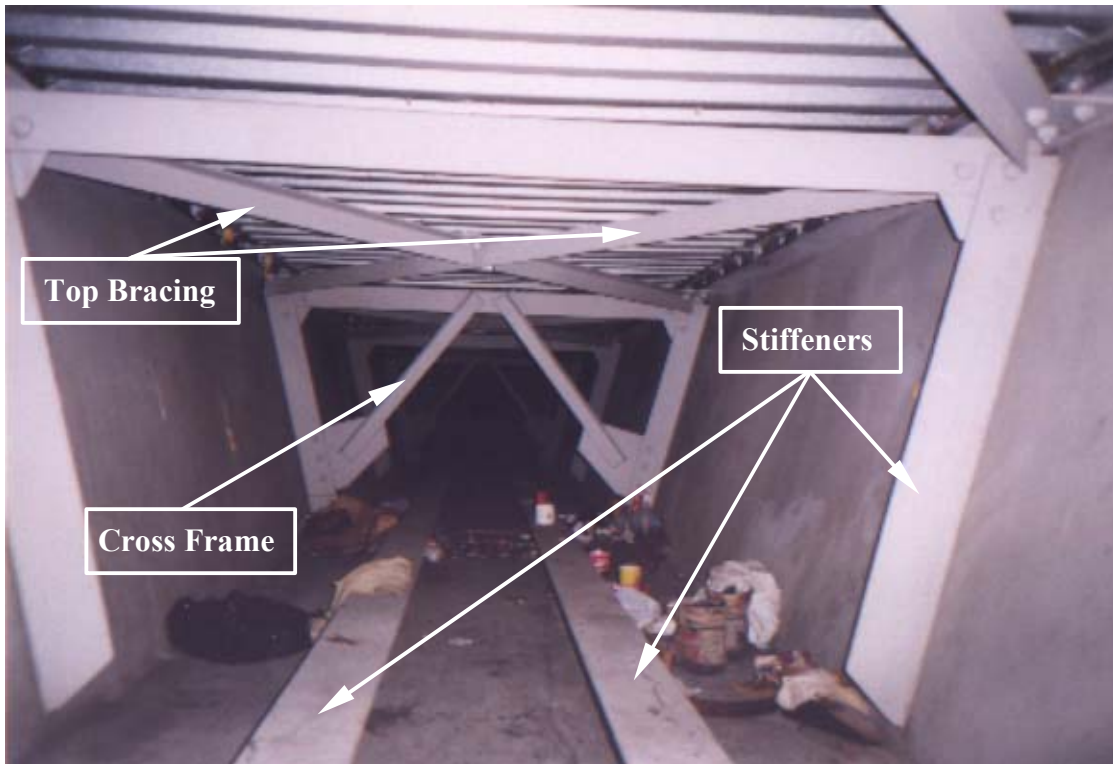


Figure 1.2: Interior of a box girder. Note the vertical cross-frames (comprised of sloping truss members), web stiffeners, bottom flange stiffeners, and top bracing.

1.2 Motivation and Research Objectives

As stated earlier, current code provisions pertaining to curved box girder bridges are based on decades-old studies. As a result, engineers designing curved composite box girder bridges are frequently faced with situations where the guidance in these codes is either insufficient or nonexistent. There is undoubtedly an immediate need for a code review to address issues that are not adequately treated in current specifications.

A prominent example illustrating the need for new information about curved box girders pertains to access holes, which are provided so that maintenance personnel can enter the interior of box girders for inspection purposes. Access hatches are usually placed before and after an expansion joint where bending moments are minimum. The spans covered by box girders are often long spans, and the girders are constructed as continuous girders over two or more supports. In many cases, the distance between access hatches exceeds the limit that rescue crews can reach in the event of an emergency. Current codes do not address this issue and there is little guidance on where and how additional access hatches can be added to new

as well as existing structures to improve accessibility. The results of a study that addresses this issue are summarized in Chapter 5.

Two other topics of significance to the design of curved composite box girder bridges are also discussed in this report. First, the issue of warping (non-uniform torsion) is investigated in a detailed and comprehensive manner. Warping has been rarely the focus of researchers in the recent literature. Code provisions related to warping are based on old studies, which to say the least, offer little guidance to designers. Second, live load (LL) distribution factors are investigated with the help of a computer program specifically developed for this purpose. AASHTO-LRFD (1998) has adopted the LL distribution factor approach in its provisions to simplify the design process. This approach, while convenient for designers, has its obvious limitations. Since bridges are categorized into groups based on structural systems, each group is subject to a set of formulas that provides the LL distribution factor. Within each group, several parameters are deemed important and the code attempts to calibrate equations that are applicable for a wide range of values for these parameters. While AASHTO-LRFD (1998) intends for the distribution factors to be conservative, it is inevitable that in some cases the suggested expressions will yield unconservative estimates. Several studies have been recently published on the distribution factors for girder bridges, attempting to enhance the available expressions. However, very little has been published on distribution factors for composite box girder bridges.

1.3 Report Organization

This report is organized into five chapters. The first chapter is an introduction to the topic at hand providing the reader with the background of the topic and the motivation behind the research. In Chapter 2, a description of the computer program that is developed for the purpose of investigating composite box girder bridges is described. The study on warping stresses is presented in Chapter 3. The results from the live load distribution factor investigation are presented in Chapter 4. Chapter 5 presents a study on access hatches in composite box girder bridges. Summary and conclusions are given in Chapter 6, which is followed by a reference list and two appendices.

2 ANALYSIS OF CURVED COMPOSITE BOX GIRDER BRIDGES

2.1 Introduction

Early on in the project, a decision had to be made about what was the best analysis tool for handling the tasks at hand. The two options available were: 1) to use a commercially available package, or 2) to develop a special program tailored to the needs of the project. Commercial packages may be categorized into two main groups. The first group is research-oriented packages that often provide an abundant array of special feature including providing elements with warping capabilities. These packages are not geared towards design in general, and bridge design in particular. For example, they do not offer a loading module according to the latest code provisions. Using such packages would entail an enormous amount of work to provide the details of the bridge loading and special details of connections between different elements. Packages geared towards design are basically finite element implementations with strict code interpretations. The finite element modules are usually simpler than those in research packages. In other words, they follow the latest code provisions, but lack the ability to incorporate special effects such as warping. Some packages with warping capabilities implement a simplified *approximate* method in their analyses.

Based on the limitations stated earlier, a decision was made to develop a computer program for the analysis of curved composite box girder bridges. While this choice involves more work than resorting to available commercial packages, it was deemed necessary because of the nature of the studies involved.

This chapter describes the computer program that was developed throughout the course of this project. It is a finite element program that is specifically tailored for the analysis of curved composite box girder bridges. It is developed in the VisualBASIC environment which allowed providing it with a graphical user interface (GUI) to facilitate its use. Several issues were encountered while developing the program, all of which have been solved and are also described in this chapter.

2.2 Choice of Analysis Strategy

Analysis methods for curved box girders can be classified into two broad categories. The first is a macro approach, such as the plane grid method or space frame method. In this technique, the bridge system is discretized into a number of beam-column or grid elements, which can

be straight or curved. The focus in this type of analysis is on forces rather than on stresses. The second category of analysis techniques is the micro model approach, examples of which are the finite element method or finite strip method. In these methods, the bridge system is discretized into a number of continuum elements, and the emphasis is on stresses and corresponding strains.

Micro models are more rational than macro models, and provide more detailed information. However, they are difficult to setup and analyze, and are usually used for research purposes or to validate new designs. Macro-modeling techniques on the other hand, are simple to implement and since they yield reasonable results, are commonly used by practitioners and researchers. In fact, the plane grid method was used to calibrate the load distribution factors in the current AASHTO-LRFD specifications (1998). The analysis method adopted in the program is the space frame approach and falls under the macro-model category.

2.3 Program Structure

The program structure is not different from other finite element programs. It has five main modules; namely, Input (Pre-processor), Automatic Load Generator, Matrix Formation and Solution, Internal Force Calculation, Result Presentation (Post-processor). The details involved are numerous to be listed in this document and can be found in any textbook on matrix structural analysis. This chapter will only describe the special features of the program that needed to be addressed in developing the program. A general flow chart can be seen in Figs. 2.1 and 2.2.

2.4 Graphical User Interface

The purpose of developing a computer program is to be able to conduct special analyses needed for achieving the research goals. These goals can only be achieved by obtaining results from various parametric studies; i.e. a large number of analyses. A graphical user interface serves this effort and would simplify several aspects of the analyses such as reviewing results; checking input data, ...etc. VisualBASIC, which is the development environment chosen for this project, offers a large library of graphical tools. These tools were used in developing the pre- and post-processors for the program.

Figures 2.3 through 2.5 show how a 3-D model can be viewed through the developed GUI. A plan view of the model is given in Fig. 2.3. This view is very useful for checking proper element connectivity. The user has full control on the viewing angle, which allows him to rotate the model about all three axes. This is done with the help of a special tool developed for that purpose that requires two angles from the user as can be seen in Fig. 2.4. The deformed shape can be viewed with the user's choice of magnification factor. For example, Fig. 2.5 shows the deformed shape of a bridge model loaded with an AASHTO standard

truck using a magnification factor of 200. The model is viewed with a plan angle of 150° and an elevation angle of 15° . This view is also useful for checking the model for input errors.

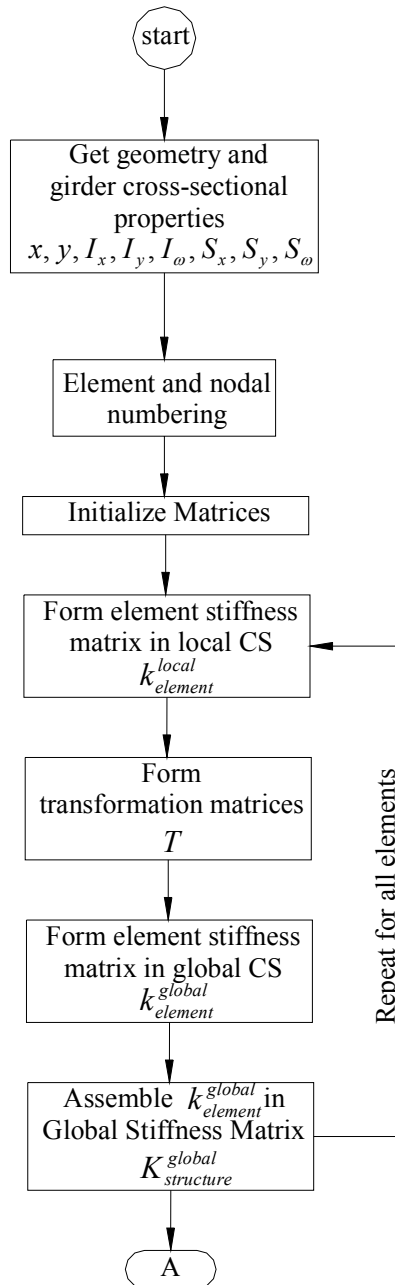


Figure 2.1: Flow chart of computer program (part I)

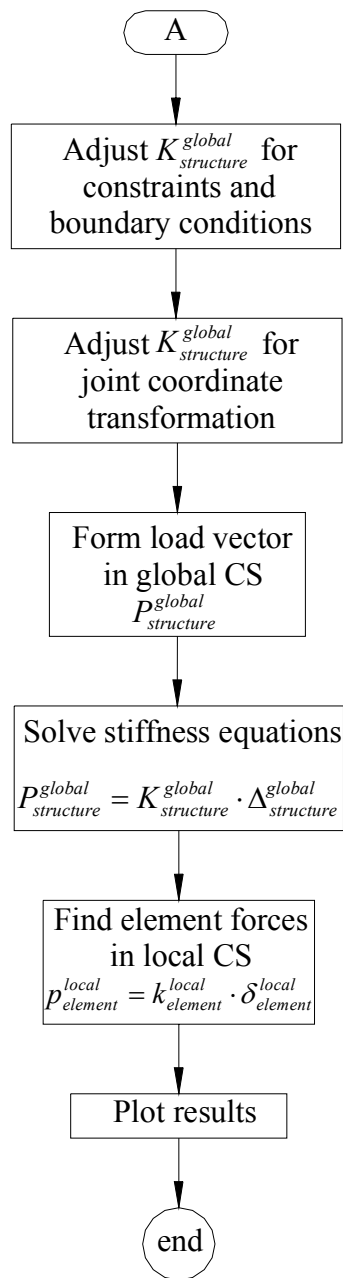


Figure 2.2: Flow chart of computer program (part II)

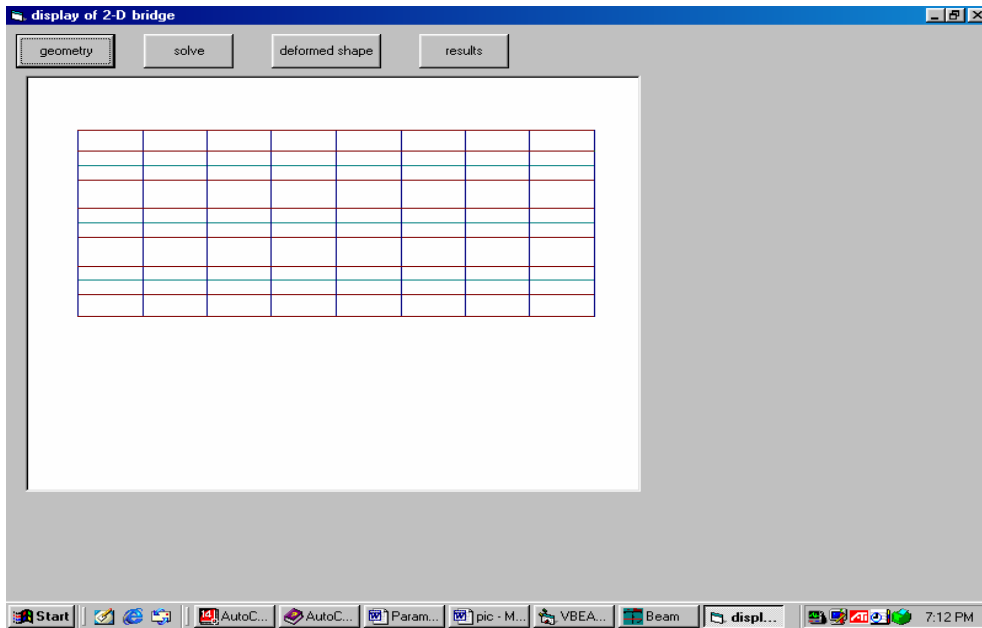


Figure 2.3: Plan view of the grid model

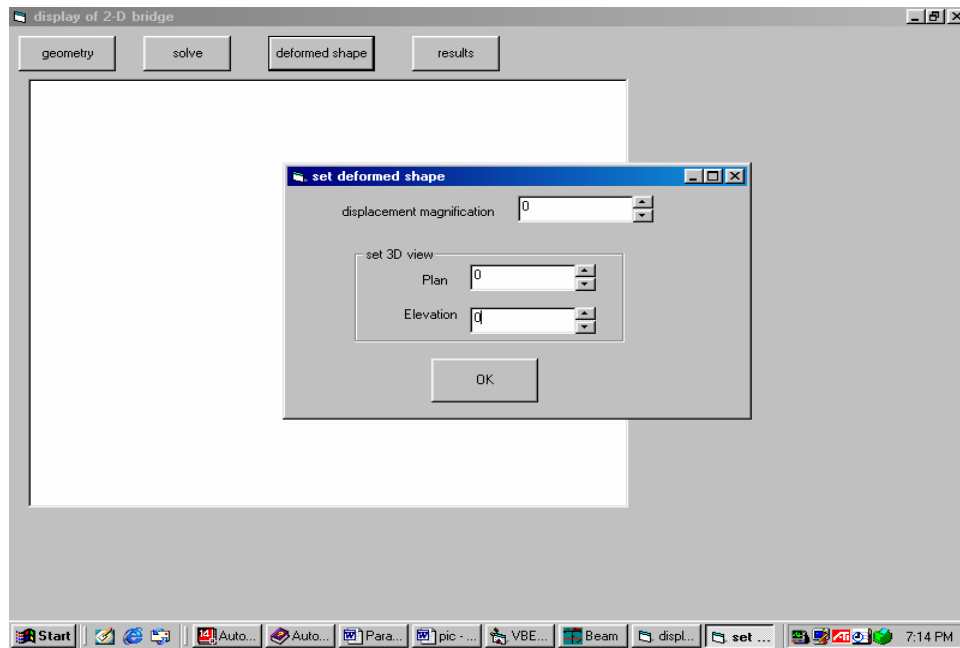


Figure 2.4: Setting 3-D viewing parameters

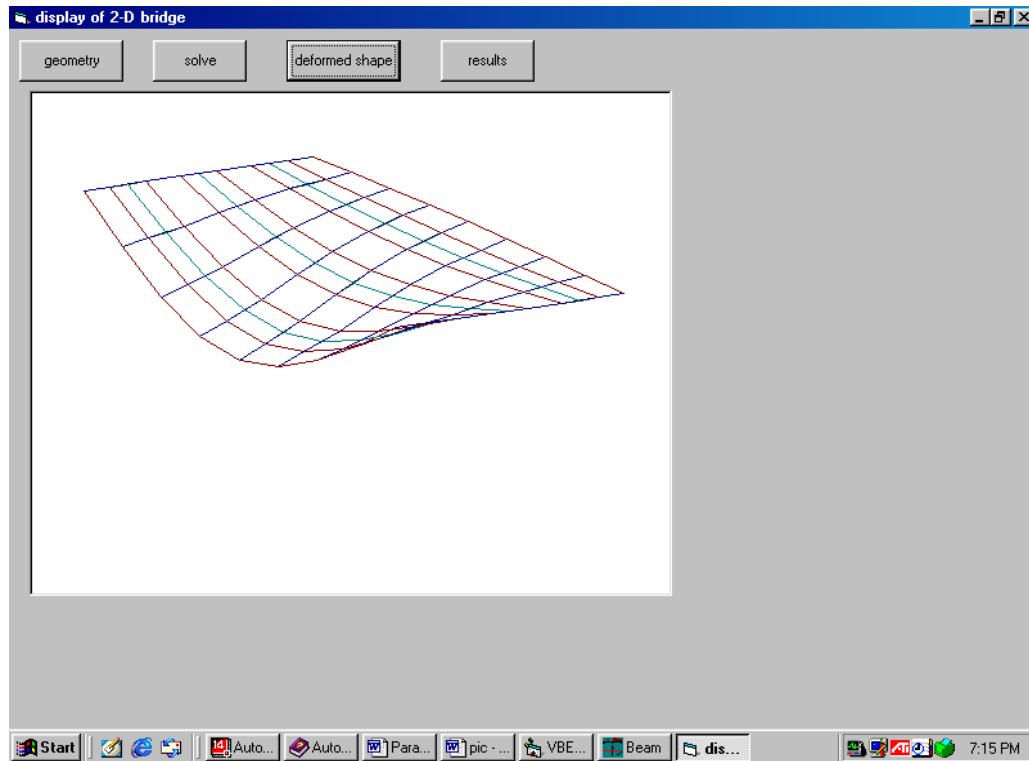


Figure 2.5: Isometric 3-D view of deformed shape

2.5 Elements Library

The program offers two elements suitable for the analysis of curved bridges. The first element is the classical frame element with 6 DOFs per node. To investigate warping effects, another element was implemented in which a seventh DOF is added to each node. Formulation for both elements is given next.

2.5.1 Six DOF Implementation

This element is the classical three-dimensional frame element with 6 DOFs per node. The DOFs are $\{u \ v \ w \ \theta_x \ \theta_y \ \theta_z\}^T$ in the local CS of the element as can be seen in Fig. 2.6. The element stiffness matrix has an order of 12x12.

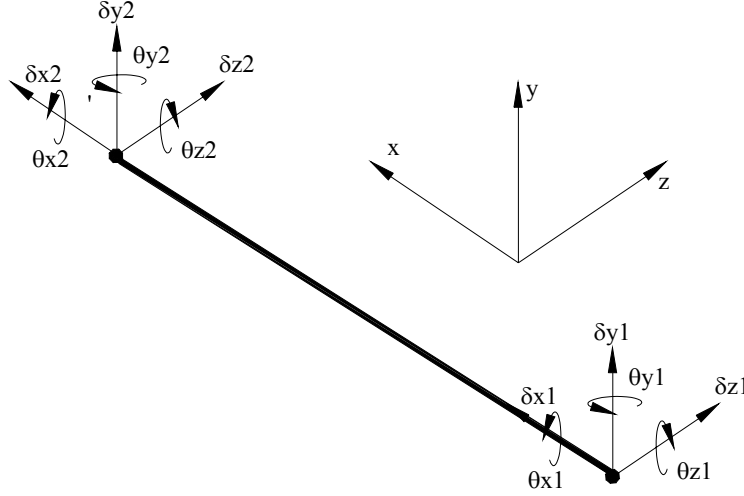


Figure 2.6: Local coordinate system for 6-DOF element

Stiffness relations for this element can be derived using the direct method or the virtual work principle. In the direct method, each DOF is released while other DOFs are restrained; one at a time. A unit deformation is then imposed on the released DOF resulting in reactions at the restrained DOFs. The reactions constitute the stiffness terms of the column elements corresponding to the released DOF. This straight forward method is suitable for simple elements where the reactions due to the imposed unit deformation can be easily quantified.

The virtual work principle is based on the concept of energy conservation. It is a well known approach, but its essential features will be outlined here for completeness. A virtual displacement, $\delta\Delta$, is imposed on the structure – in this case the element. The external work done to impose this virtual displacement has to be equal to the internal strain energy,

$$\delta W = \delta W_{\text{ext}} - \delta W_{\text{int}} = 0 \quad (2.1)$$

The virtual displacement field imposed on the element follows an assumed displacement field characterized by shape functions, $[N]$. The relationship between the displacement, Δ , at any point and nodal displacements for a general element with n DOFs is given by

$$\Delta = N_1\Delta_1 + N_2\Delta_2 + \dots + N_n\Delta_n = \sum_{i=1}^n N_i\Delta_i = \langle N \rangle \{ \Delta \} \quad (2.2)$$

where N_i is the shape function corresponding to the i^{th} DOF. The strain energy is calculated with the help of the strain displacement matrix, $[B]$, which contains derivatives of the shape functions and relates generalized strains to nodal displacements. For example, the

generalized axial strain is obtained using the first derivative of $[N_{axial}]$, where $[N_{axial}]$ contains the shape functions pertaining to the axial degrees of freedom.

$$\varepsilon_{axial} = [N'_{axial}] \{\Delta\} \quad (2.3)$$

which establishes the fact that the strain-displacement matrix for axial deformation DOFs is

$$[B_{axial}] = [N'_{axial}] \quad (2.4)$$

A relationship involving the second derivative of $[N]$ yields $[B]$ matrix for flexural terms. In general, the strain energy due to the imposed virtual displacement field is given as

$$\delta W_{int} = \int_{vol} [\delta \varepsilon] [D] [\varepsilon] d(vol) \quad (2.5)$$

where $[D]$ is the constitutive matrix, which differs based on the DOF under considerations. For example, $[D]$ for axial deformations is simply the modulus of elasticity. The external work done to impose the virtual displacement field, $\{\delta \Delta\}$, is given by

$$\delta W_{ext} = \langle \delta \Delta \rangle \{F\} \quad (2.6)$$

Equating δW_{ext} and δW_{int} leads to

$$\langle \delta \Delta \rangle \left[\int_{vol} [B]^T [D] [B] d(vol) \right] \{\Delta\} = \langle \delta \Delta \rangle \{F\} \quad (2.7)$$

Comparing Eq. 2.7 to the general stiffness relationship provides the following expression for the stiffness matrix.

$$[K] = \left[\int_{vol} [B]^T [D] [B] d(vol) \right] \quad (2.8)$$

The accuracy of the derived stiffness matrix depends on the quality of the assumed shape functions representing various displacement fields. Axial deformations are often represented by linear shape functions satisfying preliminary strength of materials requirements. The axial deformation, u , at any point within the element is given by

$$u = \langle N_{axial} \rangle \begin{Bmatrix} u_1 \\ u_2 \end{Bmatrix} \quad (2.9)$$

where for an element of length L , the assumed shape functions pertaining to the axial degrees of freedom are

$$\langle N_{axial} \rangle = \left\langle \begin{array}{cc} L-x & x \\ L & L \end{array} \right\rangle \quad (2.10)$$

Linear shape functions are also assumed for torsion and the twisting angle DOF.

$$\theta_x = \langle N_{Torsional} \rangle \begin{Bmatrix} \theta_{x1} \\ \theta_{x2} \end{Bmatrix} \quad (2.11)$$

$$\langle N \rangle = \left\langle \begin{array}{cc} L-x & x \\ L & L \end{array} \right\rangle \quad (2.12)$$

where $[N_{Torsional}]$ has the shape functions pertaining to the torsional degrees of freedom. Hermitian cubic polynomials are assumed for flexural related DOFs.

$$v = \langle N_1 \quad N_2 \quad N_3 \quad N_4 \rangle \begin{Bmatrix} v_1 \\ \theta_{x1} \\ v_2 \\ \theta_{x2} \end{Bmatrix} \quad (2.13)$$

where

$$\langle N \rangle = \begin{Bmatrix} N_1 \\ N_2 \\ N_3 \\ N_4 \end{Bmatrix}^T = \begin{Bmatrix} 1 - 3\left(\frac{x}{L}\right)^2 + 2\left(\frac{x}{L}\right)^3 \\ 3\left(\frac{x}{L}\right)^2 - 2\left(\frac{x}{L}\right)^3 \\ x\left(1 - \frac{x}{L}\right)^2 \\ x\left[\left(\frac{x}{L}\right)^2 - \frac{x}{L}\right] \end{Bmatrix}^T \quad (2.14)$$

An identical set of flexural shape functions is also assumed for the other (weak) axis of bending. The previous derivation is totally uncoupled; i.e. torsion is not affected by bending and axial DOFs are not affected by torsion, and so on. This implies that the derived stiffness matrix is formulated for small deformations. Large deformations in which secondary effects take place are not accounted for this research.

2.5.2 Seven DOF Implementation

One of the goals of this study is to investigate the warping behavior of curved composite box girder bridges. This element is developed for that purpose. Warping is accounted for through an added seventh DOF. The additional DOF is the first derivative of the twisting angle, θ'_x .

At each node, the DOFs for this element become $\{u \ v \ w \ \theta_x \ \theta_y \ \theta_z \ \theta'_x\}^T$ in the local coordinate system (CS) of the element as can be seen in Fig. 2.7. Other implementations of warping are possible; however, the formulation presented next captures the essential aspects of the behavior. It is well known that the St. Venant torsion, T_s , which is often referred to as uniform torsion, is normally expressed in terms of the torsion constant, J , and the shear modulus, G , and the twisting angle, θ_x , as follows

$$T_s = \frac{GJ\theta_x}{L} = GJ\theta'_x \quad (2.15)$$

The bimoment, M_ω , which accompanies torsion and causes out of plane deformations as those shown in Fig. 2.8 is a function of the warping constant, I_ω , the modulus of elasticity, E , and the second derivative of the twisting angle, θ''_x

$$M_\omega = EI_\omega\theta''_x \quad (2.16)$$

The total torsion may now be viewed as comprised of two components; the uniform torsion, T_s , and the non-uniform torsion, T_ω . It can be proven that the non-uniform torsion is the first derivative of the bimoment

$$T_\omega = -\frac{d}{dx}M_\omega = -EI_\omega\theta'''_x \quad (2.17)$$

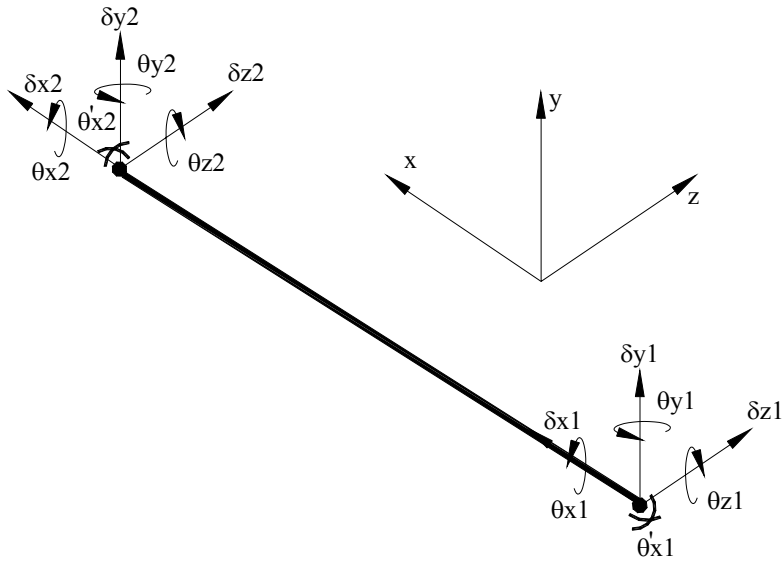


Figure 2.7: Local coordinate system for 7-DOF element

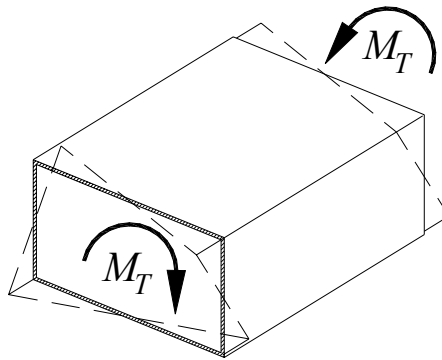


Figure 2.8: Warping of a closed thin-walled cross-section

Thus, the total applied torsion can be expressed as

$$M_x = T = T_s + T_\omega = GJ\theta'_x - EI_w\theta'''_x \tag{2.18}$$

Formulating the element stiffness matrix equations by employing virtual work principles leads to the following expressions for the internal and external virtual work

$$\delta W_{\text{ext}} = M_{\omega} \cdot \delta \theta'_x + T \cdot \delta \theta_x \quad (2.19)$$

$$\delta W_{\text{int}} = \int_0^L \delta \theta'_x EI_{\omega} \theta''_x dx + \int_0^L \delta \theta'_x GJ \theta'_x dx \quad (2.20)$$

the element stiffness for the four DOFs related to torsion, $\langle \theta_{x1} \quad \theta_{x2} \quad \theta'_{x1} \quad \theta'_{x2} \rangle^T$ can now be expressed as

$$[k] = \left[\int_0^L \langle N' \rangle G \{N'\} J dx + \int_0^L \langle N'' \rangle E \{N''\} I_{\omega} dx \right] \quad (2.21)$$

If the displacement field for the twisting angle is assumed to be a cubic polynomial as follows

$$\theta_x = a_1 + a_2 x + a_3 x^2 + a_4 x^3 \quad (2.22)$$

the first derivative of the twisting angle can be expressed as

$$\theta'_x = a_2 + 2a_3 x + 3a_4 x^2 \quad (2.23)$$

The coefficients, a_i , in the previous expressions can be found using the appropriate boundary conditions, which leads to the same expressions as those obtained previously for bending (Eqs. 2.13 and 2.14). Substituting for the coefficients in the previous equations yields the following submatrix for torsion related DOFs.

$$[k] = GJ \begin{bmatrix} \frac{6}{5L} & -\frac{6}{5L} & \frac{1}{10} & \frac{1}{10} \\ & \frac{6}{5L} & -\frac{1}{10} & -\frac{1}{10} \\ & & \frac{2L}{15} & -\frac{L}{30} \\ \text{sym} & & & \frac{2L}{15} \end{bmatrix} + \frac{EI_{\omega}}{L} \begin{bmatrix} \frac{12}{L^2} & -\frac{12}{L^2} & \frac{6}{L} & \frac{6}{L} \\ & \frac{12}{L^2} & -\frac{6}{L} & -\frac{6}{L} \\ & & \frac{4}{4} & \frac{2}{2} \\ \text{sym} & & & 4 \end{bmatrix} \quad (2.24)$$

By introducing a new parameter, $\alpha = \frac{EI_\omega}{GJL^2}$, both terms in Eq. 2.24 can be lumped into the following matrix

$$[k] = \frac{GJ}{L} \begin{bmatrix} \left(\frac{6}{5} + 12\alpha\right) & -\left(\frac{6}{5} + 12\alpha\right) & L\left(\frac{1}{10} + 6\alpha\right) & L\left(\frac{1}{10} + 6\alpha\right) \\ & \left(\frac{6}{5} + 12\alpha\right) & -L\left(\frac{1}{10} + 6\alpha\right) & -L\left(\frac{1}{10} + 6\alpha\right) \\ & & L^2\left(\frac{2}{15} + 4\alpha\right) & L^2\left(-\frac{1}{30} + 2\alpha\right) \\ \text{sym} & & & L^2\left(\frac{2}{15} + 4\alpha\right) \end{bmatrix} \quad (2.25)$$

This submatrix is added to the other uncoupled DOFs to obtain the full 14x14 stiffness matrix. The assumption of uncoupled DOFs does not always hold and special treatments are necessary. The following sections illustrate some of the special treatments implemented in the program.

2.6 Special Features

2.6.1 Shear Deformations

Shear deformations are quite small in most civil engineering applications and they are therefore often ignored with no impact on the quality of results. However, shear deformations may be dominant in some situations where bending moments are small compared to shear forces acting on the member. This is normally true for short span beams. In a structural system such as a curved box girder bridge, this is also true for diaphragms connecting box girders in the transverse directions. To account for shear deformations, the concept of *equivalent shear area*, A_s , is used. According to this concept, the applied shear force, F_y , is equal to the equivalent shear area multiplied by the shear stress at the centroid of the cross section. The component of complementary internal virtual work due to shear can be expressed as

$$\delta W_{\text{int}(S)} = \int_0^l \left(\frac{\delta F_y}{A_s} \right) \frac{1}{G} \left(\frac{F_y}{A_s} \right) A_s dx = \frac{\delta F_y \cdot F_y L}{A_s G} \quad (2.26)$$

The total strain energy is equal to the summation of the bending and shear components

$$\delta W_{\text{int}} = \delta W_{\text{int}(B)} + \delta W_{\text{int}(S)} = \langle \delta F_y \quad \delta M_z \rangle \begin{bmatrix} \frac{L^3}{3EI_z} + \frac{L}{A_s G} & \frac{L^2}{2EI_z} \\ \frac{L^2}{2EI_z} & \frac{L}{EI_z} \end{bmatrix} \begin{Bmatrix} F_y \\ M_z \end{Bmatrix} \quad (2.27)$$

The middle term of the above expression is the flexibility matrix taking into account shear deformations. The stiffness matrix is then obtained by transforming the flexibility matrix which leads to the following (McGuire et al. 2000)

$$\begin{Bmatrix} F_{y1} \\ M_{z1} \\ F_{y2} \\ M_{y2} \end{Bmatrix} = \frac{EI_z}{L \left(\frac{L^2}{12} + \eta \right)} \begin{bmatrix} 1 & \frac{L}{2} & -1 & \frac{L}{2} \\ \frac{L^2}{3} + \eta & -\frac{L}{2} & \frac{L^2}{6} - \eta & \\ & 1 & -\frac{L}{2} & \\ & & \frac{L^2}{3} + \eta & \end{bmatrix} \begin{Bmatrix} v_1 \\ \theta_1 \\ v_2 \\ \theta_2 \end{Bmatrix} \quad (2.28)$$

symmetric

where a new term, η , is introduced to account for shear deformations. η is given as

$$\eta = \eta_z = \frac{EI_z}{A_s G} \quad (2.29)$$

Satisfactory results were obtained when A_s was taken equal to the area of the webs in the appropriate direction. The resulting stiffness matrix for the 6-DOF implementation is now given as

$$K_{(e)}^0 = \begin{bmatrix} K_{(e)(1)}^0 & K_{(e)(2)}^0 \\ K_{(e)(3)}^0 & K_{(e)(4)}^0 \end{bmatrix} \quad (2.30)$$

where the four submatrices of $K_{(e)}^0$ are given next

$$K_{(e)(1)}^0 = \begin{bmatrix} \frac{EA}{L} & 0 & 0 & 0 & 0 & 0 \\ 0 & \frac{12EI_z}{L^3 + 12L\eta_z} & 0 & 0 & 0 & \frac{6EI_z}{L^2 + 12\eta_z} \\ 0 & 0 & \frac{12EI_y}{L^3 + 12L\eta_y} & 0 & \frac{-6EI_y}{L^2 + 12\eta_y} & 0 \\ 0 & 0 & 0 & \frac{GJ}{L} & 0 & 0 \\ 0 & 0 & \frac{-6EI_y}{L^2 + 12\eta_y} & 0 & \frac{EI_y}{L} \frac{L^2/3 + \eta_y}{L^2/12 + \eta_y} & 0 \\ 0 & \frac{6EI_z}{L^2 + 12\eta_z} & 0 & 0 & 0 & \frac{EI_z}{L} \frac{L^2/3 + \eta_z}{L^2/12 + \eta_z} \end{bmatrix} \quad (2.31)$$

$$K_{(e)(2)}^0 = \begin{bmatrix} -\frac{EA}{L} & 0 & 0 & 0 & 0 & 0 \\ 0 & \frac{-12EI_z}{L^3 + 12L\eta_z} & 0 & 0 & 0 & \frac{6EI_z}{L^2 + 12\eta_z} \\ 0 & 0 & \frac{-12EI_y}{L^3 + 12L\eta_y} & 0 & \frac{-6EI_y}{L^2 + 12\eta_y} & 0 \\ 0 & 0 & 0 & -\frac{GJ}{L} & 0 & 0 \\ 0 & 0 & \frac{6EI_y}{L^2 + 12\eta_y} & 0 & \frac{EI_y}{L} \frac{L^2/3 + \eta_y}{L^2/12 + \eta_y} & 0 \\ 0 & \frac{-6EI_z}{L^2 + 12\eta_z} & 0 & 0 & 0 & \frac{EI_z}{L} \frac{L^2/6 - \eta_z}{L^2/12 + \eta_z} \end{bmatrix} \quad (2.32)$$

$$K_{(e)(3)}^0 = \begin{bmatrix} \frac{EA}{L} & 0 & 0 & 0 & 0 & 0 \\ 0 & \frac{-12EI_z}{L^3 + 12L\eta_z} & 0 & 0 & 0 & \frac{-6EI_z}{L^2 + 12\eta_z} \\ 0 & 0 & \frac{-12EI_y}{L^3 + 12L\eta_y} & 0 & \frac{6EI_y}{L^2 + 12\eta_y} & 0 \\ 0 & 0 & 0 & \frac{GJ}{L} & 0 & 0 \\ 0 & 0 & \frac{-6EI_y}{L^2 + 12\eta_y} & 0 & \frac{EI_y}{L} \frac{L^2 / 6 - \eta_y}{L^2 / 12 + \eta_y} & 0 \\ 0 & \frac{6EI_z}{L^2 + 12\eta_z} & 0 & 0 & 0 & \frac{EI_z}{L} \frac{L^2 / 6 - \eta_z}{L^2 / 12 + \eta_z} \end{bmatrix} \quad (2.33)$$

$$K_{(e)(4)}^0 = \begin{bmatrix} \frac{EA}{L} & 0 & 0 & 0 & 0 & 0 \\ 0 & \frac{12EI_z}{L^3 + 12L\eta_z} & 0 & 0 & 0 & \frac{-6EI_z}{L^2 + 12\eta_z} \\ 0 & 0 & \frac{12EI_y}{L^3 + 12L\eta_y} & 0 & \frac{6EI_y}{L^2 + 12\eta_y} & 0 \\ 0 & 0 & 0 & \frac{GJ}{L} & 0 & 0 \\ 0 & 0 & \frac{6EI_y}{L^2 + 12\eta_y} & 0 & \frac{EI_y}{L} \frac{L^2 / 3 + \eta_y}{L^2 / 12 + \eta_y} & 0 \\ 0 & \frac{-6EI_z}{L^2 + 12\eta_z} & 0 & 0 & 0 & \frac{EI_z}{L} \frac{L^2 / 3 + \eta_z}{L^2 / 12 + \eta_z} \end{bmatrix} \quad (2.34)$$

in the previous expressions

J is the torsional constant

I_y and I_z are the moments of inertia about the y and z direction, respectively

E and G are the modulus of elasticity and shear modulus, respectively

$\eta_y = \frac{EI_y}{A_{S_z}G}$ is the shear deformation term in the z direction of the local CS based on the shear area A_{S_z}

$\eta_z = \frac{EI_z}{A_{S_y}G}$ is the shear deformation term in the y direction of the local CS based on the shear area A_{S_y}

The corresponding matrix for the 7-DOF implementation is

$$K_{(e)}^0 = \begin{bmatrix} K_{(e)(1)}^0 & K_{(e)(2)}^0 \\ K_{(e)(3)}^0 & K_{(e)(4)}^0 \end{bmatrix} \quad (2.35)$$

where the submatrices are

$$K_{(e)(1)} = \begin{bmatrix} \frac{EA}{L} & 0 & 0 & 0 & 0 & 0 & 0 \\ 0 & \frac{12EI_z}{L^3 + 12L\eta_z} & 0 & 0 & 0 & \frac{6EI_z}{L^2 + 12\eta_z} & 0 \\ 0 & 0 & \frac{12EI_y}{L^3 + 12L\eta_y} & 0 & \frac{-6EI_y}{L^2 + 12\eta_y} & 0 & 0 \\ 0 & 0 & 0 & \frac{GJ}{L} \left(\frac{6}{5} + 12\alpha \right) & 0 & 0 & GJ \left(\frac{1}{10} + 6\alpha \right) \\ 0 & 0 & \frac{-6EI_y}{L^2 + 12\eta_y} & 0 & \frac{EI_y}{L} \frac{L^2/3 + \eta_y}{L^2/12 + \eta_y} & 0 & 0 \\ 0 & \frac{6EI_z}{L^2 + 12\eta_z} & 0 & 0 & 0 & \frac{EI_z}{L} \frac{L^2/3 + \eta_z}{L^2/12 + \eta_z} & 0 \\ 0 & 0 & 0 & GJ \left(\frac{1}{10} + 6\alpha \right) & 0 & 0 & GJ \left(\frac{2}{15} + 4\alpha \right) \end{bmatrix} \quad (2.36)$$

$$K_{(e)(2)} = \begin{bmatrix} \frac{EA}{L} & 0 & 0 & 0 & 0 & 0 & 0 \\ 0 & \frac{-12EI_z}{L^3+12L\eta_z} & 0 & 0 & 0 & \frac{6EI_z}{L^2+12\eta_z} & 0 \\ 0 & 0 & \frac{-12EI_y}{L^3+12L\eta_y} & 0 & \frac{-6EI_y}{L^2+12\eta_y} & 0 & 0 \\ 0 & 0 & 0 & -\frac{GJ}{L}\left(\frac{6}{5}+12\alpha\right) & 0 & 0 & GJ\left(\frac{1}{10}+6\alpha\right) \\ 0 & 0 & \frac{6EI_y}{L^2+12\eta_y} & 0 & \frac{EI_y}{L}\frac{L^2/3+\eta_y}{L^2/12+\eta_y} & 0 & 0 \\ 0 & \frac{-6EI_z}{L^2+12\eta_z} & 0 & 0 & 0 & \frac{EI_z}{L}\frac{L^2/6-\eta_z}{L^2/12+\eta_z} & 0 \\ 0 & 0 & 0 & -GJ\left(\frac{1}{10}+6\alpha\right) & 0 & 0 & GJ\left(-\frac{1}{30}+2\alpha\right) \end{bmatrix} \quad (2.37)$$

$$K_{(e)(3)} = \begin{bmatrix} \frac{EA}{L} & 0 & 0 & 0 & 0 & 0 & 0 \\ 0 & \frac{-12EI_z}{L^3+12L\eta_z} & 0 & 0 & 0 & \frac{-6EI_z}{L^2+12\eta_z} & 0 \\ 0 & 0 & \frac{-12EI_y}{L^3+12L\eta_y} & 0 & \frac{6EI_y}{L^2+12\eta_y} & 0 & 0 \\ 0 & 0 & 0 & -\frac{GJ}{L}\left(\frac{6}{5}+12\alpha\right) & 0 & 0 & -GJ\left(\frac{1}{10}+6\alpha\right) \\ 0 & 0 & \frac{-6EI_y}{L^2+12\eta_y} & 0 & \frac{EI_y}{L}\frac{L^2/6-\eta_y}{L^2/12+\eta_y} & 0 & 0 \\ 0 & \frac{6EI_z}{L^2+12\eta_z} & 0 & 0 & 0 & \frac{EI_z}{L}\frac{L^2/6-\eta_z}{L^2/12+\eta_z} & 0 \\ 0 & 0 & 0 & GJ\left(\frac{1}{10}+6\alpha\right) & 0 & 0 & GJ\left(-\frac{1}{30}+2\alpha\right) \end{bmatrix} \quad (2.38)$$

$$K_{(e)(4)} = \begin{bmatrix} \frac{EA}{L} & 0 & 0 & 0 & 0 & 0 & 0 \\ 0 & \frac{12EI_z}{L^3+12L\eta_z} & 0 & 0 & 0 & \frac{-6EI_z}{L^2+12\eta_z} & 0 \\ 0 & 0 & \frac{12EI_y}{L^3+12L\eta_y} & 0 & \frac{6EI_y}{L^2+12\eta_y} & 0 & 0 \\ 0 & 0 & 0 & \frac{GJ}{L}\left(\frac{6}{5}+12\alpha\right) & 0 & 0 & -GJ\left(\frac{1}{10}+6\alpha\right) \\ 0 & 0 & \frac{6EI_y}{L^2+12\eta_y} & 0 & \frac{EI_y}{L}\frac{L^2/3+\eta_y}{L^2/12+\eta_y} & 0 & 0 \\ 0 & \frac{-6EI_z}{L^2+12\eta_z} & 0 & 0 & 0 & \frac{EI_z}{L}\frac{L^2/3+\eta_z}{L^2/12+\eta_z} & 0 \\ 0 & 0 & 0 & -GJ\left(\frac{1}{10}+6\alpha\right) & 0 & 0 & GJ\left(\frac{2}{15}+4\alpha\right) \end{bmatrix} \quad (2.39)$$

2.6.2 Eccentricity between Shear Center and Centroid

The previous derivation of the stiffness matrix is based on the assumption that the centroid and the shear center of the cross section coincide. This assumption is true for many engineering shapes, however, it is not the case for box girder cross sections. The eccentricity between the centroid and shear center is relatively small for closed cross sections. But as will be seen later, the cross section is not fully closed (quasi-closed) during construction. At this stage, the shear center often falls below the bottom flange while the centroid is usually within the plates (flanges and webs). Hence, a large eccentricity is created. Not accounting for this eccentricity is inaccurate modeling. Therefore, the derived stiffness matrix is treated by a special transformation for that purpose. For a general cross section with non-coincident shear center and centroid as in Fig. 2.9

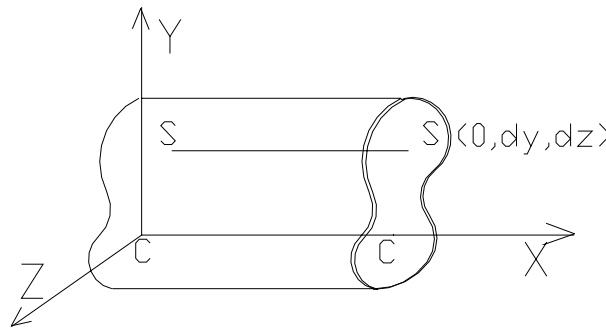


Figure 2.9: A general element showing non-coincident shear center and centroid

The eccentricity between the shear center and centroid leads to a coupling between torsion and bending DOFs. It is assumed that the local coordinate system x passes through the centroid line of the straight beam, and that the y and z represent the weak and strong bending axes, respectively. A shear force acting at the centroid of the cross section, but not the shear center, generates extra torsion because of the eccentricity. The effect of the eccentricity ($0, d_y, d_z$) is accounted for using the following transformation

$$K_{SC} = T_{SC} * K * T_{SC}^T \quad (2.40)$$

where the transformation matrix is given as (Dubigeon and Kim 1982)

$$T_{sc} = \begin{bmatrix} 1 & 0 & 0 & 0 & 0 & 0 & 0 & 0 & 0 & 0 & 0 & 0 & 0 & 0 \\ 0 & 1 & 0 & 0 & 0 & 0 & 0 & 0 & 0 & 0 & 0 & 0 & 0 & 0 \\ 0 & 0 & 1 & 0 & 0 & 0 & 0 & 0 & 0 & 0 & 0 & 0 & 0 & 0 \\ 0 & -dz & dy & 1 & 0 & 0 & 0 & 0 & 0 & 0 & 0 & 0 & 0 & 0 \\ 0 & 0 & 0 & 0 & 1 & 0 & 0 & 0 & 0 & 0 & 0 & 0 & 0 & 0 \\ 0 & 0 & 0 & 0 & 0 & 1 & 0 & 0 & 0 & 0 & 0 & 0 & 0 & 0 \\ 0 & 0 & 0 & 0 & 0 & 0 & 1 & 0 & 0 & 0 & 0 & 0 & 0 & 0 \\ 0 & 0 & 0 & 0 & 0 & 0 & 0 & 1 & 0 & 0 & 0 & 0 & 0 & 0 \\ 0 & 0 & 0 & 0 & 0 & 0 & 0 & 0 & 1 & 0 & 0 & 0 & 0 & 0 \\ 0 & 0 & 0 & 0 & 0 & 0 & 0 & 0 & 0 & 1 & 0 & 0 & 0 & 0 \\ 0 & 0 & 0 & 0 & 0 & 0 & 0 & 0 & -dz & dy & 1 & 0 & 0 & 0 \\ 0 & 0 & 0 & 0 & 0 & 0 & 0 & 0 & 0 & 0 & 0 & 1 & 0 & 0 \\ 0 & 0 & 0 & 0 & 0 & 0 & 0 & 0 & 0 & 0 & 0 & 0 & 1 & 0 \\ 0 & 0 & 0 & 0 & 0 & 0 & 0 & 0 & 0 & 0 & 0 & 0 & 0 & 1 \end{bmatrix} \quad (2.41)$$

corresponding to the 14 degree of freedom in the following order $\langle u_1, v_1, w_1, \theta_{x1}, \theta_{y1}, \theta_{z1}, \theta'_{x1}, u_2, v_2, w_2, \theta_{x2}, \theta_{y2}, \theta_{z2}, \theta'_{x2} \rangle^T$.

2.6.3 Support Boundary Conditions

Due to the nature of curved bridges, it was necessary to handle support DOFs in a special manner. Supports of curved girders restrain movement in the vertical and horizontal directions. The vertical movement does not require special handling because the local y -axis is normally chosen to be parallel to the global y -axis. Horizontally, the x - and z -axes usually coincide with global axes at one support only, and in most other some cases they do not as can be seen in Fig. 2.10. Therefore, special handling of these boundary conditions through constraints was necessary.

This is done using a transformation matrix that relates the DOFs in the local $x - y$ and the global coordinate systems $X - Y$. The relationship for the 6-DOF implementation is given by Equation 2.42.

The transformation for the 7-DOF element is similar except for the additional warping DOF. Since the physical meaning of warping is two bending moments with same magnitude and opposite directions as illustrated for example in Fig. 2.11 for an I-section beam, bimoment has no direction. Therefore, the bimoment in the local coordinate system and that in global coordinate system are the same.

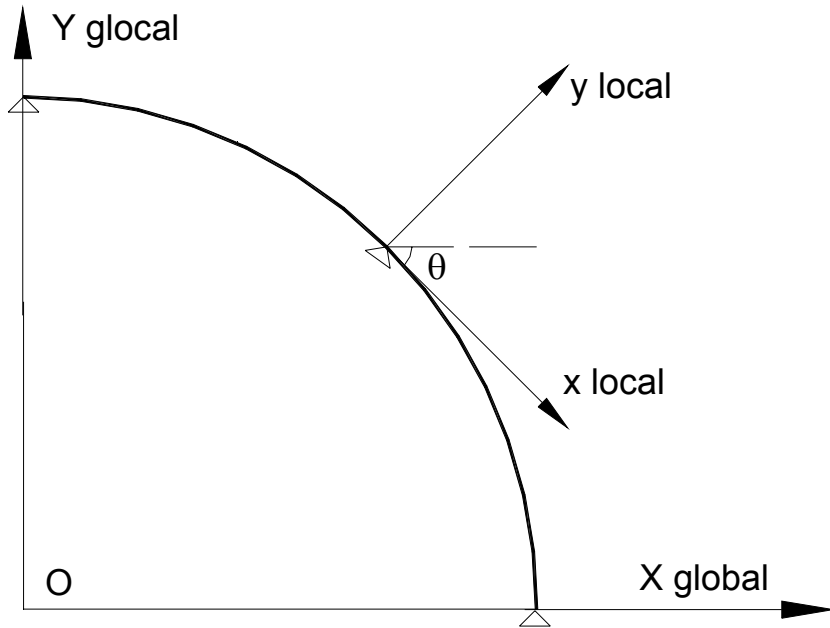


Figure 2.10: Local and global CS for handling of restrained DOFs

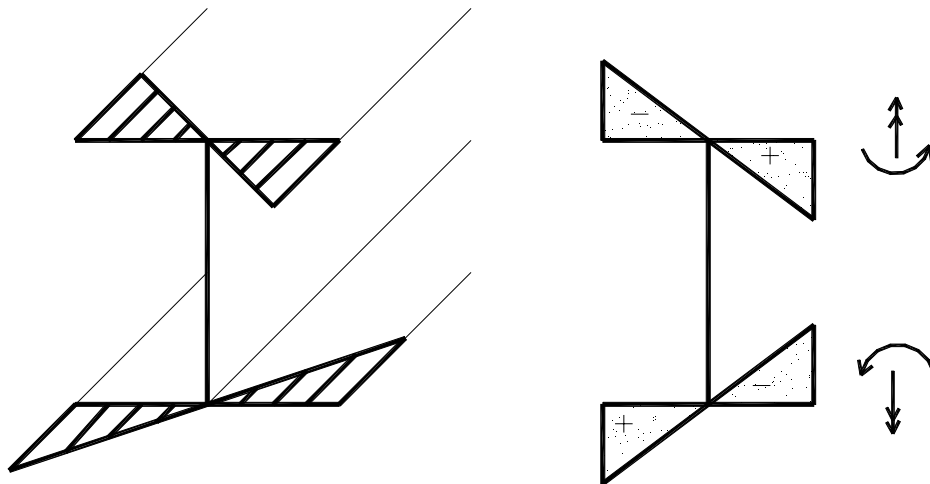


Figure 2.11: Normal stress distribution under warping for a I-section beam

$$\begin{pmatrix} u_g \\ v_g \\ w_g \\ \theta_{xg} \\ \theta_{yg} \\ \theta_{zg} \end{pmatrix} = \begin{bmatrix} \cos \theta & \sin \theta & 0 & 0 & 0 & 0 \\ -\sin \theta & \cos \theta & 0 & 0 & 0 & 0 \\ 0 & 0 & 1 & 0 & 0 & 0 \\ 0 & 0 & 0 & \cos \theta & \sin \theta & 0 \\ 0 & 0 & 0 & -\sin \theta & \cos \theta & 0 \\ 0 & 0 & 0 & 0 & 0 & 1 \end{bmatrix} \begin{pmatrix} u \\ v \\ w \\ \theta_x \\ \theta_y \\ \theta_z \end{pmatrix} \quad (2.42)$$

This means that the transformation matrix for the 7-DOF implementation is

$$\begin{pmatrix} u_g \\ v_g \\ w_g \\ \theta_{xg} \\ \theta_{yg} \\ \theta_{zg} \\ \theta'_{xg} \end{pmatrix} = \begin{bmatrix} \cos \theta & \sin \theta & 0 & 0 & 0 & 0 & 0 \\ -\sin \theta & \cos \theta & 0 & 0 & 0 & 0 & 0 \\ 0 & 0 & 1 & 0 & 0 & 0 & 0 \\ 0 & 0 & 0 & \cos \theta & \sin \theta & 0 & 0 \\ 0 & 0 & 0 & -\sin \theta & \cos \theta & 0 & 0 \\ 0 & 0 & 0 & 0 & 0 & 1 & 0 \\ 0 & 0 & 0 & 0 & 0 & 0 & 1 \end{bmatrix} \begin{pmatrix} u \\ v \\ w \\ \theta_x \\ \theta_y \\ \theta_z \\ \theta'_x \end{pmatrix} \quad (2.43)$$

It is clear that both transformation matrices contain many zero terms. The full transformation matrix (14x14) has more zeros than shown in Eq. 2.43 because more DOFs are completely uncoupled. Direct execution of the transformation resulted in unnecessary computation and increased runtime. A sparse-matrix implementation was therefore adopted to reduce running time and storage requirements.

2.6.4 Implementation using Sparse Matrices

The nature of grillage models for curved bridges requires handling many sparse matrices. A sparse matrix is a matrix with all but few cells holding zero values. The existence of some sparse matrices does not affect the overall computational time or memory requirements in small programs that handle all matrices the same way. However, preliminary runs with this general implementation showed that more than 90% of the computational time is consumed by transformations that involve large sparse matrices. To overcome this obstacle, a sparse matrix implementation was needed.

Since most of the matrix multiplication operations are of zero terms, it is possible to skip most of these operations by just focusing on the nonzero matrix terms. The best approach is to use algorithms that handle these matrices as reduced sparse matrices. In addition to the savings in execution time, sparse implementations also save storage requirements. Following the work of Horowitz et al. (1993), these sparse matrices were compressed into special data structures. The following example is chosen to better illustrate the method. In the example an 8x8 sparse matrix $[A]$ is given as:

$$[A] = \begin{bmatrix} 15 & 0 & 0 & 22 & 0 & -15 \\ 0 & 11 & 3 & 0 & 0 & 0 \\ 0 & 0 & 0 & -6 & 0 & 0 \\ 0 & 0 & 0 & 0 & 0 & 0 \\ 91 & 0 & 0 & 0 & 0 & 0 \\ 0 & 0 & 28 & 0 & 0 & 0 \end{bmatrix} \quad (2.44)$$

The first step in handling this sparse matrix is to convert it into a data structure, $[\bar{A}]$, with a number of elements equal to the number of non-zero cells in $[A]$; i.e. eight elements. Each of the elements in the new data structure holds three pieces of information; namely row number, column number and value. The resulting data structure is stored in a sequential manner as in Eq. 2.45

	row #	col #	value	
$[\bar{A}] =$	1	1	15	
	1	4	22	
	1	6	-15	
	2	2	11	
	2	3	3	
	3	4	-6	
	5	1	91	
	6	3	28	

(2.45)

The total number of cells in $[\bar{A}]$ is 24 compared to 36 in original matrix, $[A]$. Matrix manipulation (e.g. transpose, multiplication, ...etc.) is executed for $[\bar{A}]$ with the help of several subroutines written for that purpose. Timesavings in this example may not seem worthwhile the effort. However, the savings are quite substantial when dealing with much larger matrices with fewer active cells (non-zero terms), as is the case with many of the matrices in this program. It should also be noted that such matrices are an integral part of the calculation and that the transformation and multiplication operations are repeated extensively. The amount of timesavings was immediately felt by reducing the run time from tens of minutes to less than a few seconds.

2.7 Program Verification

Before embarking on any intensive analyses, a thorough verification study was needed. In this section three verification problems are described. Each problem is designed to check a

specific feature in the program. Results obtained from the program were compared to those obtained from commercially available packages. Also comparisons with closed-formed solutions were performed for one of the problems. The verification study showed that the program is capable of capturing the general behavior of curved box girder bridges. It is also capable of capturing the most important aspects of warping behavior.

2.7.1 Comparison with closed-form solution

This verification problem is for a simply-supported curved beam with span length, $L = 40''$, radius, $R = 100''$. A single concentrated load is applied at midspan, $P = 10$ lb. A total of 160 elements are used to model the problem. Results obtained from the program were compared to closed-form solution proposed by Konishi and Komatsu (Nakai et al. 1982). In their solution, a parameter κ is defined

$$\kappa = L \sqrt{\frac{GJ}{EI_{\omega}}} \quad (2.46)$$

For κ values larger than 9.0, bimoment values can be accurately estimated using the following expression

$$M_w = \frac{PR}{2\alpha^2} * R * \tan \frac{\phi}{2} \quad (2.47)$$

in which L is the span length, R is the radius of curvature, and P is the concentrated load acting at mid-span. The central angle is calculated as L/R in radians and the parameter α is given as

$$\alpha = R \sqrt{\frac{GJ}{EI_{\omega}}} \quad (2.48)$$

Table 2.1 lists the results as obtained from Eq. 2.47 and from the developed program. Three cross sectional properties were attempted to test the validity of the program over a wide range of κ . It can be seen that the difference between both methods is relatively low, especially for high values of κ . The larger difference at lower values of κ should not be considered a deficiency because 1) the closed-form solution is not an *exact* solution but rather a solution based on several assumptions that are often made to simplify the derivation, 2) it will be seen later that κ values of existing bridges fall in a higher range than the case considered in this verification study. The conclusion of this study is that the program is capable of capturing the warping behavior by accurately estimating the bimoment values for a curved simply supported girder.

Table 2.1: M_w verification results – Program vs. closed form solutions

κ	Eq. 2.47	Program	Difference
122	0.1082	0.1118	3.30%
70	0.321	0.325	1.20%
23	2.921	2.682	8.20%

2.7.2 Comparison with beam element models (ABAQUS)

In this verification example, results obtained from the developed program are compared with ABAQUS results reported in Okeil et al. (2000). The reported results are for the bimoment distribution of an existing curved box-girder bridge (Bridge 521 of the FDOT inventory – see Chapter 3) under dead loads. They are obtained using the computer program ABAQUS (1997) which offers a beam element with warping capabilities (Element Type BO31S). Identical models were built using ABAQUS and the developed program, in which 816 elements were used.

Figures 2.12 and 2.13 show the bimoment distribution along the bridge as obtained from the program and from ABAQUS, respectively. The figures show that the results are identical except at the interior supports. At these positions, the bimoment results from the program are larger than those obtained using ABAQUS. Doubling the element number (using 1632 elements) showed that results were converging, though convergence is not rapid.

2.7.3 Comparison with full shell element models (SAP2000)

A thin-walled cantilever-beam verification exercise was also conducted by comparing between program results and response data from the SAP2000 software package. Due to the presence of bimoment, which complicates the total normal stress distribution, several different models are set up and analyzed.

The cross section of the cantilever beam is square with different flange and web plate thickness to allow for warping to develop (see Fig. 2.14). Cross-sectional properties were computed and used in the analysis done by the computer program. The cantilever beam is curved with total length 40 inches and radius 100 inches from the center of curvature to centroid line of the beam. The beam is discretized into a 160-element model. Uniform meshing was used leading to equal element lengths of 0.25 inch. A single concentrated torque, $T = 10$ lb-in acting at the free end (see Fig. 2.15). To make sure that the results given by the 160-element model are accurate, different models with different element number were

also studied. Twenty, forty, and eighty element models were considered. Convergence of the results was observed for models using less than 80 elements. The results showed that there is almost no difference between results given by 80-element model and 160-element model.

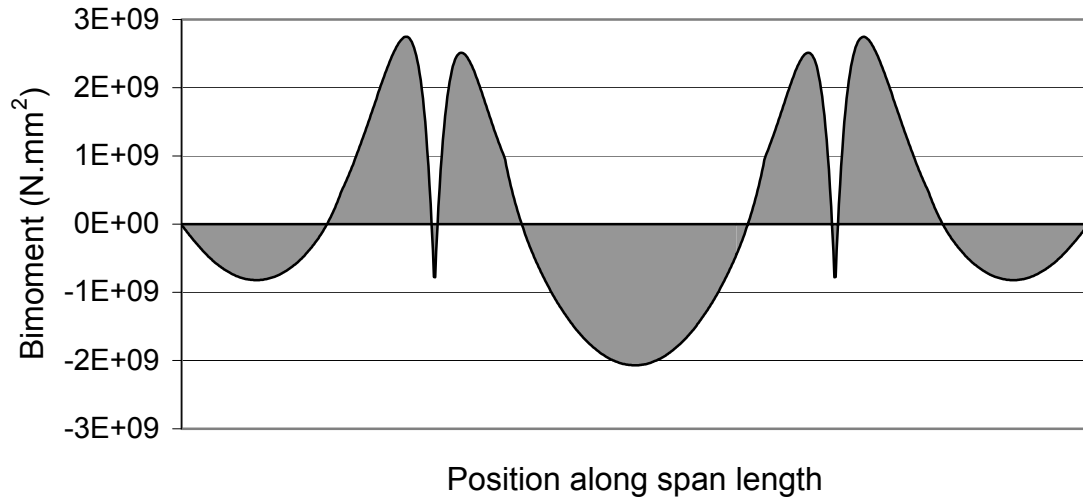


Figure 2.12: Bimoment distribution along the entire length of Bridge 521 (program results)

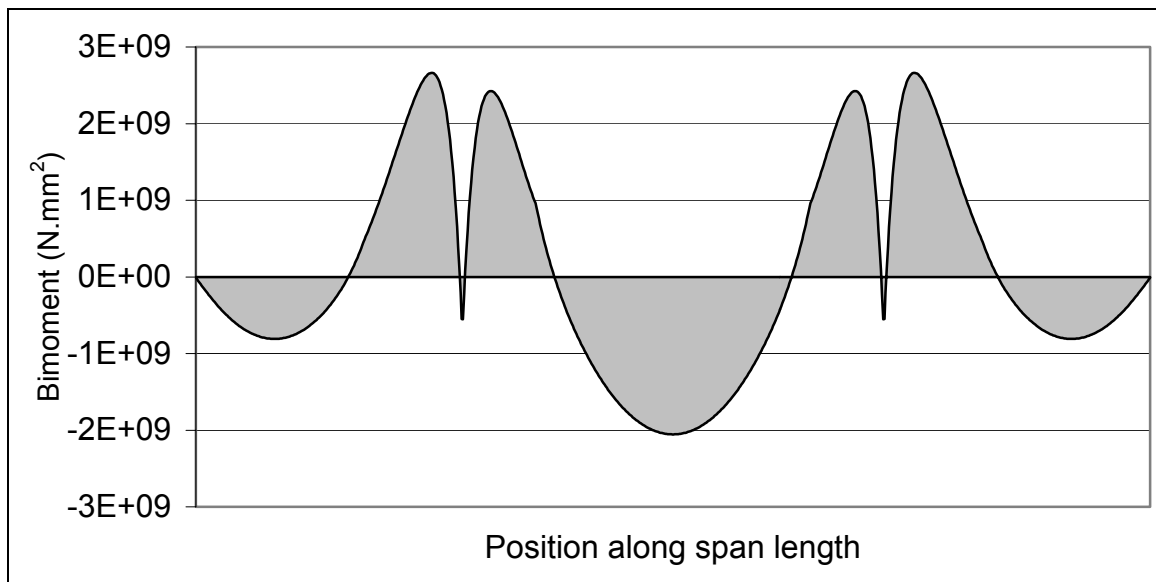


Figure 2.13: Bimoment distribution along the entire length of Bridge 521 (ABAQUS results)

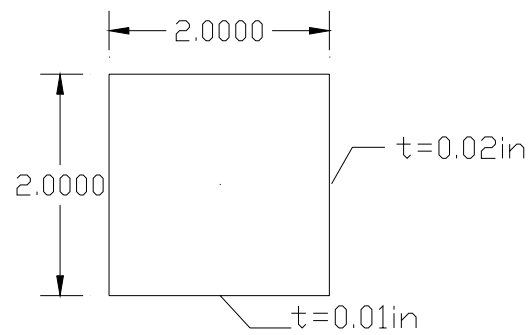


Figure 2.14: Dimensions of the cross section for verification example (in inches)

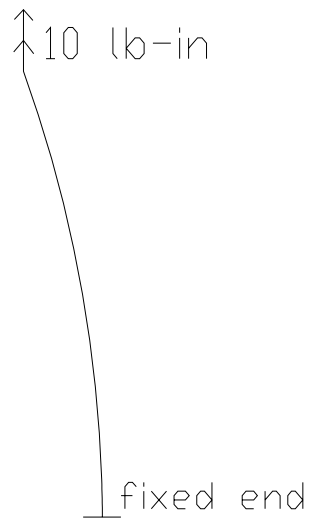


Figure 2.15: Loading of verification example

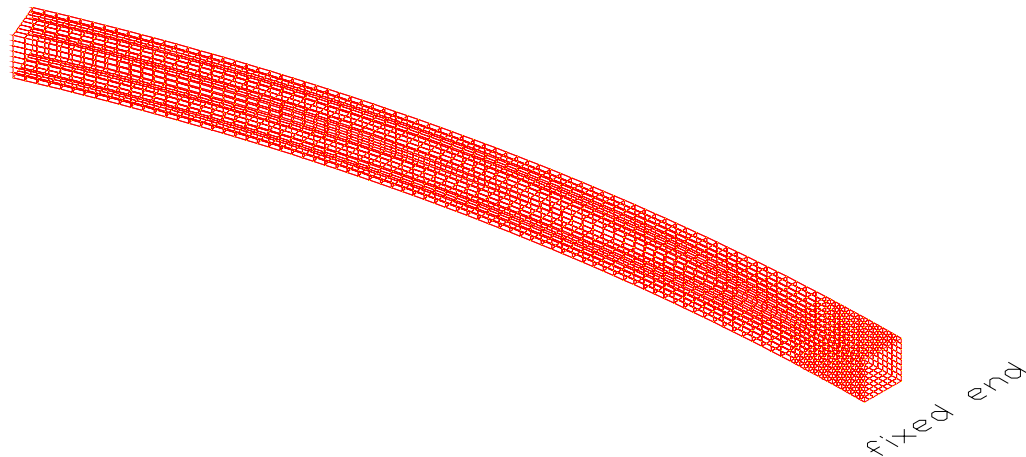


Figure 2.16: 3D-view of Model A in SAP 2000

The same example was modeled using SAP 2000. Full shell elements with six DOF per node were used to model the walls of the box as seen in Fig. 2.16. In addition to the fixity of the supported end of the cantilever, additional intermediate constraints were added to simulate diaphragms and cross frames to help the cross section maintain its preloading shape. The lack of these additional constraints would introduce distortion which is not the focus of this study. Other straining actions (bimoment, bending moment, ...etc.) are not affected by the additional constraints if the deformation is small. This measure was necessary since the element implemented in the program does not account for any distortional deformations. It is also known that current code provisions require the use of cross frames, which if provided appropriately, will drop any distortional effects to negligible levels. The positions of diaphragms are shown in Fig. 2.17. The spacing between adjacent diaphragms is 4.0 inches, but in the area close to the fixed end, where the normal stress caused by bimoment is more significant than the normal stress caused by bending moment, more diaphragms are added to resist distortion, the spacing of diaphragms is reduced to 0.5 inch. Between adjacent diaphragms which has spacing 4.0 inches, the wall is discretized transversely into 8 elements and longitudinally into 8 elements. So the element size is 0.25"x0.5". Where the spacing of diaphragms is 0.5 inch, the wall is discretized transversely into 8 elements and longitudinally into 2 elements, 4 elements, 8 elements respectively. The corresponding element sizes are 0.25"x0.25", 0.25"x0.125", 0.25"x0.0625", respectively. No more refined mesh is discussed here because of the tolerance in SAP2000 and also, when aspect ratio of shell element is larger than 4, the accuracy of results will be an issue. The 3 models are designated A, B, and C respectively. Table 2.2 lists the element size and element number for the three models.

Table 2.2: Summary of SAP2000 shell models

Model	Element Size	Total Element Number
A	0.25"x0.25"	2816
	0.25"x0.5"	
B	0.25"x0.125"	3328
	0.25"x0.5"	
C	0.25"x0.0625"	4352
	0.25"x0.5"	

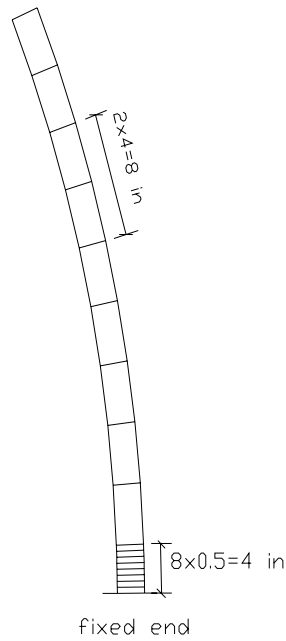


Figure 2.17: Layout of diaphragms

Figures 2.18 and 2.19 show that the developed program yields deformation results that are almost identical to those obtained from all 3 shell models.

For a square section subjected to both bending moment and bimoment, the maximum normal stress happens at the corner. The normal stress is calculated from the bimoment and bending moment extracted from the computer program as follows:

$$\sigma = \frac{M_x}{I_x} y + \frac{M_y}{I_y} x + \frac{M_\omega}{I_\omega} \omega \quad (2.49)$$

Results from the SAP2000 model are processed as follows. The top and bottom nodal stresses are averaged to obtain the membrane nodal stress. The final nodal stress considered in the verification study is the mean of the average nodal stresses obtained from each element attached to the node in question. Table 2.3 lists the mean normal stresses at different positions along the length of models A, B, C, and the results are plotted in Figs. 2.20 and 2.21. Figure 2.21 is an enlarged plot of the same distribution shown in Fig. 2.20 for the last 5 inches of the beam.

The results show that the normal stresses from the developed program and from SAP2000 models are in good agreement in most locations except for the region in the vicinity of the fixed end of the cantilever beam. In this small region (about 1/20 of the total length), stress gradient are very high, and Models A, B, and C are not sufficiently refined to pick up the severe stress changes that occur. The large stress gradient is largely due to the sudden spike in bimoment near the fixed end, where the bimoment reaches its maximum value.

In summary, the comparisons between SAP2000 and the program indicate that the program is quite accurate in predicting the behavior of curved box girders. The quality of the results is naturally dependent on how fine the used mesh is. However, it is obvious that the finite element is more sensitive to the element size than is the proposed model because of the spikes in the bimoment distribution that are harder to capture with a shell model. Based on this verification studies described, it is believed that the program is acceptable and deemed accurate for the purpose of investigating box girder bridges.

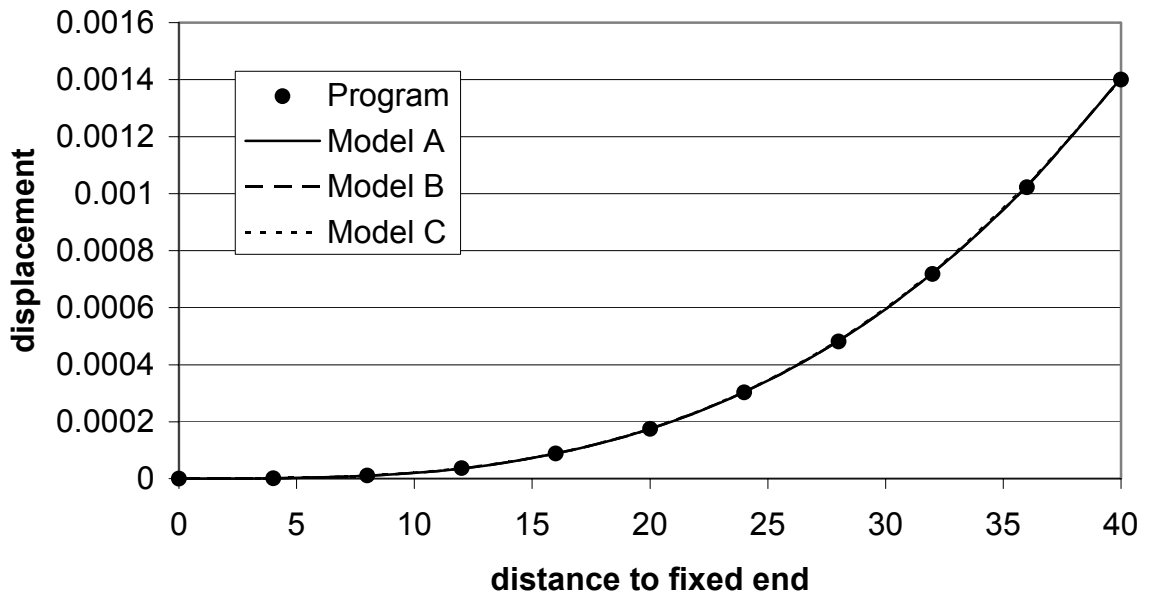


Figure 2.18: Comparison of vertical displacement

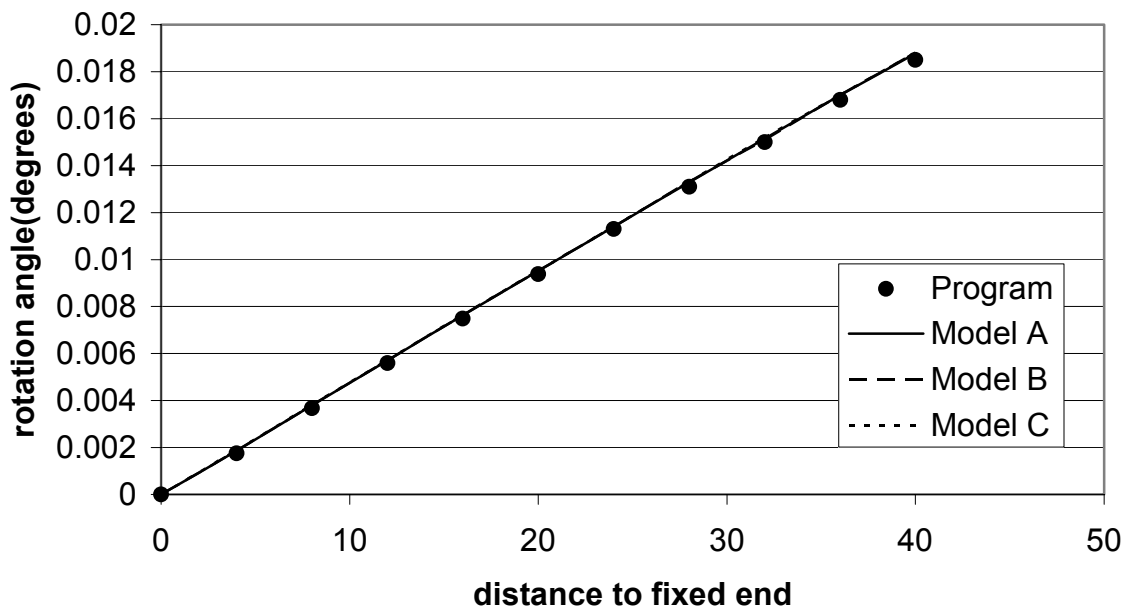


Figure 2.19: Comparison of twisting angle

Table 2.3: Maximum normal stress from program and Models A, B, and C

Distance to fixed end (inch)	Program	Model A	Model B	Model C
0.000	245.0	100.0	110.0	122.0
0.125	181.0	N/A	94.2	93.0
0.250	116.0	75.0	73.0	71.0
0.500	54.0	52.5	51.9	51.3
0.750	26.0	35.0	35.0	35.5
1.000	14.0	31.0	31.0	31.7
1.250	8.0	23.0	21.6	22.0
1.500	5.4	19.5	20.0	20.0
1.750	4.0	14.5	14.0	13.9
2.000	3.0	13.7	14.6	15.0
4.000	6.0	8.0	8.0	8.5
6.000	9.0	10.0	10.3	10.3
8.000	12.0	13.4	13.4	13.1
10.000	15.0	15.5	15.5	15.6
12.000	18.0	20.5	20.2	20.1
14.000	21.0	21.7	22.0	22.0
16.000	24.0	26.7	26.7	26.8
18.000	27.0	28.0	56.4	24.0
20.000	30.0	33.5	33.4	33.4
22.000	33.0	34.3	34.2	34.2
24.000	36.0	40.0	40.0	40.1
26.000	39.0	40.5	40.3	40.3
28.000	42.0	47.3	46.6	46.6
30.000	45.0	46.5	46.4	46.4
32.000	47.0	53.0	53.0	52.7
34.000	52.0	52.3	52.3	52.2
36.000	53.0	59.3	59.2	59.3
38.000	56.0	55.2	55.2	55.2

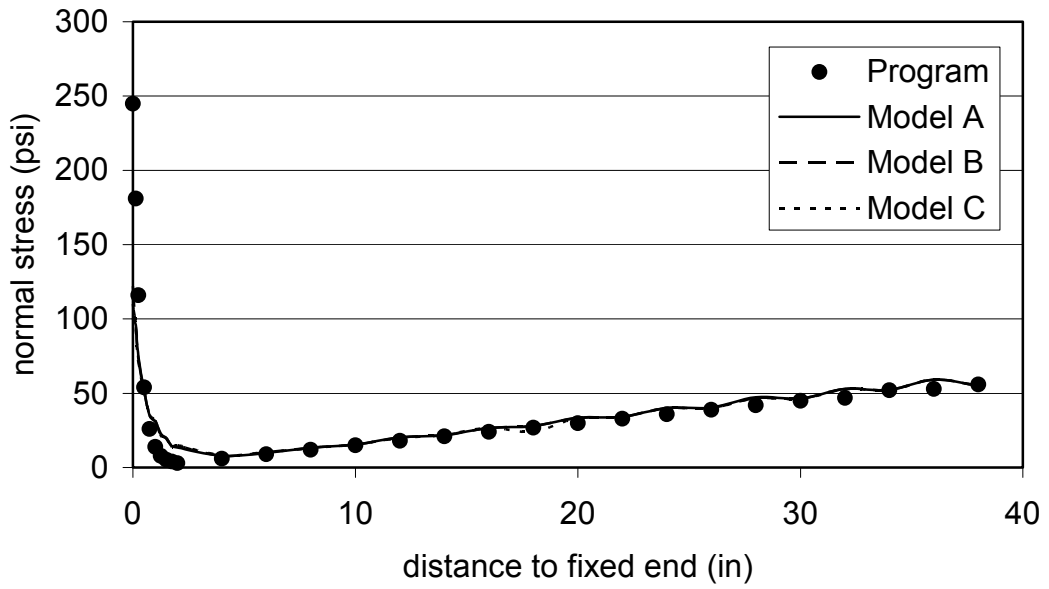


Figure 2.20: Maximum normal stress comparison along entire beam length

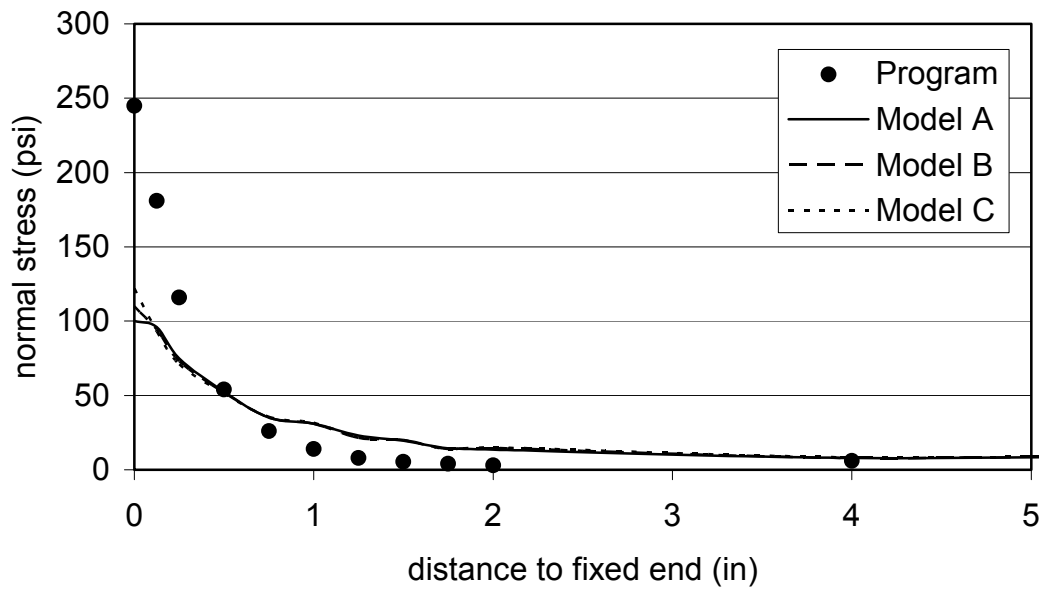


Figure 2.21: Maximum normal stress comparison in the vicinity of fixed end

3 WARPING STRESSES IN COMPOSITE CURVED BOX GIRDER BRIDGES

3.1 Background

This chapter presents a detailed investigation of warping related stresses in eighteen existing box girder bridges chosen from the Florida Department of Transportation inventory. The bridges are carefully selected to cover a wide range of design parameters including horizontal curvature, cross sectional properties, and number of spans. They were designed by different firms and were constructed at different times and are considered to be representative of current design practice. Forces are evaluated from analyses that account for the construction sequence and the effect of warping. Loading is considered following the 1998 AASHTO-LRFD provisions. The differences between stresses obtained taking into account warping and those calculated by ignoring warping are used to evaluate the effect of warping. Analysis results show that warping has little effect on both shear and normal stresses in all bridges. Current design provisions are discussed in light of the analysis results.

3.2 Non-uniform Torsion

A complicated state of forces develops in curved girders when they are loaded. The forces that are developed include bending moments, shear forces, pure (i.e. St. Venant) torsion, warping (i.e. nonuniform) torsional moments, and bimoments. Torsional moments and bimoments due to cross-section distortion also develop. However, distortion-related effects can be easily reduced to insignificant levels by providing an adequate number of cross frames (Oleinik and Heins 1975).

The out of plane deformation of cross sections subjected to torsion (see Fig. 3.8) violate the main assumption of the Bernoulli's Beam Theory: *plane sections remain plane*. If restrained, these out of plane deformations create additional normal and shear stresses, which when integrated over the cross-section yield the bimoment and warping torsional moment respectively. In general, the torsional moments acting on curved girders are larger than those encountered in straight girders.

Calculating warping related stresses is not a straightforward process. The current curved box bridge specification (AASHTO Curved 1997) insists that the effects of nonuniform torsion must be considered in design, but does not provide any assistance or guidance on how to do so. The only guidance given to determine when warping stresses could be important falls under a section in the commentary dealing with top bracing and appears to pertain to this

particular section only (i.e. during construction). This guidance is adapted from the work of Nakai and Heins (1977), who investigated a variety of curved bridge types and proposed criteria based on cross-section properties, bridge length, and subtended angle that would allow engineers to determine when warping is significant. The study by Nakai and Heins (1977) has several limitations including: 1) idealized loading and boundary conditions were assumed; 2) although, normal stresses due to warping were considered, shear stresses due to warping were ignored; and 3) the effects of centrifugal forces were not accounted for. Centrifugal forces always occur in curved bridges and can be substantial.

Other researchers have also tried to quantify the significance of warping in curved box girders. Trukstra and Fam (1978) investigated the effect of diaphragms on the behavior of curved box girder bridges. They conducted a parametric study using finite element models and investigated for simple load cases the ratio between stresses calculated from the finite element model and corresponding stresses obtained from idealized beam models. Both concrete and composite single box girders were considered. As expected, the results showed that diaphragms improve load distribution and positively influence stress ratios. A wide range of radii was covered in the study. Girders that showed large stress ratios belong to a group with small radii, which fall into an impractical range ($R < 30.48\text{m}$ [100 ft]). Shear stresses were also not investigated in this study.

More recently, Waldron (1988) investigated the effect of warping on normal stresses in single box girders. Forces were calculated by deriving closed form solutions of the fundamental equation governing torsion and warping for special loading cases. Using concrete box examples, it was shown that warping could increase normal stresses by as much as 29%. This high stress ratio corresponds to a theoretical loading condition where a single concentrated load acts on one of the webs at midspan. For truck loads (following the British code), stress ratios drop to around 5%. Based on the study, it was concluded that the width-to-depth ratio significantly impacts the normal warping stress ratio.

The studies summarized above all suffer from a number of common drawbacks. They did not address warping shear stresses and were based on idealized loading and boundary conditions. They also did not address the construction sequence of composite box girders. This study addresses all of these issues and presents a detailed investigation of warping stresses in curved composite box girders. The study is conducted on 18 bridges from the Florida Department of Transportation (FDOT) inventory. The bridges are carefully selected to cover a wide range of design parameters including horizontal curvature, cross sectional properties, and number of spans. The bridges were designed by different firms and were constructed at different times and are considered to be representative of current design practice. A summary of the main properties of the bridges is given in Table 3.1 and further information can be found in Okeil et al. (2000) and Okeil and El-Tawil (2002). The 1998 AASHTO-LRFD load provisions are considered in the study and the effect of warping on both normal and shear stresses is quantified. The implications of the analysis results with respect to current design provisions are then discussed.

Table 3.1: Summary data for analyzed existing bridges

Bridge	Spans	Lanes	Span lengths		Radius of curvature		Finite element length (mm)	Number of finite elements	Number of load cases
			Min (m)	Max (m)	Min (m)	Max (m)			
390	5	1	54.86	71.17	188.98	188.98	152.4	1923	74
521	3	1	23.16	36.58	1758.90	1758.90	101.6	816	35
525	2	1	41.54	49.59	Straight	Straight	101.6	897	37
528	5	1	48.16	58.52	1746.38	1746.38	152.4	1658	68
537	5	1	30.48	64.92	218.30	218.30	152.4	1390	58
538a	5	2	37.19	52.43	436.60	3033.17	152.4	1585	65
538b	5	2	46.33	64.31	436.60	873.19	152.4	1762	69
538c	4	2	50.90	64.01	873.19	873.19	152.4	1508	61
538d	7	2	36.88	64.01	436.60	873.19	152.4	2486	100
539	5	1	39.62	55.93	218.60	218.60	152.4	1539	63
540	6	1	23.77	54.25	290.76	290.76	152.4	1661	69
541a	5	1	38.25	63.09	250.40	431.51	152.4	1686	69
541b	5	1	32.16	61.26	250.40	645.52	152.4	1604	60
542a	6	1	43.89	62.18	349.58	349.03	152.4	2096	84
542b	6	1	34.75	59.13	349.58	8732.18	152.4	1834	74
598	4	1	44.35	52.27	107.56	211.68	152.4	1895	51
606	3	2	56.08	80.37	438.88	875.00	101.6	1310	69
607	3	2	46.94	66.85	870.91	Straight	101.6	1582	60

3.3 Analysis of Existing Bridges

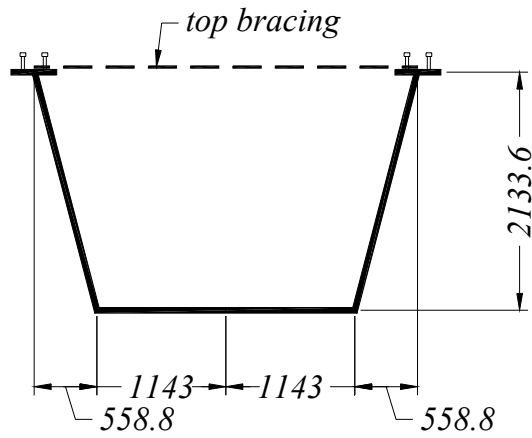
3.3.1 Geometric properties of closed cross sections

Accurate cross-sectional properties are essential for conducting a successful analysis. Expressions for these properties can be found in textbooks (e.g. Guohao 1987 and Nakai and Yoo 1988). A summary of relevant expressions can be found in Appendix I. Two conditions are considered for each box girder. The first condition represents the cross section during construction; i.e. before the concrete deck hardens. At this stage, diagonal bracing between the top steel flanges is provided to ensure stability. The cross-section cannot be considered as an open cross-section because of the top bracing. Since the section is not a closed section either, it is considered as quasi-closed, i.e. with a fictitious top plate to represent the effect of the top bracing. Several expressions for the thickness of the equivalent plate have been proposed in the past, of which the one proposed by Kohlbrunner and Basler (1969) is used in this study:

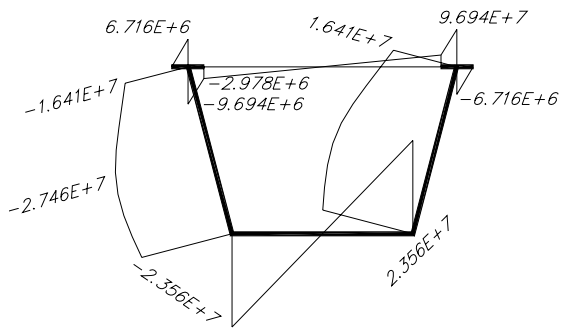
$$t_{eq} = \frac{E}{G} \frac{ab}{\frac{d^3}{F_d} + \frac{2a^3}{3F_o}} \quad (3.1)$$

where E is the modulus of elasticity, G is the shear modulus, a the spacing between cross frames, b is the distance between flanges, d is the length of bracing member, F_o is the area of top flange, and F_d is the area of bracing member.

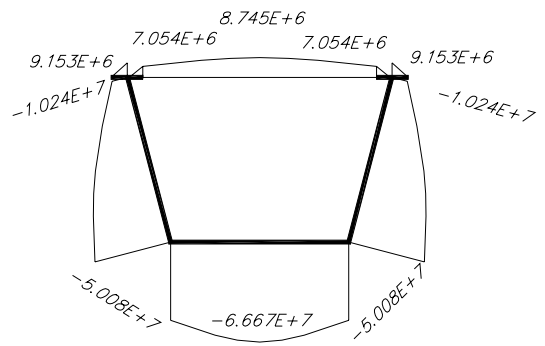
After hardening, the concrete deck becomes an integral part of the cross section and its contribution is accounted for. The equivalent plate's contribution becomes small compared to the deck, and is ignored. In accounting for the concrete deck, it is first transformed into an equivalent steel plate using an appropriate modular ratio; E_c/E_s . This transformation is justified when the deck is completely in compression, but is approximate when the deck or parts of it are under tension. Since 1) it is not clear when the deck will be completely in tension because of the combined effect of moment and torsion, and 2) the contribution of the top bracing is being ignored, the use of the uncracked properties is deemed reasonable in this work. Other researchers have also made use of this approximation in the past including Johnson and Mattock (1967), whose work forms the basis of several provisions in AASHTO LRFD (1998). Figures 3.1 and 3.2 show a few of the geometric functions for one of the bridges considered before and after integration of the deck in the cross section.



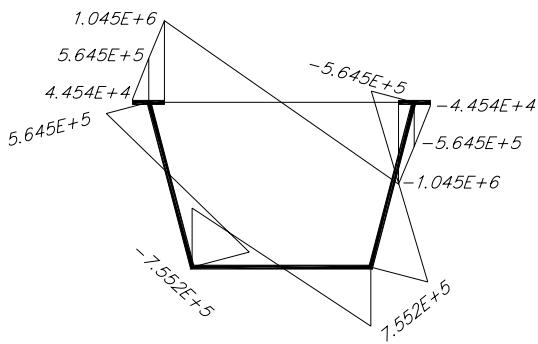
(a) quasi-closed cross section



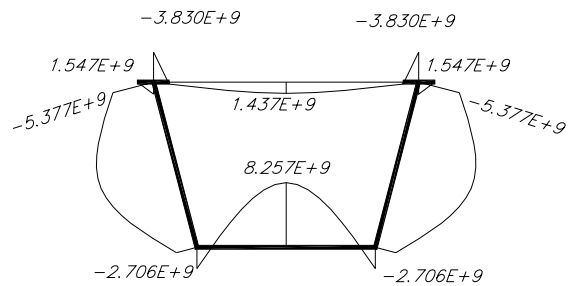
(b) S_x



(c) S_y

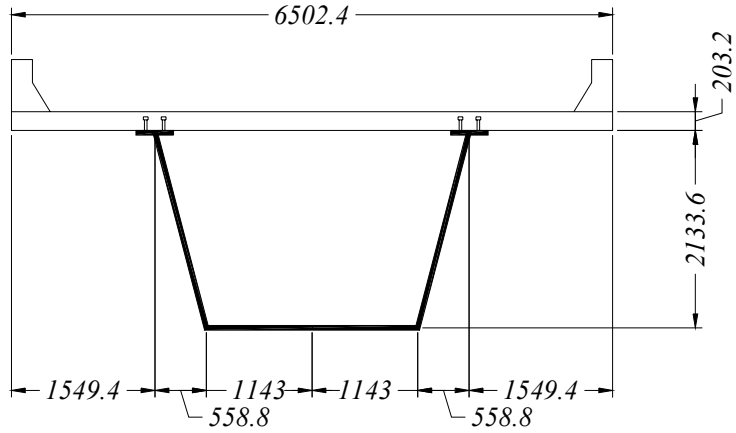


(d) ω

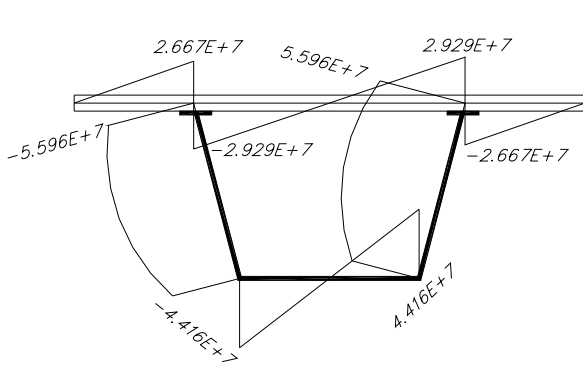


(e) S_ω

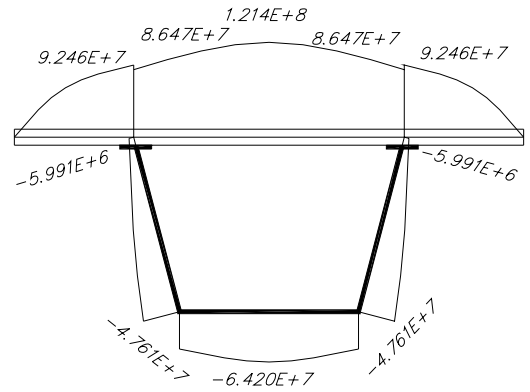
Figure 3.1: Geometric properties of quasi-closed cross section (Dimensions in mm, ω in mm^2 , S_x S_y in mm^3 , S_ω in mm^4)



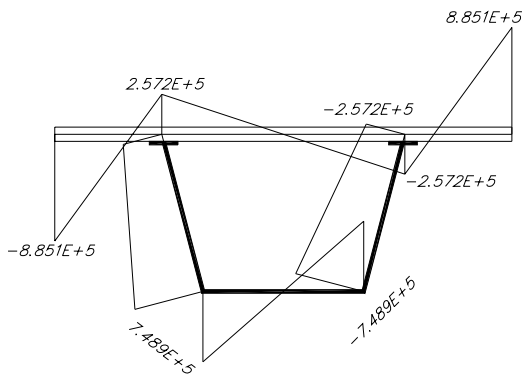
(a) closed cross section



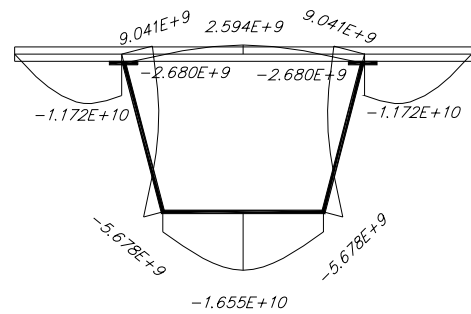
(b) S_x



(c) S_y



(d) ω



(e) S_ω

Figure 3.2: Geometric properties of closed cross section (Dimensions in mm, ω in mm^2 , S_x S_y in mm^3 , S_ω in mm^4)

For simple geometries (regular spans, curvatures, ...etc.) and loadings (uniform torque, single concentrated torque), girder forces are a function of a dimensionless parameter, κ , which is given as (Nakai and Yoo 1988)

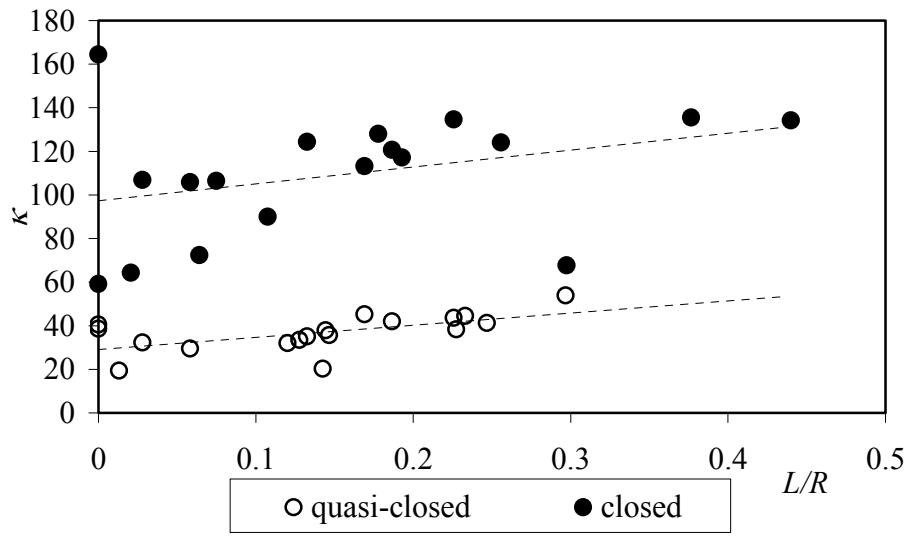
$$\kappa = L \sqrt{\frac{GK}{EI_{\omega}}} \quad (3.2)$$

where L is the span length, G is the shear modulus, K is the torsional constant, E is the modulus of elasticity, and I_{ω} is the warping constant. A large κ implies that the contribution of warping to stiffness is small and that warping related stresses are therefore low. On the other hand, a small κ implies that the warping contribution to stiffness is large and that warping related stresses could be high.

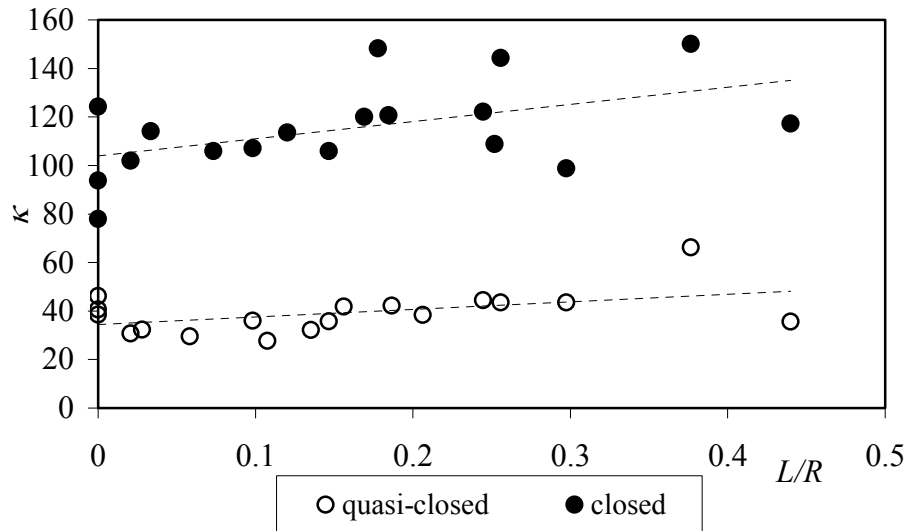
The reliance of member forces on κ is true only for certain idealized loading, geometric, and boundary conditions. In real bridges, the cross-section and radius of horizontal curvature both vary along each span as well as from span to span, which renders the use of Eq. 3.2 impossible. To account for these variations, a weighted κ (calculated for each span) is used as follows. The relationship between this weighted κ parameter and warping stresses is discussed later on.

$$\kappa = \int_L \sqrt{\frac{GK}{EI_{\omega}}} dL \quad (3.3)$$

Two κ values are computed for each span of each bridge corresponding to quasi-closed and closed conditions. Figures 3.3 show a plot of these κ values versus the average L/R ratio for corresponding spans. The κ values are calculated for spans where the critical normal stresses (Fig. 3.3a) and shear stresses (Fig. 3.3b) take place as described later. As expected, Fig. 3.3 clearly shows that closed cross-sections possess better torsional qualities than open cross-sections, i.e. higher κ values. Although there is some scatter, it is clear that current design practices yield κ values with an average of about 38 for quasi-closed cross sections and 114 for closed cross sections. A slight increase in the trend of κ is also observed with higher L/R , which reflects the more efficient designs for spans with a sharper radius of curvature.



(a)



(b)

Figure 3.3: Geometric properties of closed cross section (Dimensions in mm, ω in mm^2 , S_x , S_y in mm^3 , S_ω in mm^4)

3.3.2 Bridge models

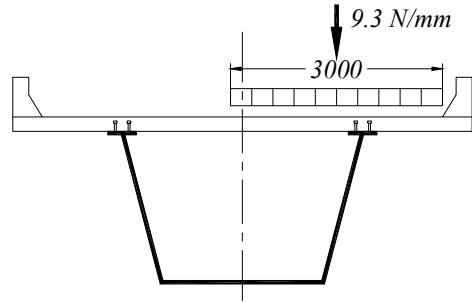
Detailed descriptions of the 18 bridges considered in this study can be found in Okeil et al. (2000). For completeness, a summary of the modeling details is provided next.

The analyses are conducted using the computer program ABAQUS (1997). All 18 girders considered in this study are modeled using a three-dimensional beam-column element (BO31S) that accounts for warping. The element has 7 degrees of freedom per node, and is similar to the element described in Chapter 2. Although several of the bridges have more than one box, only one box girder is modeled per bridge to reduce the modeling and computational effort. Each box girder is assumed to support a slab that is wide enough to accommodate at least one traffic lane. This implies a load distribution factor of at least 1.0 lane per girder, which is conservative when compared to distribution factors from AASHTO-LRFD specifications (1998) for straight girders.

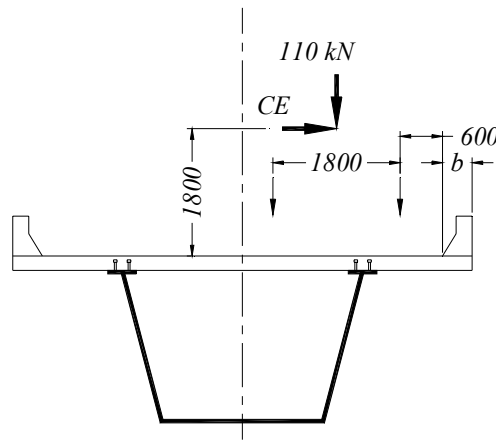
Small elements (101.6mm [4in] or 152.4mm [6in]) are used to model the bridges resulting in hundreds of elements per girder. This is necessary in order to accurately calculate the warping related forces. For example, the bimoment experiences large spikes at supports, which are difficult to capture unless small elements are used. Verification studies confirmed that the chosen element sizes are sufficient to provide reasonable accuracy. Intermediate support locations are restrained against vertical and transverse translations, and twisting rotations. The warping degree of freedom is not restrained anywhere because diaphragms are not capable of providing significant resistance to out of plane deformations. However, continuity over intermediate supports leads to the development of bimoments and torsional warping moments, which is not the case at end supports where the developed bimoment is zero. Table 3.1 lists the number elements used for each bridge, which ranged from 816 to 2486. The table also lists other details for the bridges covered in this study.

3.3.3 Bridge loading and resulting forces

Dead loads are estimated based on the dimensions and material properties given in blueprints provided by FDOT. Live loads are considered according to AASHTO-LRFD (1998). Following the HL-93 loading, a uniform lane load of 9.3 N/mm, uniformly distributed load over a 3000 mm width, is considered in addition to a tandem load (two 110kN axles). Transversely, the loads are positioned at the outermost possible location to generate the maximum torsional effects (see Fig. 3.4). The centrifugal force (CF) is taken into account for curved segments of the bridges. From these loads, the dead load force distributions and envelopes for the live load force distributions are generated. Each set included, M_x , M_y , M_ω , V_x , V_y , T , T_s , and T_ω , which are described in the next section. Figure 3.5 shows an example of the live load factored (*Strength I* limit state) envelopes for warping related forces obtained from the analysis of an idealized 3-span pilot bridge.



Lane Load



Tandem Load (one axle shown)

Figure 3.4: Positioning of live loads for a single lane bridge (dimension in mm)

Since ABAQUS does not provide results for the warping torsional moment, T_ω , the fact that it is the derivative of the bimoment (i.e. $T_\omega = M'_\omega$) is used to obtain these results. A numerical differentiation scheme (Greenspan and Casulli 1988) of the bimoment, M_ω , is utilized. To enhance the quality of the numerical results, three points are used to numerically differentiate M_ω at any point; the point under consideration and the points before and after. For example, determining the warping torsional moment at node i involves the values of the warping moment at the nodes $i - 1$ and $i + 1$ as well as the elements' length, L_{elem}

$$(T_\omega)_i = \frac{-(M_\omega)_{i-1} + (M_\omega)_{i+1}}{2L_{\text{elem}}} \quad (3.4)$$

At points where abrupt changes take place such as supports, a forward (point under consideration and two following points), or a backward (point under consideration and two previous points), differentiation scheme are used so that the spikes can be accurately captured. Equations 3.5 and 3.6 Give the expressions for the forward and backward numerical differentiation, respectively.

$$(T_{\omega})_i = \frac{-3(M_{\omega})_i + 4(M_{\omega})_{i+1} + (M_{\omega})_{i+2}}{2L_{\text{elem}}} \quad (3.5)$$

$$(T_{\omega})_i = \frac{(M_{\omega})_{i-2} - 4(M_{\omega})_{i-1} + 3(M_{\omega})_i}{2L_{\text{elem}}} \quad (3.6)$$

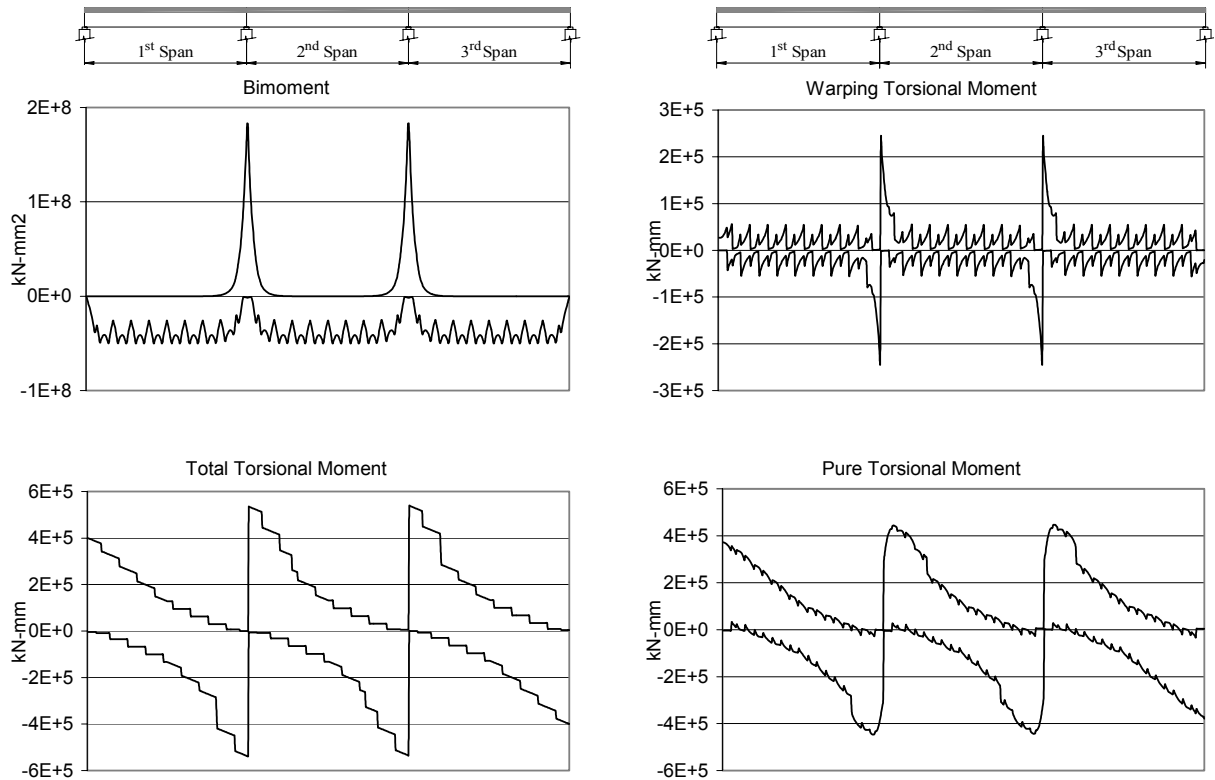


Figure 3.5: Envelope of warping-related straining actions due to live loads for idealized bridge

3.3.4 Stress Calculations

Normal stresses – including the effect of warping - are calculated as follows (Nakai and Yoo 1988):

$$\sigma_{\text{exact}} = \frac{M_x}{I_x} y + \frac{M_y}{I_y} x + \frac{M_\omega}{I_\omega} \omega = \sigma_{\text{approx}} + \frac{M_\omega}{I_\omega} \omega \quad (3.7)$$

where I_x and I_y are the moments of inertia about the x - and y -axes, and x and y are the distances from the centroid of the cross section. Equation 3.7 shows that the *exact* normal stress, σ_{exact} , is generated by the bending moments (M_x , M_y) and bimoment (M_ω) which causes warping. The sum of the first two terms is from classical beam theory, which does not account for warping, and will be referred to as σ_{approx} . The third term is a function of the warping constant, I_ω , and the warping function, ω .

The approximate shear stress, τ_{approx} , is calculated from classical beam theory (i.e. by ignoring the effects of warping) using the following equation:

$$\tau_{\text{approx}} = \frac{V_y}{tI_x} S_x(s) + \frac{V_x}{tI_y} S_y(s) + \frac{T}{2tA_c} \quad (3.8)$$

where V_x and V_y are the shear forces and T is the torsional moment acting on the cross section. The other terms in the expression represent the geometric properties of the closed cross section; namely, wall thickness (t), moments of area ($S_x(s)$ and $S_y(s)$), and enclosed cross-sectional area (A_c). The third term assumes that the entire torsional moment is St. Venant torsion. If warping is considered, the torsional moment must be split into its two constituent terms (pure torsion, T_s , and warping torsion, T_ω), and the shear stresses can be calculated as follows:

$$\tau_{\text{exact}} = \frac{V_y}{tI_x} S_x(s) + \frac{V_x}{tI_y} S_y(s) + \frac{T_s}{2tA_c} + \frac{T_\omega}{tI_\omega} S_\omega(s) \quad (3.9)$$

The geometric properties I_ω (warping constant) and $S_\omega(s)$ (sectoral area) are used to calculate the shear stress due to warping torsional moments (last term in Eq. 3.6).

3.4 Warping Stress Ratio

One of the main goals of this research is to determine the effect of warping on both shear and normal stresses. This is achieved by investigating the ratio between *approximate* stresses calculated using classical beam theory (i.e. ignoring warping) and *exact* stresses which include the effect of warping. For each bridge, ratios pertaining to both normal and shear stresses are calculated at selected key points in critical sections with the highest *exact* stresses (calculated according to Eqs. 3.7 and 3.9). The key points considered in each cross-section are shown in Fig. 3.6. The warping stress ratios for both normal stresses ($WSR - N$) and shear stresses ($WSR - S$) are then calculated as follows. The results are given in Table 3.2.

$$WSR - N = \frac{\sigma_{\text{exact}} - \sigma_{\text{approx}}}{\sigma_{\text{approx}}} \quad (3.10)$$

$$WSR - S = \frac{\tau_{\text{exact}} - \tau_{\text{approx}}}{\tau_{\text{approx}}} \quad (3.11)$$

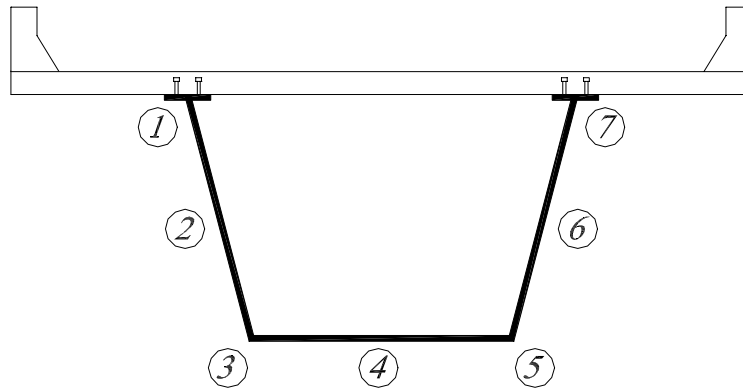


Figure 3.6: Keypoints considered for stress calculations

Table 3.2: Definitions of Warping Stress Ratio (WSR)

Exact Stress Calculations	Approximate Stress Calculations	Stress Ratios
$\sigma_{DL, \text{exact}} = \frac{M_{xDL}}{I_{xO}} y + \frac{M_{yDL}}{I_{yO}} x + \frac{M_{\omega DL}}{I_{\omega O}} \omega$	$\sigma_{DL, \text{approx}} = \frac{M_{xDL}}{I_{xO}} y + \frac{M_{yDL}}{I_{yO}} x$	$WSR_{DL}^{\sigma} = \frac{\frac{M_{\omega DL}}{I_{\omega O}} \omega}{\sigma_{DL, \text{approx}}}$
$\sigma_{LL, \text{exact}} = \frac{M_{xLL}}{I_{xC}} y + \frac{M_{yLL}}{I_{yC}} x + \frac{M_{\omega LL}}{I_{\omega C}} \omega$	$\sigma_{LL, \text{approx}} = \frac{M_{xLL}}{I_{xC}} y + \frac{M_{yLL}}{I_{yC}} x$	$WSR_{LL}^{\sigma} = \frac{\frac{M_{\omega LL}}{I_{\omega C}} \omega}{\sigma_{LL, \text{approx}}}$
$\sigma_{T, \text{exact}} = \sigma_{DL, \text{exact}} + \sigma_{LL, \text{exact}}$	$\sigma_{T, \text{approx}} = \sigma_{DL, \text{approx}} + \sigma_{LL, \text{approx}}$	$WSR_T^{\sigma} = \frac{\frac{M_{\omega DL}}{I_{\omega O}} \omega + \frac{M_{\omega LL}}{I_{\omega C}} \omega}{\sigma_{T, \text{approx}}}$
$\tau_{DL, \text{exact}} = \frac{V_{yDL}}{tI_{xO}} S_{xO}(s) + \frac{V_{xDL}}{tI_{yO}} S_{yO}(s) + \frac{T_{sDL}}{2tA_{cO}} + \frac{T_{\omega DL}}{tI_{\omega O}} S_{\omega O}(s)$	$\tau_{DL, \text{approx}} = \frac{V_{yDL}}{tI_{xO}} S_{xO}(s) + \frac{V_{xDL}}{tI_{yO}} S_{yO}(s) + \frac{T_{DL}}{2tA_{cO}}$	$WSR_{DL}^{\tau} = \frac{\tau_{DL, \text{approx}} - \tau_{DL, \text{exact}}}{\tau_{DL, \text{approx}}}$
$\tau_{LL, \text{exact}} = \frac{V_{yLL}}{tI_{xC}} S_{xC}(s) + \frac{V_{xLL}}{tI_{yC}} S_{yC}(s) + \frac{T_{sLL}}{2tA_{cC}} + \frac{T_{\omega LL}}{tI_{\omega C}} S_{\omega C}(s)$	$\tau_{LL, \text{approx}} = \frac{V_{yLL}}{tI_{xC}} S_{xC}(s) + \frac{V_{xLL}}{tI_{yC}} S_{yC}(s) + \frac{T_{LL}}{2tA_{cC}}$	$WSR_{LL}^{\tau} = \frac{\tau_{LL, \text{approx}} - \tau_{LL, \text{exact}}}{\tau_{LL, \text{approx}}}$
$\tau_{T, \text{exact}} = \tau_{DL, \text{exact}} + \tau_{LL, \text{exact}}$	$\tau_{T, \text{approx}} = \tau_{DL, \text{approx}} + \tau_{LL, \text{approx}}$	$WSR_T^{\tau} = \frac{\tau_{T, \text{approx}} - \tau_{T, \text{exact}}}{\tau_{T, \text{approx}}}$

3.5 Results

The WSR for all cases summarized in Table 3.2 are calculated using the procedures described earlier. Two sets of plots are generated in an attempt to identify trends in the results. Figures 3.7 and 3.8 show the WSR for normal and shear stresses plotted versus the average L/R ratios for corresponding spans. The WSR are also plotted versus κ , as shown in Figs. 3.9 and 3.10. Each of the four figures provides three plots corresponding to the ratios due to dead, live and total (combined dead and live) loads. The dashed line in each plot represents the average level. In spite of significant scatter in some of the plots, several observations are evident from Figures 3.7 through 3.10. These observations are discussed next.

3.5.1 Normal stresses

During construction (i.e. quasi-closed cross-section under dead load), ignoring warping implies that normal stresses are underestimated by an average of 0.84%. The most critical case is underestimated by 1.90%. In designing for live loads (closed section), the average effect of warping is an additional 0.25% with the most severe case being 1.88%. The average WSR for total stress effect (closed section subjected to dead and live loads) is 0.34% with a maximum of 3.16%. In evaluating these numbers, readers should keep in mind that the locations at which the maximum WSR for dead, live, and combined loading are different. Although the plots in Figs. 10 and 12 do not show any conclusive trends because of scatter in the data, it is clear that the magnitude of the WSR are quite small (less than 3.16% for all cases).

3.5.2 Shear stresses

Although the WSR 's pertaining to shear are somewhat higher than those corresponding to normal stresses, the ratios are still relatively low. The calculations show that the average dead load shear stresses are underestimated by 1.57% with a maximum of 7.42%. After casting the concrete deck, the cross section's properties are greatly enhanced, and ignoring warping is actually on the conservative side with a tendency to overestimate stresses by an average of 1.52%. For combined loading (Fig. 3.10 (c)), total stresses are underestimated if warping is not taken into account by an average of 1.37%.

3.5.3 Effect of κ

As previously discussed, Fig. 3.3 indicates that κ improves slightly as L/R increases, reflecting the greater torsional resistance provided by designers for spans with a sharper radius of curvature. Figures 3.9 and 3.10 show the relationship between κ and $WSR - N$ as well as $WSR - S$ respectively. Since κ is a measure of the contribution of warping to stiffness, it is logical to see some correlation in Figs. 3.9 and 3.10. However, the data in both

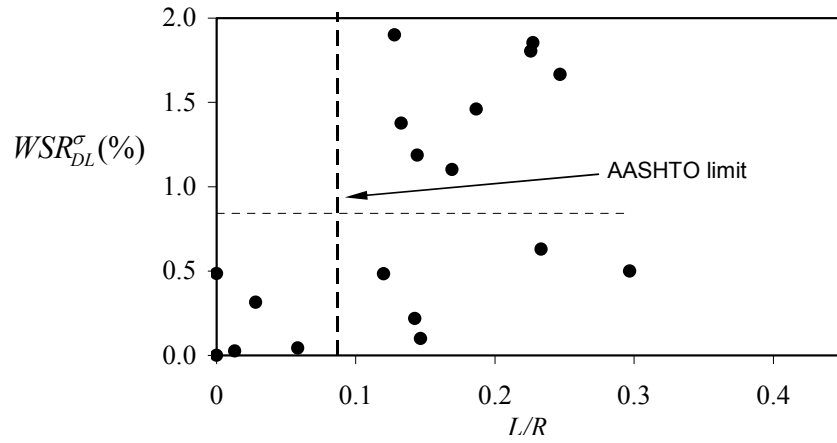
figures is scattered and does not appear to have a specific trend. There are several reasons that can be put forward to explain this: 1) although spans with a larger κ are torsionally stronger, they are probably subjected to larger demands; 2) the bridges were designed by different firms and hence the level of conservatism in design as well as the design models and tools vary from one bridge to another; 3) κ calculated according to Eq. 3.3 is a weighted value that may not accurately reflect the vulnerability of a critical cross-section to warping as well as κ calculated from Eq. 3.2 would for idealized conditions.

3.6 Design Implications

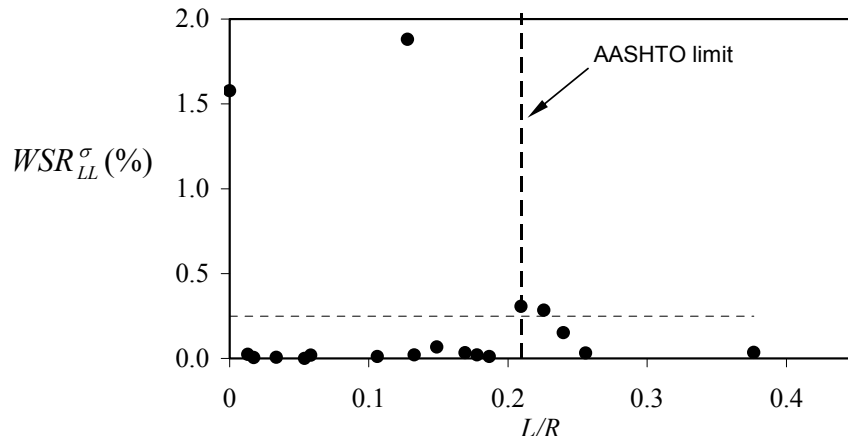
Although no trends are evident in Figs. 3.7 and 3.8, one important observation can be made; i.e. the effect of warping on both normal and shear stresses in all 18 bridges is quite small. Since each point plotted in the figures represents the largest ratio at the most critical point of the most critical span of each bridge, it appears that the effect of warping on overall behavior is rather insignificant.

The vertical lines in Figures 3.7 and 3.8 indicate the critical L/R ratio as defined by AASHTO-LRFD (1998) below which bridges may be analyzed and designed as straight. Bridge designers prefer to deal with straight bridges because they are easier to analyze and design. Straight bridges must still be designed to resist some torsional forces, which result from eccentrically placed loading. However, torsional demands – and corresponding warping effects – in straight box girder bridges are quite small and are negligible in many cases. There are two limits permitted by AASHTO-LRFD (1998). For open cross-sections (defined as quasi-closed in this research because of the top bracing), three span bridges with a subtended angle less than 5° ($L/R=0.087$) can be treated as straight. For closed cross-sections the critical L/R is 0.21.

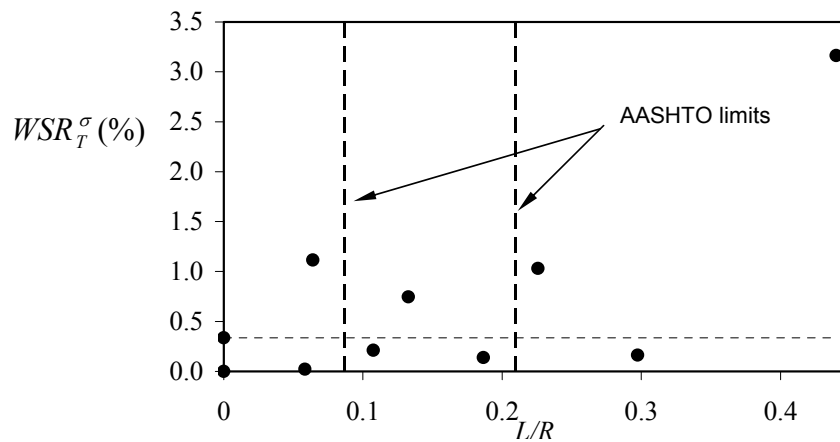
It is clear that a significant portion of the bridges fall outside these limits. For these bridges, AASHTO Curved (1997) becomes the applicable design code. This implies that the effect of horizontal curvature and the resulting torsional demands could be significant and should be taken into consideration. Although AASHTO Curved (1997) clearly states that non-uniform torsion should be explicitly considered, this study shows that the effect of warping is still small in all these bridges. This is true even in bridges where L/R is greater than twice the limit permitted by AASHTO-LRFD for closed cross-sections, and more than 4 times for quasi-closed sections.



(a) due to dead loads

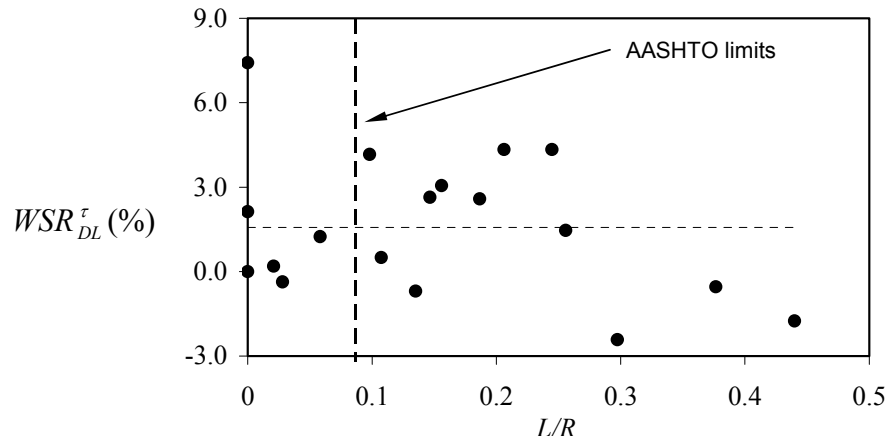


(b) due to live loads

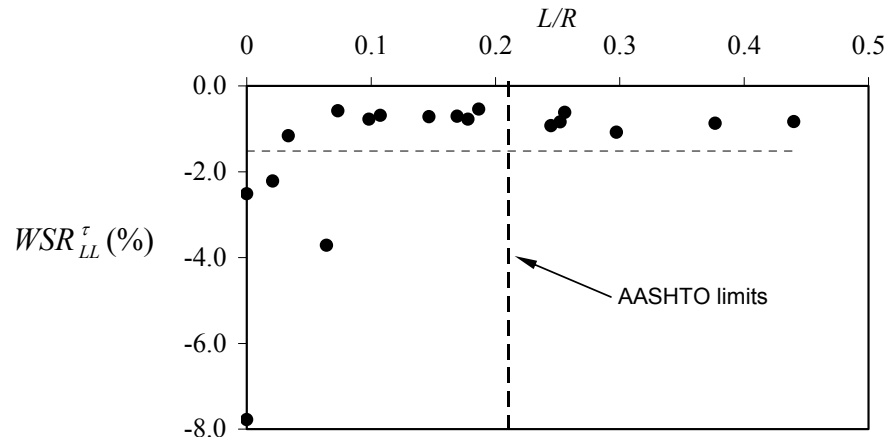


(c) due to total loads

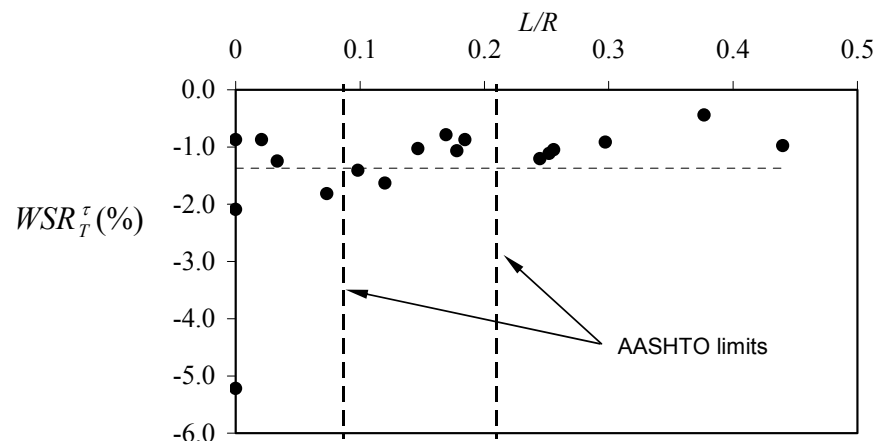
Figure 3.7: Normal Warping Stress Ratios vs. L/R



(a) due to dead loads

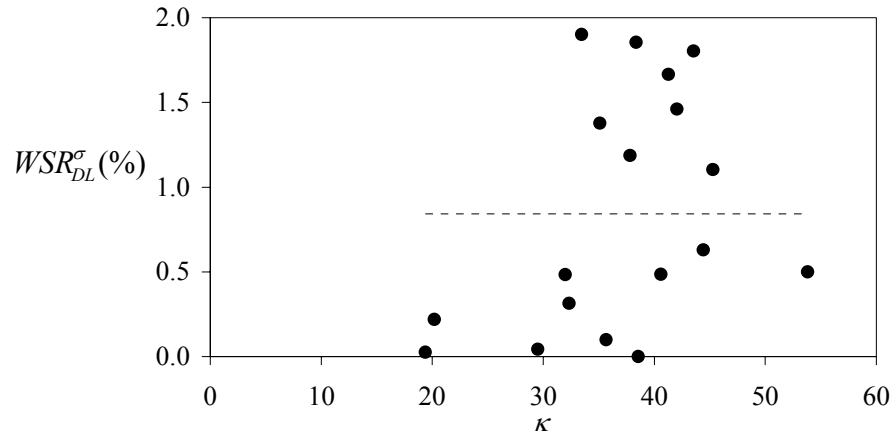


(b) due to live loads

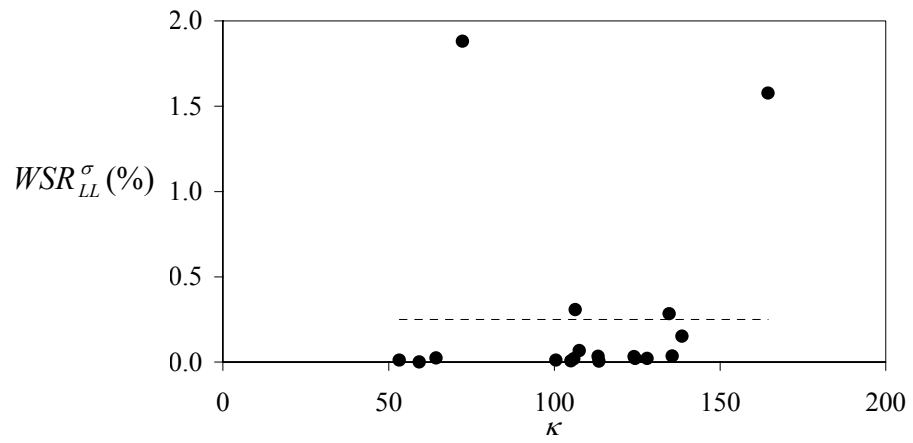


(c) due to total loads

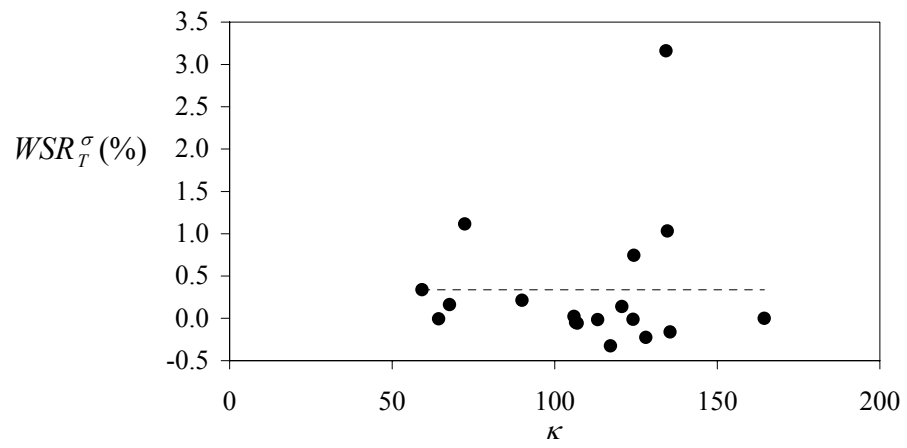
Figure 3.8: Shear Warping Stress Ratios vs. L/R



(a) due to dead loads

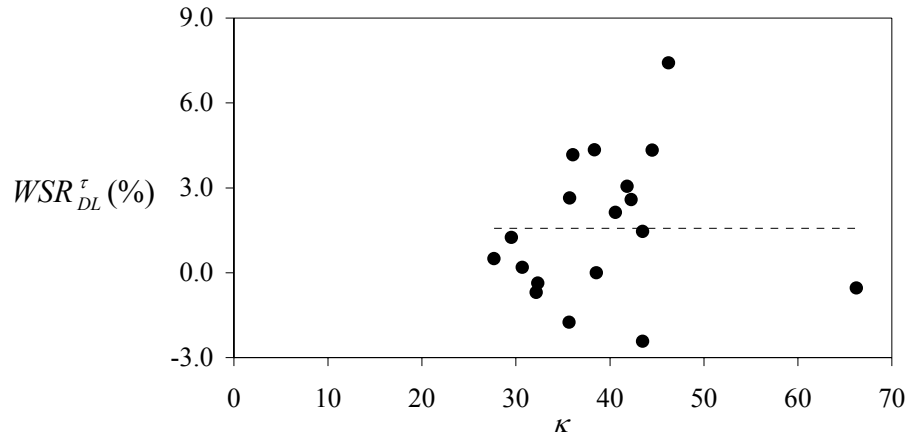


(b) due to live loads

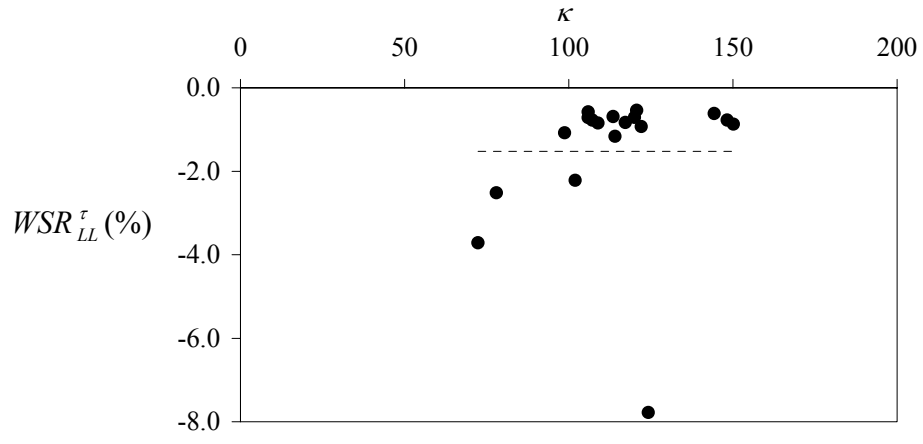


(c) due to total loads

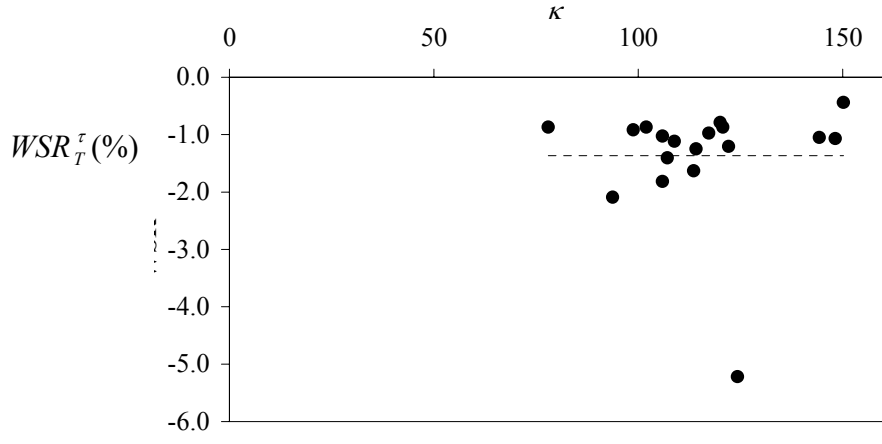
Figure 3.9: Normal Warping Stress Ratios vs. κ



(a) due to dead loads



(b) due to live loads



(c) due to total loads

Figure 3.10: Shear Warping Stress Ratios vs. κ

3.7 Summary and Conclusions

This chapter presents a detailed investigation on the effects of warping on the stress levels in eighteen existing box girder bridges chosen from the Florida Department of Transportation inventory. The bridges cover a wide range of design parameters including horizontal curvature, cross sectional properties, and number of spans. Forces are evaluated from analyses that account for the construction sequence and the effect of warping. Loading is considered following the 1998 AASHTO-LRFD provisions. By considering the differences between stresses obtained taking into account warping and those calculated by ignoring warping, it is shown that warping has little effect on both shear and normal stresses in the limited sample of bridges considered.

The results presented herein should not be construed to imply that warping is not important. Rather, this work points out that there could be a large subset of bridges where the warping effect is small enough to be ignored in structural calculations. This is particularly useful to designers because warping calculations are complicated and time consuming. Additional work is needed to define relevant parameters that can be used to identify bridges where warping calculations are warranted. The authors also believe that there is a need for a validated approximate design method that accounts for the effect of warping, without which it is hard to envision designers performing detailed analyses such as those presented here.

4 LIVE LOAD DISTRIBUTION FACTORS FOR COMPOSITE CURVED BOX GIRDERS

4.1 Introduction

This chapter describes an investigation of the live load distribution factor (DF). The live load distribution factor is an integral part of current AASHTO design codes. AASHTO LRFD (1998) provides distribution factors for several structural systems including composite box girder bridges. The suggested DFs are limited to straight bridges and bridges with slight curvatures and are based on the work of Ho (1972). The AASHTO Curved (1997) does not provide specifications regarding DF's for composite curved box girder bridges. However, the commentary of AASHTO Curved (1997) provides alternate expressions for DF's that can be used for composite curved box girder bridges. The provided expressions are based on the work of Ho and Reilly (1971) and Heins (1972). The expressions in the commentary consider three variables only in determining the DF's; namely number of girders, G , girder spacing, S , and the number of lanes, N . Equations 4.1 and 4.2 show these expressions for bending and torsional moments.

$$g_M = \frac{S}{-2.6 + 0.6 \frac{GS}{N}} \quad (4.1)$$

$$g_T = \frac{S}{-15.3 + 1.5 \frac{GS}{N}} \quad (4.2)$$

Since the previous expressions are derived based on analyses of straight girder, curvature still needs to be accounted for. This is done through modifiers following Eq. 4.3 and 4.4 for bending and torsional moments, respectively:

$$\xi_M = 1.0 + \frac{A}{R} + \frac{B}{R^2} \quad (4.3)$$

$$\xi_T = C + \frac{D}{R^2} \quad (4.4)$$

This simplification of a very complex behavior leads to ignoring other parameters such as the ratio between the lateral and longitudinal stiffness of the system. Furthermore, the torsional stiffness of each box is not accounted for. It should also be noted that the studies based on which the current DF's were derived, were conducted decades ago with the available tools at the time. Current advancements allow more in-depth studies with more sophisticated models than were available before. Such shortcomings led to a call by the National Cooperative Highway Research Program (NCHRP) to revisit the current expressions for live-load DF's for all types of bridges. This part of the study serves as a good preliminary investigation to the research program announced by NCHRP.

4.2 Concept of Distribution Factor

The concept of live load distribution is appealing to practicing engineers. Regardless of advancements in available design tools, DF's remain popular because of they are easily comprehended, easy to use, and have gained acceptance over the years. In this method, a simplified single-girder system is analyzed for a single lane of loading regardless of the transverse dimensions and properties of the bridge. The forces developed in this simplified system are determined using basic structural analysis methods. Forces in specific girders of the real system are obtained by multiplying the results of the simplified system by the distribution factor. For example, the shear force in a certain girder, V^{girder} , is obtained according to Eq. 4.5 through the use of the appropriate DF for shear, g_v , and the shear force obtained from analyzing the simplified single girder system, $V^{\text{simplified}}$.

$$V^{\text{girder}} = g_v V^{\text{simplified}} \quad (4.5)$$

The expressions for DF's are usually obtained through analyses similar to those described here, except that they are done in reverse order; i.e. the distribution factor is obtained by dividing results obtained from analyzing the real system by those of the simplified system. A regression of results leads to the expression of the DF's. The main benefit of using the DF is that it is possible to determine internal forces in a three-dimensional (3-D) system such as a bridge by analyzing a simplified single girder system.

4.3 Analysis Procedure and Model Verification

Obtaining a reliable distribution factor depends on several factors including the quality of modeling the entire bridge system, the number of cases used in the development of the DF expression, and the accuracy of the regression analysis used in deriving these expressions. Each of these factors is essential to the success of any proposed DF. Many DF studies utilized grillage models to obtain forces in the actual bridge systems. Other researchers adopt a more sophisticated analysis scheme by modeling the entire system using shell

element. In choosing for the study at hand, the advantages and disadvantages of both approaches were weighed in. The findings are summarized next

4.3.1 Shell Models vs. Grillage Models

Modeling the entire system using shell elements is undoubtedly more involved and provides additional information that other models are not capable of providing. However, shell elements provide results on a stress or stress resultant level, which introduces the following shortcomings. First, current codes focus more on the member level rather than on the material level. This is because the LRFD approach requires determining the strength of the member being designed in contrast with the allowable stress design method (ASD), which sets an allowable stress at the material level. Converting stresses obtained from shell model analyses to section forces is possible by integration of the appropriate stresses over the desired cross section. The integration process is tedious and time consuming. Second, the quality of stresses or stress resultants obtained from shell models are sensitive to various factors such as stress concentrations due to shear lag or any other sort of disruptions in the cross section such as stiffeners. Stresses are also affected by the type of element being used in the analysis, which in the opinion of the authors has an effect on how reliable the resulting DF's are.

Grillage models are more straightforward and provide direct results in the form of internal forces and moments. The simplicity of grillage models comes at the cost of losing some of the details in modeling three-dimensional objects, especially box girders systems. This could lead to inaccurate estimates of the DF's. However, many of the details that cause such discrepancies can be adequately modeled using grillage models. For example, an analysis of a box girder bridge using linear elements to model girders as well as the concrete deck leads to inaccurate results because the span of the deck is exaggerated as can be seen in Fig. 4.1. In the figure, the deck spans the distance between the box upper flanges. However, linear elements passing through the centroid implies a deck system as shown in the lower system.

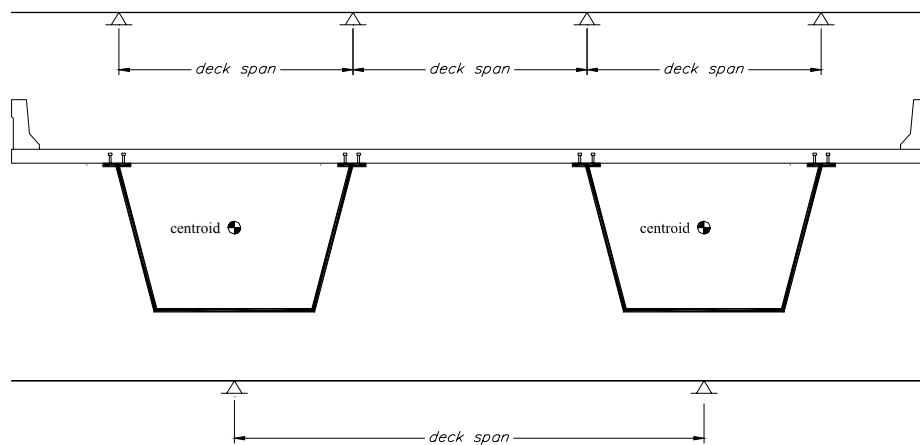


Figure 4.1: Grillage modeling and its effect on deck span length

As will be seen later, it is possible to overcome such drawbacks of grillage models through modeling adjustments. Accordingly, the choice of a shell model was deemed not necessary and a sophisticated grillage model was used for the DF study.

4.3.2 Determination of Distribution Factors

For each bridge configuration, two bridge models were built. The first model is a single girder model, which represents what the designer would normally use in every day design. For engineers, the analysis of such a model is quite simple and straightforward with readily available analysis tools. Figure 4.2 shows a schematic of one of the single girder models loaded with a group of concentrated loads representing a standard truck (HS-20) loading.

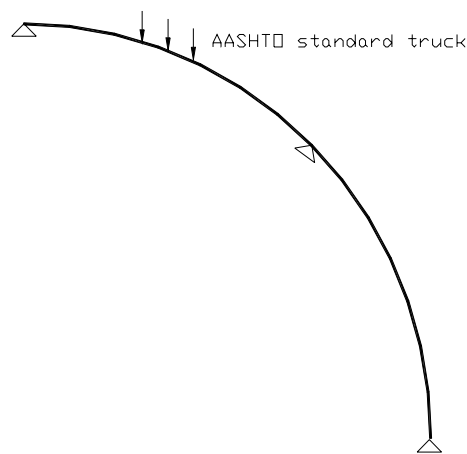


Figure 4.2: Schematic of single girder models used in determining the distribution factor

The second model is a detailed grillage model of the bridge system. Linear elements were used to model the bridge components such as girders, deck, and diaphragms. Figure 4.3 shows a schematic of the node and element arrangements for one of these models having three box girders. As it appears from the figure, girder elements (bold lines) connect nodes that are not shared with deck elements. Deck elements connect nodes according to deck dimensions, however avoiding direct contact with girder nodes. The connectivity of the deck and the girders is achieved through rigid links that apply constraints between nodes at their ends. The constraints are imposed in a master/slave type of relationship in such a way that achieves a continuity condition similar to that of the real structure. This arrangement avoids overestimating deck span lengths as described earlier.

The grillage model is verified by comparing results to those obtained using folded plate theory for a straight three-cell box-girder bridge (Johnson et al. 1967). The verification example is provided with only two diaphragms at the supports, thus the combined torsional rigidity method is used to model distortional behavior. The combined torsional rigidity

method is based on Beam-on-Elastic-Foundation analogy (BEF). A summary of the procedure is given next based on the cross sectional dimensions in Fig. 4.4.

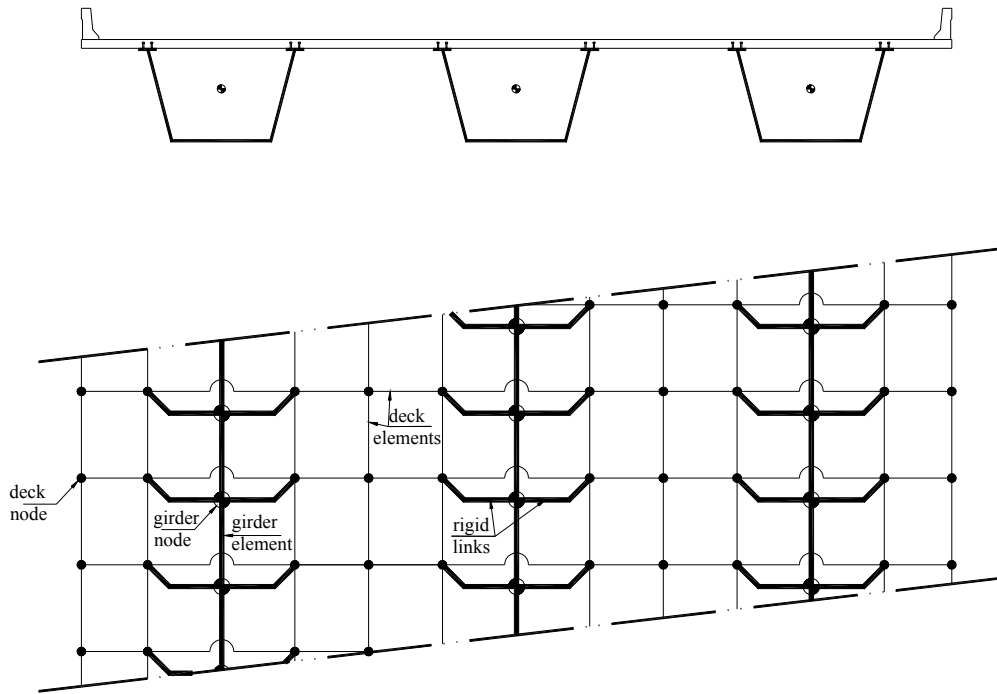


Figure 4.3: Schematic of grillage models used in determining the distribution factor

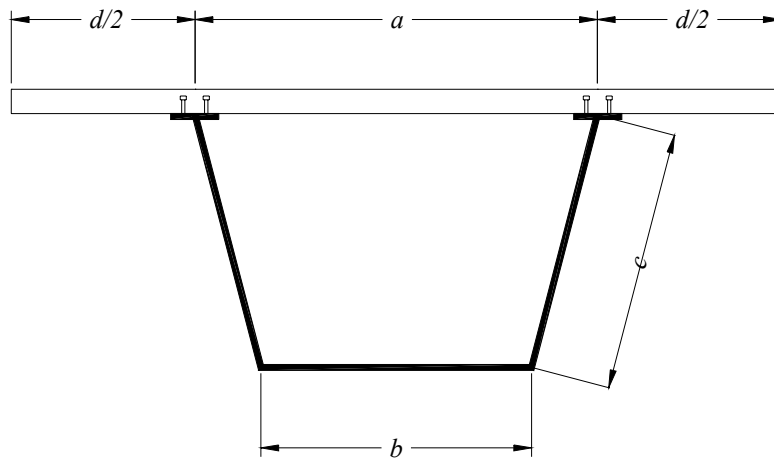


Figure 4.4: Dimensions for calculation of total torsional constant based on BEF

- The flexural rigidity of the top flange D_a , bottom flange D_b , web D_c is first determined:

$$D = \frac{Et^3}{12(1-\nu^2)} \quad (4.6)$$

- The out-of-plane shear in the bottom flange per unit torsional load is then calculated:

$$\gamma = \frac{\frac{1}{D_c} [(2a+b)abc] + \frac{ba^3}{D_a}}{(a+b) \left[\frac{a^3}{D_a} + \frac{2c}{D_c} (a^2 + ab + b^2) + \frac{b^3}{D_b} \right]} \quad (4.7)$$

- The vertical deflection of one web per unit torsional load can now be calculated as:

$$\delta = \frac{ab}{24(a+b)} \left\{ \frac{c}{D_c} \left[\frac{2ab}{a+b} - \gamma(2a+b) \right] + \frac{a^2}{D_a} \left[\frac{b}{a+b} - \gamma \right] \right\} \quad (4.8)$$

- A parameter β is then determined:

$$\beta = \left\{ \frac{1}{EI_c \delta} \right\}^{0.25} \quad (4.9)$$

- The reduced torsional rigidity is then calculated according to:

$$C = \frac{a^2 I_c (\beta l)^3}{l^2 1.6w} \quad (4.10)$$

in which l is the unbraced length between two adjacent diaphragms; c is the reduced torsional rigidity due to distortion and I_c is the moment of inertia for vertical bending. It should be noted that this expression is only valid for simply supported bridges. Similar expressions can be derived for curved bridges using space frame models.

- Finally, the combined torsional rigidity is calculated:

$$\frac{1}{J_t} = \frac{1}{C} + \frac{1}{J} \quad (4.11)$$

in which J is the classic torsional constant for closed cross sections (see Appendix A).

The three-girder bridge example reported in Johnson et al. (1967) was modeled using the suggested grillage model after obtaining the torsional constant following the above procedure. Figure 4.5 Show a comparison between results obtained from the suggested model and those reported by Johnson et al. The results are for the deflections of the deck at mid-span of the bridge due to an eccentrically positioned standard truck acting at midspan. As expected, the lateral flexibility leads to unequal deflections. Figure 4.5 shows that deflections under the loads are about 2.5 times the average deflection. It can be seen that the grillage model predicts deflections that are in good agreement with those reported by Johnson et al. (1967). Experimental results obtained from a 1:50 scale model were in good agreement with the same results.

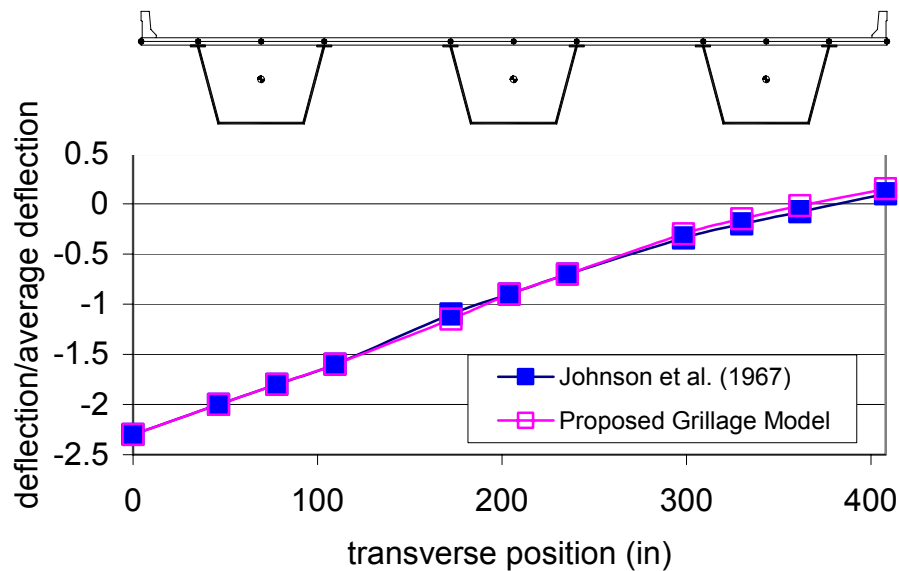


Figure 4.5: Verification results for proposed grillage model

The single girder and grillage models are used in the subsequent analyses which are performed in three stages:

- Stage I: A single girder model is built for each of the bridges in the parametric study. The model is then analyzed by loading it with AASHTO-LRFD (1998) loads for a full lane width (HL-93) by sweeping the truck along the longitudinal axis of the model. These analyses will yield the maximum force effects (bending moments, shear forces, and torsional moments) in the single girder bridge model,

P^{single} . The maximum forces are recorded for later use in determining the distribution factor. Truck locations causing these maximum forces are also stored. These locations serve as a starting point for Stage II analyses.

- Stage II: A grillage model is built for each of the bridges. Analyses of the grillage model are conducted for the same loading (HL-93) as linear models, however, the number of lanes loaded is based on the actual roadway width. The truck positioning in the longitudinal direction is predetermined from the single girder analyses in Stage I. The transverse location causing the maximum force effects is determined by sweeping the whole loading of the lane (truck + lane) laterally. The maximum forces caused by the most severe positioning of loads are recorded for all girders (exterior and interior), P^{girder} .
- Stage III: The distribution factors are determined according to Eq. 4.12 based on the results obtained in Stages I and II.

$$g_p = \frac{P^{\text{girder}}}{P^{\text{single}}} \quad (4.12)$$

4.4 Parametric Study

As stated earlier, a distribution factor is as reliable as the models used in producing it. This is not only pertinent to the quality of the structural analysis model, but also to the number and range of variables used in producing the distribution factor expression. In this study, several variables were identified as important to the load distribution capability of a curved box girder bridge system. Some these parameters are the same as those considered in earlier studies focusing on straight bridges, while others pertain only to curved bridges. The parameters considered are the number of girders, N , roadway width expressed by number of lanes, N_L , girder spacing, S , span length, L , and radius of curvature, R . Each bridge was analyzed for three possible numbers of continuous spans. Table 4.1 shows the details of the parameters included in this study. The cross-dimensional dimensions (plate thicknesses, ...etc.) were determined based on comparable existing designs in the FDOT inventory (eighteen bridges used in Chapter 3). The concrete deck was assumed to have a thickness of 205 mm (8 inches) for all cases considered. A total of 265 bridges were generated for this range of parameters.

Table 4.1: Details of variables considered in parametric study

Number of Lanes, N_L	Number of Girders, N	Girder Spacing, S (m)	Span Length, L (m)	Radius of Curvature, R (m)	Number of Spans
2	2	4.10	25 50 100	100 250 500	2 3 4
2	3	2.74			
3	2	5.90			
3	3	3.94			
3	4	2.95			
4	3	5.14			
4	4	3.85			
4	5	3.08			

4.5 Results and Conclusions

Models for all bridges were created based on the grillage model described in Section 4.3.2 and analyses following the procedure described earlier were conducted. The analyses generated a huge database of distribution factors for several types of internal forces (positive and negative bending moments, shear forces, and torsional moments). The distribution factor is extracted for each girder and the maximum values for all interior girders as well as the two exterior girders are chosen. Tables 4.2 through 4.4 list some of the data generated by this process. The tables show the distribution factors as obtained from this study and from Eq. 4.1, and the difference between both values. The tables provide the data organized by span length; $L=25\text{m}$, 50m , and 100m , respectively. While research is currently ongoing to process this data and propose new LL distribution factors, it is disturbing to observe that errors of up to 25% can occur when current DF expressions are used for the limited pool of bridges studied herein.

Table 4.2: Comparison of distribution factor results (L=25 m)

R	Spans	N_L	N	S	g_M	$g_{M^+}^e$		$g_{M^+}^i$		$g_{M^-}^e$		$g_{M^-}^i$	
					Eq. 4.1	Prog	Diff. (%)						
100	2	2	3	3.60	0.735	0.942	-21.9	0.777	-5.3	0.970	-24.2	0.759	-3.1
100	2	3	3	3.60	1.316	1.149	14.6	1.064	23.8	1.167	12.8	1.051	25.2
100	2	3	4	3.60	0.862	1.093	-21.1	0.952	-9.4	1.125	-23.4	0.963	-10.5
100	2	4	3	5.14	1.690	1.562	8.2	1.509	12.0	1.575	7.3	1.516	11.5
100	2	4	4	3.60	1.316	1.200	9.7	1.119	17.6	1.217	8.1	1.128	16.7
100	2	4	5	3.08	1.015	0.937	8.3	0.942	7.8	0.942	7.7	0.947	7.1
100	3	4	3	5.14	1.690	1.563	8.1	1.511	11.9	1.571	7.6	1.523	11.0
100	3	4	4	3.60	1.316	1.202	9.5	1.121	17.5	1.216	8.3	1.129	16.6
100	3	4	5	3.08	1.015	0.938	8.2	0.943	7.6	0.939	8.1	0.948	7.1
100	4	3	3	3.60	1.316	1.151	14.4	1.064	23.7	1.167	12.8	1.055	24.8
100	4	4	3	5.14	1.690	1.563	8.1	1.511	11.9	1.571	7.6	1.523	11.0
100	4	4	4	3.60	1.316	1.202	9.5	1.121	17.5	1.216	8.3	1.129	16.6
100	4	4	5	3.08	1.015	0.938	8.2	0.943	7.6	0.939	8.1	0.948	7.0
250	2	2	3	3.60	0.735	0.933	-21.2	0.776	-5.3	0.969	-24.1	0.759	-3.2
250	2	3	4	3.60	0.862	1.074	-19.7	0.950	-9.2	1.116	-22.8	0.964	-10.5
250	2	4	3	5.14	1.690	1.532	10.3	1.508	12.1	1.551	9.0	1.516	11.5
250	2	4	4	3.60	1.316	1.173	12.2	1.110	18.5	1.194	10.3	1.124	17.1
250	2	4	5	3.08	1.015	0.907	11.9	0.928	9.3	0.920	10.3	0.941	7.9
250	3	3	3	3.6	1.316	1.133	16.2	1.065	23.6	1.153	14.1	1.055	24.8
250	3	4	3	5.14	1.690	1.534	10.2	1.510	11.9	1.548	9.2	1.522	11.1
250	3	4	4	3.6	1.316	1.175	12.1	1.112	18.4	1.193	10.4	1.125	17.0
250	3	4	5	3.08	1.015	0.908	11.8	0.929	9.2	0.917	10.7	0.941	7.8
250	4	3	3	3.6	1.316	1.133	16.2	1.065	23.6	1.154	14.1	1.055	24.7
250	4	4	3	5.14	1.690	1.534	10.2	1.510	11.9	1.549	9.1	1.523	11.0
250	4	4	4	3.6	1.316	1.175	12.1	1.112	18.4	1.193	10.3	1.125	17.0
250	4	4	5	3.08	1.015	0.908	11.8	0.930	9.2	0.917	10.6	0.942	7.7
500	2	2	3	3.6	0.735	0.929	-20.8	0.776	-5.2	0.968	-24.0	0.759	-3.1
500	2	3	3	3.6	1.316	1.125	17.0	1.064	23.7	1.147	14.7	1.052	25.2
500	2	3	4	3.6	0.862	1.067	-19.2	0.948	-9.1	1.113	-22.5	0.964	-10.5
500	2	4	4	3.6	1.316	1.163	13.1	1.107	18.9	1.185	11.0	1.122	17.3
500	2	4	5	3.08	1.015	0.897	13.2	0.923	9.9	0.912	11.3	0.938	8.2
500	3	3	3	3.6	1.316	1.126	16.9	1.065	23.6	1.148	14.6	1.055	24.7
500	3	4	4	3.6	1.316	1.165	13.0	1.108	18.8	1.185	11.1	1.123	17.2
500	3	4	5	3.08	1.015	0.898	13.1	0.925	9.8	0.910	11.6	0.939	8.1
500	4	3	3	3.6	1.316	1.027	28.2	1.065	23.6	1.149	14.5	1.056	24.7
500	4	4	3	5.14	1.690	1.524	10.9	1.510	11.9	1.541	9.7	1.523	11.0
500	4	4	4	3.6	1.316	1.165	13.0	1.109	18.7	1.185	11.0	1.124	17.1
500	4	4	5	3.08	1.015	0.898	13.1	0.925	9.7	0.910	11.5	0.940	8.0

Table 4.3: Comparison of distribution factor results (L=50 m)

R	Spans	N_L	N	S	g_M	$g_{M^+}^e$		$g_{M^+}^i$		$g_{M^-}^e$		$g_{M^-}^i$	
					Eq. 4.1	Prog	Diff. (%)						
100	2	2	3	2.74	0.819	0.734	11.47	0.695	17.84	0.738	10.99	0.685	19.44
100	2	3	3	3.94	1.254	1.120	11.95	1.060	18.31	1.121	11.85	1.046	19.88
100	2	3	4	2.95	0.941	0.860	9.38	0.818	14.98	0.863	9.10	0.823	14.38
100	2	4	3	5.14	1.690	1.508	12.12	1.424	18.69	1.521	11.15	1.422	18.89
100	2	4	4	3.85	1.269	1.165	8.90	1.101	15.17	1.164	9.02	1.114	13.89
100	2	4	5	3.08	1.015	0.949	6.94	0.920	10.37	0.945	7.39	0.920	10.35
100	3	2	3	2.74	0.819	0.735	11.45	0.695	17.82	0.739	10.85	0.686	19.26
100	3	3	3	3.94	1.254	1.120	11.90	1.060	18.26	1.123	11.60	1.049	19.46
100	3	3	4	2.95	0.941	0.861	9.34	0.819	14.94	0.863	9.02	0.825	14.10
100	3	4	3	5.14	1.690	1.509	12.03	1.425	18.63	1.524	10.90	1.429	18.30
100	3	4	4	3.85	1.269	1.166	8.84	1.102	15.12	1.165	8.89	1.117	13.55
100	3	4	5	3.08	1.015	0.949	6.90	0.916	10.76	0.945	7.42	0.921	10.14
100	4	2	3	2.74	0.819	0.735	11.45	0.695	17.82	0.740	10.69	0.688	18.97
100	4	3	3	3.94	1.254	1.120	11.89	1.060	18.26	1.121	11.87	1.054	18.89
100	4	3	4	2.95	0.941	0.861	9.34	0.819	14.94	0.864	8.92	0.827	13.75
100	4	4	3	5.14	1.690	1.509	12.03	1.425	18.63	1.527	10.70	1.436	17.70
100	4	4	4	3.85	1.269	1.166	8.84	1.102	15.11	1.167	8.72	1.120	13.22
100	4	4	5	3.08	1.015	0.949	6.90	0.916	10.76	0.945	7.41	0.924	9.88
250	2	2	3	2.74	0.819	0.711	15.20	0.694	17.98	0.725	12.98	0.686	19.28
250	2	3	3	3.94	1.254	1.091	14.93	1.059	18.33	1.104	13.54	1.047	19.73
250	2	3	4	2.95	0.941	0.824	14.17	0.808	16.43	0.841	11.86	0.818	14.99
250	2	4	3	5.14	1.690	1.472	14.81	1.423	18.80	1.499	12.79	1.423	18.77
250	2	4	4	3.85	1.269	1.123	13.00	1.088	16.65	1.137	11.56	1.109	14.38
250	2	4	5	3.08	1.015	0.901	12.61	0.894	13.46	0.915	10.90	0.909	11.60
250	3	2	3	2.74	0.819	0.710	15.35	0.694	17.94	0.728	12.51	0.690	18.69
250	3	3	3	3.94	1.254	1.091	14.95	1.060	18.28	1.111	12.86	1.057	18.61
250	3	3	4	2.95	0.941	0.823	14.33	0.808	16.53	0.844	11.52	0.825	14.13
250	3	4	3	5.14	1.690	1.472	14.80	1.423	18.74	1.506	12.26	1.439	17.50
250	3	4	4	3.85	1.269	1.122	13.04	1.088	16.65	1.142	11.12	1.118	13.50
250	3	4	5	3.08	1.015	0.900	12.76	0.893	13.62	0.916	10.80	0.915	10.86
250	4	2	3	2.74	0.819	0.710	15.35	0.694	17.94	0.728	12.50	0.690	18.68
250	4	3	3	3.94	1.254	1.091	14.94	1.060	18.27	1.111	12.83	1.057	18.60
250	4	3	4	2.95	0.941	0.823	14.33	0.808	16.53	0.844	11.50	0.825	14.10
250	4	4	3	5.14	1.690	1.472	14.79	1.423	18.74	1.506	12.23	1.439	17.47
250	4	4	4	3.85	1.269	1.122	13.03	1.088	16.65	1.142	11.09	1.118	13.47
250	4	4	5	3.08	1.015	0.900	12.76	0.893	13.60	0.916	10.78	0.916	10.84
500	2	2	3	2.74	0.819	0.700	16.95	0.693	18.16	0.718	13.97	0.686	19.26
500	2	3	3	3.94	1.254	1.078	16.26	1.058	18.46	1.097	14.28	1.047	19.71
500	2	3	4	2.95	0.941	0.809	16.36	0.802	17.27	0.832	13.11	0.816	15.30
500	2	4	3	5.14	1.690	1.457	16.00	1.421	18.94	1.489	13.48	1.423	18.74
500	2	4	4	3.85	1.269	1.105	14.82	1.081	17.38	1.126	12.62	1.107	14.60
500	2	4	5	3.08	1.015	0.881	15.15	0.884	14.85	0.903	12.39	0.905	12.12
500	3	2	3	2.74	0.819	0.700	16.95	0.694	17.96	0.722	13.43	0.690	18.64
500	3	3	3	3.94	1.254	1.079	16.19	1.060	18.28	1.104	13.55	1.057	18.56
500	3	3	4	2.95	0.941	0.809	16.37	0.803	17.17	0.835	12.69	0.823	14.36
500	3	4	3	5.14	1.690	1.458	15.92	1.423	18.80	1.497	12.91	1.439	17.46
500	3	4	4	3.85	1.269	1.106	14.75	1.082	17.24	1.131	12.12	1.116	13.67
500	3	4	5	3.08	1.015	0.881	15.16	0.884	14.77	0.904	12.23	0.912	11.32
500	4	2	3	2.74	0.819	0.700	16.95	0.694	17.96	0.722	13.42	0.690	18.64
500	4	3	3	3.94	1.254	1.079	16.18	1.060	18.28	1.104	13.52	1.058	18.54
500	4	3	4	2.95	0.941	0.809	16.37	0.803	17.17	0.835	12.66	0.823	14.33
500	4	4	3	5.14	1.690	1.458	15.91	1.423	18.79	1.498	12.87	1.439	17.44
500	4	4	4	3.85	1.269	1.106	14.74	1.082	17.24	1.132	12.08	1.116	13.64
500	4	4	5	3.08	1.015	0.881	15.16	0.884	14.76	0.905	12.20	0.912	11.27

Table 4.4: Comparison of distribution factor results (L=100 m)

R	Spans	N_L	N	S	g_M	$g_{M^+}^e$		$g_{M^+}^i$		$g_{M^-}^e$		$g_{M^-}^i$	
					Eq. 4.1	Prog	Diff. (%)						
100	2	2	3	2.73	0.819	0.758	8.11	0.694	18.10	0.729	12.35	0.676	21.28
100	2	3	3	3.93	1.255	1.148	9.27	1.054	19.05	1.118	12.17	1.022	22.72
100	2	3	4	2.95	0.941	0.891	5.66	0.823	14.33	0.860	9.45	0.809	16.36
100	2	4	3	5.13	1.691	1.541	9.77	1.416	19.42	1.524	10.95	1.384	22.20
100	2	4	4	3.85	1.269	1.188	6.79	1.106	14.73	1.159	9.50	1.091	16.31
100	2	4	5	3.08	1.015	0.986	2.92	0.926	9.59	0.950	6.83	0.907	11.91
100	3	2	3	2.73	0.819	0.758	8.11	0.693	18.29	0.716	14.49	0.690	18.80
100	3	3	3	3.93	1.255	1.148	9.27	1.052	19.23	1.113	12.71	1.010	24.17
100	3	3	4	2.95	0.941	0.891	5.60	0.823	14.40	0.858	9.73	0.789	19.26
100	3	4	3	5.13	1.691	1.542	9.68	1.415	19.56	1.509	12.11	1.371	23.40
100	3	4	4	3.85	1.269	1.189	6.72	1.105	14.84	1.152	10.08	1.069	18.70
100	3	4	5	3.08	1.015	0.987	2.84	0.926	9.63	0.948	7.05	0.883	14.89
100	4	2	3	2.73	0.819	0.758	8.11	0.693	18.29	0.716	14.49	0.690	18.80
100	4	3	3	3.93	1.255	1.148	9.27	1.052	19.23	1.113	12.71	1.010	24.17
100	4	3	4	2.95	0.941	0.891	5.60	0.823	14.40	0.858	9.73	0.789	19.26
100	4	4	3	5.13	1.691	1.542	9.68	1.415	19.56	1.509	12.11	1.371	23.40
100	4	4	4	3.85	1.269	1.189	6.72	1.105	14.84	1.152	10.08	1.069	18.70
100	4	4	5	3.08	1.015	0.987	2.84	0.926	9.63	0.948	7.05	0.883	14.89
250	2	2	3	2.73	0.819	0.721	13.66	0.692	18.46	0.727	12.68	0.679	20.62
250	2	3	3	3.93	1.255	1.100	14.01	1.051	19.35	1.103	13.77	1.027	22.14
250	2	3	4	2.95	0.941	0.838	12.34	0.807	16.56	0.846	11.20	0.807	16.54
250	2	4	3	5.13	1.691	1.481	14.20	1.410	19.97	1.496	13.09	1.389	21.80
250	2	4	4	3.85	1.269	1.128	12.42	1.084	17.07	1.133	11.95	1.088	16.65
250	2	4	5	3.08	1.015	0.918	10.56	0.897	13.08	0.925	9.72	0.899	12.92
250	3	2	3	2.73	0.819	0.721	13.63	0.691	18.53	0.729	12.37	0.681	20.39
250	3	3	3	3.93	1.255	1.101	13.94	1.051	19.38	1.107	13.32	1.031	21.66
250	3	3	4	2.95	0.941	0.838	12.28	0.807	16.54	0.848	10.93	0.811	16.04
250	3	4	3	5.13	1.691	1.483	14.04	1.410	19.95	1.502	12.64	1.397	21.06
250	3	4	4	3.85	1.269	1.130	12.29	1.084	17.05	1.137	11.59	1.093	16.04
250	3	4	5	3.08	1.015	0.919	10.45	0.895	13.36	0.926	9.58	0.903	12.43
250	4	2	3	2.73	0.819	0.721	13.63	0.691	18.53	0.727	12.74	0.679	20.65
250	4	3	3	3.93	1.255	1.101	13.94	1.051	19.38	1.102	13.88	1.033	21.45
250	4	3	4	2.95	0.941	0.838	12.28	0.807	16.54	0.844	11.54	0.806	16.69
250	4	4	3	5.13	1.691	1.483	14.03	1.410	19.95	1.489	13.59	1.394	21.31
250	4	4	4	3.85	1.269	1.130	12.29	1.084	17.05	1.129	12.33	1.085	16.92
250	4	4	5	3.08	1.015	0.919	10.44	0.895	13.36	0.921	10.23	0.895	13.40
500	2	2	3	2.73	0.819	0.705	16.31	0.692	18.51	0.717	14.25	0.680	20.58
500	2	3	3	3.93	1.255	1.079	16.29	1.051	19.39	1.089	15.19	1.028	22.06
500	2	3	4	2.95	0.941	0.813	15.77	0.800	17.65	0.831	13.23	0.804	17.08
500	2	4	3	5.13	1.691	1.453	16.39	1.408	20.12	1.478	14.43	1.390	21.72
500	2	4	4	3.85	1.269	1.101	15.23	1.074	18.11	1.116	13.69	1.084	17.01
500	2	4	5	3.08	1.015	0.886	14.58	0.880	15.39	0.905	12.15	0.892	13.83
500	3	2	3	2.73	0.819	0.705	16.26	0.691	18.56	0.720	13.86	0.681	20.32
500	3	3	3	3.93	1.255	1.079	16.22	1.051	19.41	1.094	14.65	1.032	21.54
500	3	3	4	2.95	0.941	0.813	15.68	0.800	17.62	0.834	12.85	0.808	16.49
500	3	4	3	5.13	1.691	1.455	16.23	1.408	20.08	1.485	13.90	1.398	20.95
500	3	4	4	3.85	1.269	1.102	15.09	1.074	18.09	1.120	13.23	1.091	16.32
500	3	4	5	3.08	1.015	0.887	14.44	0.880	15.29	0.907	11.90	0.896	13.24
500	4	2	3	2.73	0.819	0.705	16.26	0.691	18.56	0.717	14.37	0.682	20.21
500	4	3	3	3.93	1.255	1.079	16.22	1.051	19.40	1.088	15.34	1.036	21.12
500	4	3	4	2.95	0.941	0.813	15.68	0.800	17.62	0.828	13.71	0.805	16.94
500	4	4	3	5.13	1.691	1.455	16.22	1.408	20.08	1.471	14.98	1.397	21.06
500	4	4	4	3.85	1.269	1.102	15.08	1.074	18.09	1.111	14.16	1.083	17.10
500	4	4	5	3.08	1.015	0.887	14.44	0.880	15.29	0.899	12.84	0.889	14.10

5 ACCESS HATCHES IN CONTINUOUS CURVED COMPOSITE BOX GIRDER BRIDGES

5.1 Introduction

Bridge officials are required to inspect all bridges periodically (biannually) to detect any deficiencies or deterioration. The task of bridge inspection is especially difficult to perform in box girder bridges. Almost half the inspection task is performed from inside the box due to its tunnel-like nature. Other types of bridges (I-girders) do not require such extra effort as all inspections are exterior in nature. The interior of the box, which can be dangerous because of high temperatures and poor ventilation, is reached through access hatches that are usually provided in the bottom flange immediately before or after an expansion joint. These locations are chosen because: 1) bending moments are small close to the expansion joint, and 2) the abutment/pier over which the expansion joint is located facilitates access; inspection crews can climb up the abutment or use simple tools such as a ladder to reach the access hole. Since the spans covered by box girders are often long and the girders are constructed as continuous segments over three or more supports, the distance between access hatches frequently exceeds the limit that rescue crews can reach in the event of an emergency. The addition of new access holes to an existing bridge should satisfy certain practical constraints (discussed shortly) and should not adversely affect the structural behavior of the bridge, i.e. it should not impair serviceability nor decrease the ultimate strength and fatigue life. If the access hole is placed in a critical location the bridge may need to be strengthened, which is generally costly. Alternatively, access holes could be placed in low stress regions where strengthening is not necessary thereby significantly reducing the cost of rehabilitation.

5.2 Practical Constraints for Choosing Access Hole Location

In addition to the bottom flange location, which is already used in existing bridges, new access holes may also be provided in the webs of the steel girder or in the concrete deck. Figure 5.1 shows possible access hole locations. The advantages and disadvantages of each of these alternatives are discussed with respect to their impact on the following issues:

5.2.1 Strength

Holes in the bottom flange can significantly reduce the flexural strength of the cross section and the entire structure, especially if they are placed in the vicinity of continuous supports where high negative moments develop or in high positive moment regions. Away from high moment regions, normal stresses due to flexure are small and adding a hole in the bottom

flange may be possible without strengthening. Web access holes can greatly reduce the shear resistance of the web, which is made of relatively thin steel plates. Therefore, this alternative should only be considered around midspan where low shear forces and torsional moments exist. Since concrete deck dimensions are usually predetermined by traffic considerations (road width) rather than by structural need, the effect of opening an access hole in the concrete deck has the least impact on strength of all three alternatives.

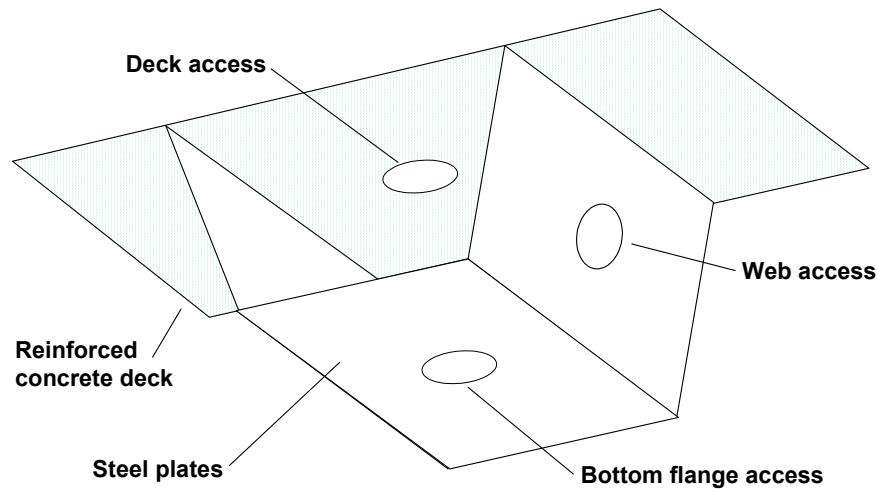


Figure 5.1: Alternative access hole locations

5.2.2 Feasibility

Access holes that will interfere with structural elements such as stiffeners and cross frames should be avoided. Longitudinal bottom flange stiffeners are provided to stiffen the plate and prevent buckling in the negative moment region over supports. These stiffeners are discontinued in regions where the negative moment drops to zero. Narrow boxes are provided with one stiffener in the middle of the plate, which creates an obstacle to adding access holes in the bottom flange near a support. Boxes with two bottom flange stiffeners can be provided with an access hole between the stiffeners if the distance in between the stiffeners is sufficient. Web access holes can be added in the space between web stiffeners. Top flange bracing may block access through reinforced concrete deck hatches. Since, braces are provided to stabilize the steel cross-section before casting the concrete deck they can be taken out if needed since they are not essential for the behavior of the steel/concrete composite closed cross section. Cross frame locations should be avoided since these structural components are important for the global behavior of the bridge.

5.2.3 Accessibility

Accessibility of access holes is an important issue since they are added for use in the event of an emergency. Holes in the concrete deck are easily accessible from the roadway and do not

need special equipment. Bottom flange and web alternatives that are away from the supports require special equipment such a snooper (truck with an arm that reaches over the side and below the bridge) or a bucket (which reaches from below). In the vicinity of the supports, piers and abutments facilitate access to the holes. In the case of multi cell bridges, web openings in inner cells will be hard to reach if they are located away from the piers.

5.2.4 Water Leakage

Any modifications in the bridge that would increase the potential for corrosion should be avoided. Access holes in bottom flanges and webs (except for outer webs where water may run down the sides) do not increase the chances of water getting into the steel box. The concrete deck alternative is the most critical of all three alternatives since imperfect hatch doors may cause water leakage into the box.

5.2.5 Impact on Traffic

Access holes that are accessed from the topside of the bridge (concrete deck, or web and bottom flange holes accessed with the help of a snooper) will impede traffic flow and need special arrangements to use the access hatch. No such arrangements are needed for bottom flange and web openings that will be accessed from beneath the bridge using a bucket or directly using the piers.

5.2.6 Unauthorized Access

Unauthorized people can easily reach access holes in the vicinity of the supports and in the concrete deck. Away from the supports, web or bottom flange access is not possible without the use of special equipment. In all cases, precautions should be taken to prevent unauthorized people from getting into the cells. Figure 1.2 shows the belongings of an individual who made the bridge cell his home.

Based on the previous discussions it is clear that the concrete deck option is the least attractive alternative because of the potential for water leakage to the inside of the girder and the possibility of interference with traffic flow when in use. The most appealing option is bottom flange access, which is practical and, as will be discussed later on in the report, does not have an impact on bridge strength if the location is chosen appropriately. The web option has a greater number of limitations, which makes it a last resort if the bottom flange option is not possible. Table 5.1 summarizes the advantages and disadvantages of each of the alternatives.

Table 5.1: Summary of advantages and disadvantages of access hole alternatives

Alternative	Bottom Flange	Web	Concrete Deck
Strength	Reduces flexural strength.	Reduces shear and torsional strength.	Less effect on strength than other two alternatives.
Feasibility	Stiffeners should be avoided. May be an obstacle if one stiffener is used.	Stiffeners must be avoided.	No stiffener limitations, but construction bracing may be an obstacle.
	Cross frames must be avoided.		
Access at supports	Easy	Easy	Easy access at any location.
Access between supports	Possible with the help of a snooper or a bucket.	Possible with the help of a snooper or a bucket, except for intermediate cells in multicell bridges.	
Water leakage	Not a concern.	Concern for outer cells.	Watertight doors will be needed.
Impact on traffic	No effect.	No effect.	Special arrangements will be needed for access.
Unlawful Access	Possible at supports.	Possible at supports.	Possible at any location.

5.3 Stresses in Curved Box Girder Bridges

The different types of forces acting on a curved box girder are calculated using a linear elastic finite element model. The model is based on a three-dimensional two-node beam element that accounts for warping behavior (see Chapter 2). The analyses are conducted using the commercial computer program ABAQUS (1997).

A computer program was written to determine the cross-sectional geometric properties (area, moments of inertia, warping constant, ...etc.) for composite cross sections with an overhanging deck. The program is run to determine the properties of the quasi-closed, and closed cross-sectional properties to be used in the appropriate loading stage (dead load and live load respectively). The geometric properties of the quasi-closed noncomposite girder were determined assuming a fictitious plate (representing the construction bracing) connects the top flanges of the box girder. The fictitious member is given an equivalent thickness, t_{eq} , that has the same effect on the girder as that of the construction bracing connecting the top flanges as described in Chapter 3.

Seven of the FDOT bridge girders described in Chapter 3 were also analyzed to determine the feasibility of increasing the number of access hatches. The methodology by which additional access hole locations are identified is based on identifying low stress regions

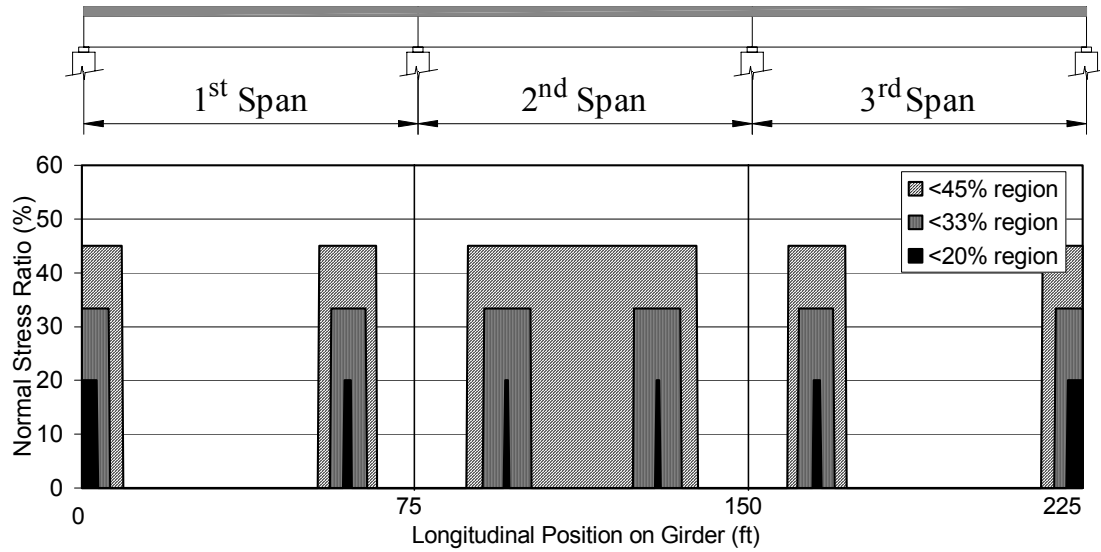
whose capacity would still exceed the demand even with the new hole. The following sections describe the details of the approaches followed in this research.

5.4 Low Stress Regions

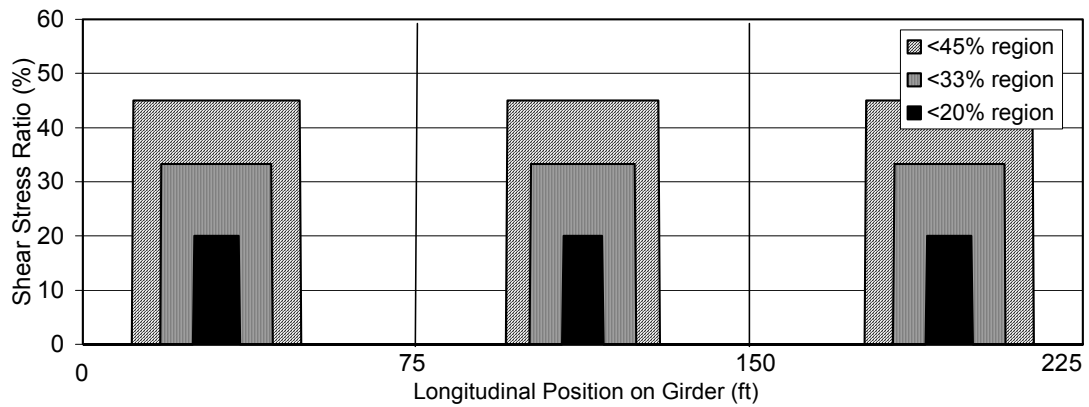
Normal and shear stresses are first determined at key points in the cross section (see Fig. 3.6) using Eqs. 3.7 and 3.9. The stresses are calculated at all locations in the longitudinal direction. Two different approaches are then used to determine low stress regions. In the first approach (Approach I), which is suitable for identifying bottom flange openings, regions are located where the maximum normal stress, σ , is less than a specific threshold, $\sigma < 33\% \sigma_{max}$. The 33% limit is important since the stress concentration factor around circular holes is 3. For comparison purposes, appropriate regions are calculated for two other thresholds $\sigma < 20\% \sigma_{max}$ and $\sigma < 45\% \sigma_{max}$. Fatigue is then incorporated in this approach by limiting suitable locations to regions where the live load stress range is less than the AASHTO-LRFD (1998) limit. The live load stress range is determined by finding the difference between the maximum and minimum stresses generated as the design vehicle crosses the bridge. In the second approach (Approach II), which is suitable for web openings, regions are located where the shear stress, τ , is less than 33% of τ_{max} . As with the first approach, other regions are calculated for $\tau < 20\% \tau_{max}$ and $\tau < 45\% \tau_{max}$.

5.4.1 Results for Idealized Bridge

The previous approaches are applied to the results obtained from the analysis of an idealized bridge model for the sake of demonstration. The idealized bridge is a three span continuous box girder. The length of each span is 75 ft. Each approach yields regions of low stresses in accordance with the assumptions made in the scheme. Figure 5.2-a shows the regions that satisfy the normal stress thresholds discussed in Approach I (without considering fatigue limitations). As expected, minimally stressed regions exist around the points of contraflexure and close to exterior supports. Approach II results in the regions seen in Fig. 5.2-b, which are located around mid-spans where low shear forces and torsional moments exist. The fatigue stress distribution for the idealized bridge is given in Fig. 5.3-a. The empty regions represent areas where stresses are compressive and are therefore not affected by fatigue. It turns out that for this particular bridge fatigue stresses are not critical anywhere along the bridge and therefore do not limit where access holes can be placed (Fig. 5.3-b). The regions suitable for access hole placement, i.e. that satisfy both strength and fatigue criteria, are obtained by imposing the regions in Figures 5.2-a and 5.3-b and are shown in Figure 5.4.

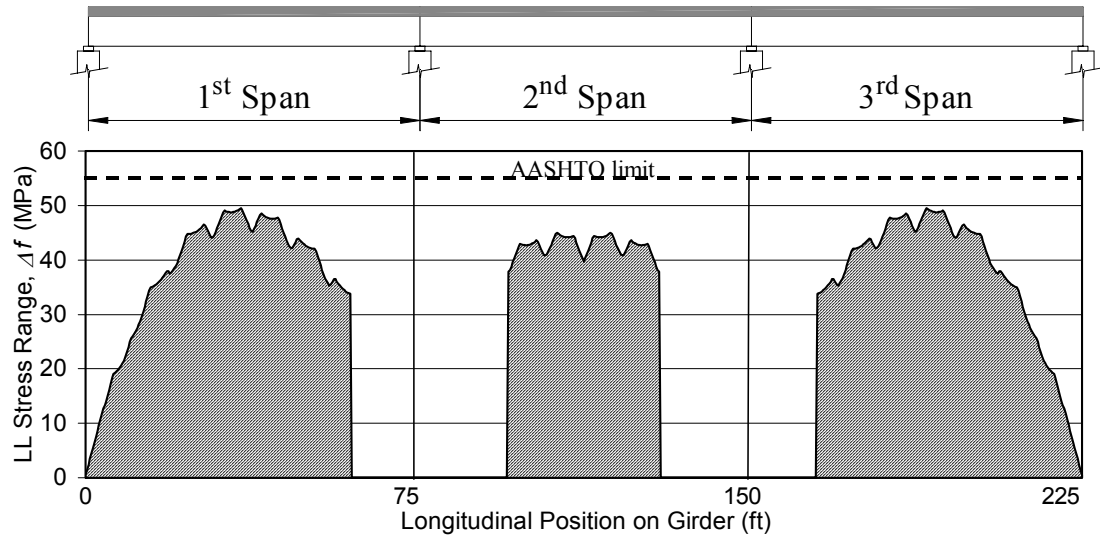


(a)

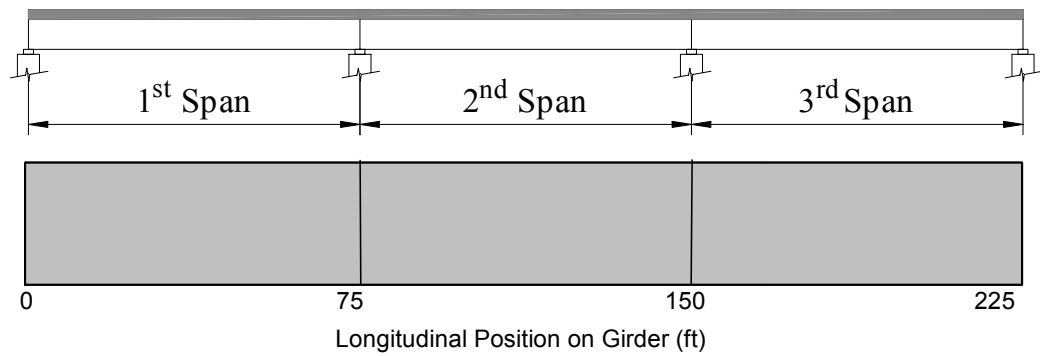


(b)

Figure 5.2: Low stress regions for idealized bridge (a - Approach I, b - Approach II).



(a)



(b)

Figure 5.3: (a) Distribution of fatigue stresses. Empty regions are areas in compression and therefore not affected by fatigue. (b) Regions not critical for fatigue considerations (entire bridge).

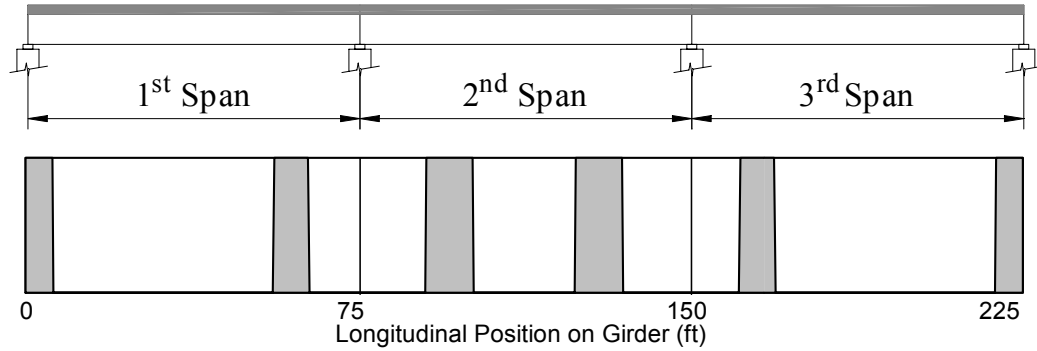


Figure 5.4: Regions that satisfy both normal stress criteria (<33% regions in Figure 5.2-a and fatigue stress criteria in Fig. 5.3-b). Shaded regions are suitable for access hole placement.

5.4.2 Study of Existing Bridges

The chosen bridges are studied using the above-described approaches to investigate whether low stress regions as defined earlier can be identified. The bridges are located in District IV of the Florida Department of Transportation and vary in dimensions covering a range of curvatures and cross sections. All bridge segments are studied. Based on the analyses conducted in this study the following results are obtained. Details for each individual bridge can be found in Okeil et al (2000).

Approach I: For spans that are continuous at both ends, the location of minimally stressed points is at a distance ranging from 20% to 42% of the span length measured from the continuous support. Corresponding values for first/last spans are 20% to 54% measured from the continuous support. The length of the minimally stressed region varies substantially. On average, the length of the region is 5.6% of the span length, L . Spans that are continuous on both sides have an average length of 6.0% L , and spans that are continuous from one side have an average region length equal to 4.7% L . Examination of the results showed that there was no clear correlation between horizontal curvature and location or size of the minimally stressed regions. The lack of a definite trend is attributed to 1) the limited number of case studies considered; 2) the complexity of the structural problem; and 3) the fact that the bridges were designed by different design firms. Different design practices can lead to some variations in design, which can substantially affect the position and size of the minimally stressed regions.

Approach II: Locations with minimal shear stress exist mainly around the middle of each span where low shear forces and torsional moments act on the girder. It is observed that for first/last spans appropriate regions are at an average distance of 37% L measured from the end support, and for spans continuous on both ends, the average distance is 50% L . The average region length for first/last spans and spans continuous on both sides is found to be 40% L and

28% L , respectively. As in Approach I, there was no clear correlation between horizontal curvature and location or size of the minimally stressed regions.

5.5 Effect of Hole Location on Strength of an Existing Bridge

A detailed finite element model of an existing bridge is created to confirm the methodology discussed above and to further investigate the effect of adding access holes at various locations on the strength of the bridge. The developed model incorporates important structural details. Shell elements are used to model the webs, bottom flange, and deck. Deck reinforcement is smeared within the concrete deck elements. Web stiffeners and cross frames are modeled using beam elements while constraint conditions simulating rigid shear connectors link the top flange of the steel box to the plane of the concrete deck. Smaller elements are used in regions of interest. Appropriate constraints connect the coarse mesh with the fine mesh. The mesh has approximately 7000 elements. Figure 5.5 shows a general view of the finite element mesh used in the analysis. A bilinear stress-strain relationship is assumed for both steel and concrete as shown in Fig. 5.6. Concrete tension stiffening is taken into account as shown in Fig. 5.6. Further details regarding the nonlinear model can be found in Okeil et al (2000).

The model is loaded with a tandem load acting at the center of the second span of the bridge and an uninterrupted lane load covers the entire second span. The model is used to study two configurations of the bridge. The first configuration is analyzed for the original condition with no holes and serves as a benchmark. The second configuration has an access hole in the low stress region identified using Approach I. The access hole is placed at a distance of 30% L from the support, just beyond the end of the bottom flange stiffeners that extended from the continuous support. The access hole is 600-mm in diameter. Figure 5.7 shows a bottom view of the model with a hole in a low stress region. Dark areas represent highly stressed regions.

Analysis of the developed model showed that introduction of the access hole in the low stress region resulted in a negligible reduction in strength. As expected, the stresses at the hole periphery are approximately 3 times the stresses that existed prior to the hole. The new stresses are still significantly lower than those in other highly stressed regions and are not expected to adversely affect the structural behavior of the bridge.

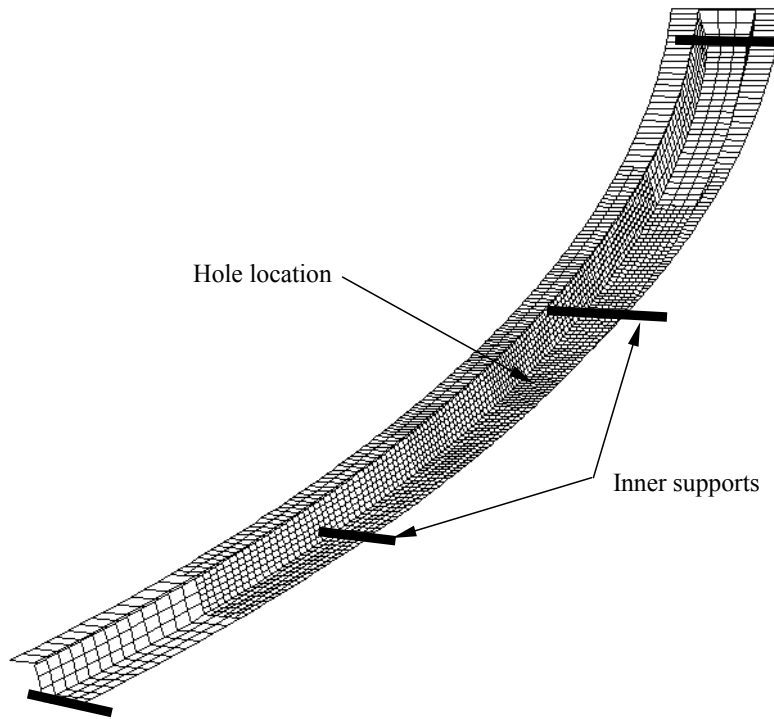


Figure 5.5: General view of finite element mesh.

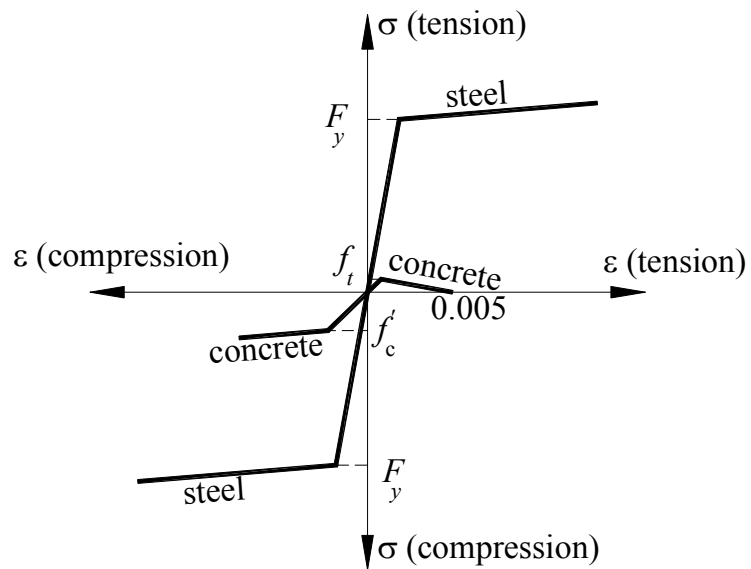


Figure 5.6: Idealized stress-strain relationships for steel and concrete.

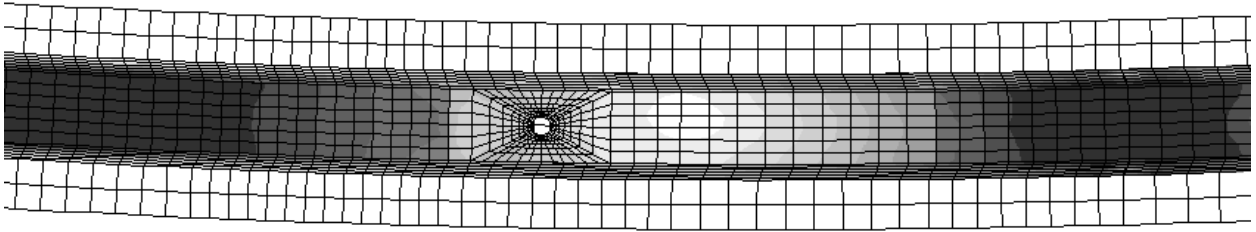


Figure 5.7: Bottom view of bridge model showing hole location in a minimally stressed region.

5.6 Summary and Conclusions

This chapter discusses practical and structural issues affecting the choice of where new access holes can be cut in existing horizontally curved box girder bridges. A methodology is presented for identifying low stress regions where access hatches can be installed without additional strengthening. Low stress regions are found using a linear elastic finite element model comprised of special beam elements that account for warping behavior of the box cross-section. The model is used to analyze 7 existing bridges that have a wide range of geometric properties and that are representative of the State of Florida inventory. For the bridges studied, it is found that an access hole can be placed in the bottom flange at a distance measured from the support ranging from 20% to 42% of the span length for spans continuous at both ends. Corresponding values for first spans are 20% to 54% measured from the continuous support. The length of the minimally stressed region varies substantially. Spans that are continuous on both sides have an average length of 6.0% of the span length, while spans that are continuous from one side have an average region length equal to 4.7% of the span length. No clear correlation was observed between horizontal curvature and position or size of the minimally stressed regions. Detailed nonlinear finite element analyses of one of the bridges confirm the methodology chosen for locating the access holes.

6 SUMMARY AND CONCLUSIONS

Current codes pertaining to analysis and design of curved composite girders are mostly based on experimental and analytical research conducted over 30 years ago as part of project CURT (Consortium of University Research Teams) funded by the Federal Highway Administration (FHWA). A new Curved Steel Bridge Research (CSBR) project is currently being conducted under the auspices of the FHWA. Although the CSBR project is expected to provide much needed information on behavior, analysis and design of curved composite bridges, it focuses more on I-girders than on box girders. The overall objective of the research reported herein is to provide information that complements existing data and that will be useful for formulating comprehensive design guidelines for composite curved box girders. Specific objectives include: 1) investigate and quantify the effect of nonuniform torsion on the behavior and design of existing curved box girders; 2) investigate existing distribution factors for curved box girder bridges; and 3) provide information that is helpful in identifying suitable locations for placement of access hatches in the steel box.

A computer program for simulating the behavior of curved box girders was developed. The program is graphically interactive and features a general purpose beam-column element that can account for the effect of warping. The developed program is used to conduct a detailed investigation of warping related stresses in eighteen existing box girder bridges chosen from the Florida Department of Transportation inventory. The bridges are carefully selected to cover a wide range of design parameters including horizontal curvature, cross sectional properties, and number of spans. They were designed by different firms and were constructed at different times and are considered to be representative of current design practice. Forces are evaluated from analyses that account for the construction sequence and the effect of warping. Loading is considered following the 1998 AASHTO-LRFD provisions.

By considering differences between stresses obtained taking into account warping and those calculated by ignoring warping, it is shown that warping has little effect on both shear and normal stresses in the limited sample of bridges considered. These results should not be construed to imply that warping is not important. Rather, this work points out that there could be a large subset of bridges where the warping effect is small enough to be ignored in structural calculations. This is particularly useful to designers because warping calculations are complicated and time consuming.

Another study was undertaken to investigate load distribution factors promoted by current specifications. Single girder and detailed grillage models were created for a variety of bridges and analyzed. The parameters investigated are the number of girders, roadway width expressed by number of lanes, girder spacing, span length, and radius of horizontal curvature. For the limited pool of bridges studied, it was observed that errors of up to 25% can occur when current DF expressions are used.

Access hatches (holes) in curved box girder bridges are usually provided in the bottom flange immediately before or after an expansion joint. If additional access hatches are required after the bridge is built, they must be placed in such a way that 1) they satisfy important practical constraints such as feasibility, accessibility, water leakage, traffic impact, and unauthorized access; 2) they do not adversely affect the structural behavior of the bridge, i.e. their installation should not impair serviceability nor decrease ultimate strength or fatigue life. Both issues are discussed and approaches that are suitable for identifying appropriate locations for access hole placement are identified. Access hatches can be installed without additional strengthening in low stress regions in the bottom steel flange. Low stress regions can be found using the computer program developed in this research.

7 REFERENCES

- AASHTO (1998), *LRFD Bridge Design Specifications – Second Edition*, American Association of State Highway and Transportation Officials, Washington, D.C.
- AASHTO (1997), *Guide Specifications for Horizontally Curved Highway Bridges*, American Association of State Highway and Transportation Officials, Washington, D.C.
- ABAQUS (1997). *Users' Manual Version 5.7*. Hibbit, Karlsson & Sorenson, Inc., Providence, RI.
- Consortium of University Research Teams – CURT (1975), “Horizontally Curved Highway Bridges”, Department of Transportation.
- Dubigeon S. and C.B. Kim (1982), “A finite element for the study of coupled bending-prevented torsion of a straight beam,” *Journal of Sound and Vibration*, Vol. 81, No. 2, pp. 255-270.
- Greenspan, D., and V. Casulli (1988), *Numerical Analysis for Applied Mathematics, Science, and Engineering*, Addison Wesley Pub. Co., Redwood City, CA.
- Guohao, L. (1987), *Analysis of Box Girder and Truss Bridges*, China Academic Publishers, Springer-Verlag, New York, NY.
- Heins, C. P. (1972), “Design data for curved bridges-summery report- the design of curved viaducts” C. E. Report No. 47, University of Maryland
- Ho, Y. S. and R. J. Reilly (1971), “Analysis and Design of Curved Composite Box Girder Bridges,” C. E. Report No. 41, University of Maryland
- Ho, Y. S. (1972), “Analysis and Design of Curved Composite Box Girder Bridges,” Ph.D. Thesis, University of Maryland.
- Horowitz, E., Sahni, S., and S. Anderson-Freed (1993), *Fundamentals of data structures in C*, Computer Science Press, New York, NY. 1993
- Kollbrunner, C.F., and K. Basler (1969), *Torsion in Structures: An Engineering Approach*. Springer-Verlag, New York, NY.

- Johnson, S.B. and A.H. Mattock (1967), "Lateral Distribution of Load in Composite Box Girder Bridges," *Highway Research Record No. 167*, Bridges and Structures.
- McGuire W., Gallagher R.H., and R.D. Ziemian (2000), *Matrix Structural Analysis*, 2nd Edition, John Wiley & Sons, Inc.
- Nakai, H., and C.P. Heins (1977), "Analysis Criteria for Curved Bridges," *Journal of Structural Engineering*, ASCE, Vol. 103, No. 7.
- Nakai, H., and C.H. Yoo (1988), *Analysis and Design of Curved Steel Bridges*, McGraw Hill, New York, N.Y.
- Okeil, A.M., S. El-Tawil, and M. Chaphalkar (2000), *New Access Hatches in Existing Curved Box Girder Bridges: A study based on practical and structural considerations*, Research Report, Department of Civil and Environmental Engineering, University of Central Florida, Orlando, Florida.
- Okeil, A.M., and S. El-Tawil (Feb. 2002), "Considerations for Opening New Access Holes in Curved Box Girders," *Practice Periodical of Structural Design and Construction*, ASCE, Vol. 7, No. 1, pp 26-36.
- Oleinik, J.C. and Heins, C.P. (Oct. 1975), "Diaphragms for Curved Box Beam Bridges," *Journal of Structural Engineering*, ASCE, Vol. 101, No. ST10, pp 2161-2178.
- Sennah, K.M., and J.B. Kennedy (Jun. 2001), "State-of-the-Art in Design of Curved Box-Girder Bridges," *Journal of Bridge Engineering*, ASCE, Vol. 6, No. 3, pp 159-167.
- Sennah, K.M., and J.B. Kennedy (Mar. 2002), "Literature Review in Analysis of Box-Girder Bridges," *Journal of Bridge Engineering*, ASCE, Vol. 7, No. 2, pp 134-143.
- Trukstra, C.J., and A.R. Fam (Mar. 1978), "Behavior Study of Curved Box Bridges," *Journal of the Structural Division*, ASCE, Vol. 104, ST3, pp 453-462.
- Waldron, P. (1988), "The Significance of Warping Torsion in the Design of Straight Concrete Box-girder Bridges," *Canadian Journal of Civil Engineering*, Vol. 15, pp 879-889.
- Zureick, A. Naqib, R. and Yadlosky, J. M. (1994), *Curved Steel Bridge Research Project; Interim Report I: Synthesis*, Publication No. FHWA-RD-93-129, Office of Engineering and High Way Operation R&D, Federal Highway Administration, 6300 Georgetwon Pike, McLean, VA 22101.

Zureick, A., Linzell, D., Leon, R. T., and Burell, J. (2000), "Curved Steel I-Girder Bridges: Experimental and Analytical Studies," *Engineering Structures*, Vol. 22, pp. 180-190.

8 APPENDIX A: Summary of Expressions used in Computing Geometric Properties

For a thin-walled open section, the shear center, S , and the centroid, O , of the cross section may not coincide. The first step of finding the geometric properties is to find the coordinates of the shear center using the following relationships:

$$x_S = \frac{\int y \omega_o dA}{\int y^2 dA} \quad (8.1a)$$

$$x_S = \frac{\int y \omega_o dA}{\int y^2 dA} \quad (8.1b)$$

where ω_o is an initially assumed warping function obtained with the centroid of the cross section as an origin using the following expression

$$\omega(s) = \omega_1(s) + \omega_1(0) \quad (8.2)$$

The first term of the previous expression is an integral of the perpendicular distance, ρ , from the point under consideration (centroid in the initial attempt) to the tangent to the point on the cross section.

$$\omega_1(s) = \int_0^s \rho ds \quad (8.3)$$

The constant $\omega_1(0)$ is obtained from the following expression

$$\omega_1(0) = -\frac{1}{A} \int \omega_1(s) dA \quad (8.4)$$

After determining the shear center, the warping function is computed, considering the shear center this time, following Eq. 8.2. The warping constant, I_ω , is then obtained using the following integral

$$I_\omega = \int \omega(s) \omega(s) dA \quad (8.5)$$

In the case of a closed cross section as the one shown in Fig. 8.1, Eq. 8.2 becomes

$$\omega(s) = \int_0^s \left(\rho - \frac{\psi}{t} \right) ds + \omega_1(0) \quad (8.6)$$

which may be viewed as two warping functions superimposed together (see Fig. 8.2). Once $\omega(s)$ is determined, Eq. 8.5 is used to obtain I_ω .

The sectoral area for a closed section is obtained using the following expression

$$S_\omega(s) = S_\omega^o(s) - \frac{1}{(ds/t)} \oint S_\omega^o(s) \frac{ds}{t} \quad (8.7)$$

In which $S_\omega^o(s)$ is the sectoral area for the same cross section assuming a slit that converts it into an open cross section. Though other tools are available for determining S_x and S_y , an approach similar to the one described for S_ω was followed.

The torsional constant used in all analyses was determined based on the following expression:

$$J = \frac{4A_c^2}{\oint \frac{ds}{t}} \quad (8.8)$$

which estimates torsional rigidity for closed cross sections and ignores the negligible contributions of elements not enclosing an are such as the deck overhangs.

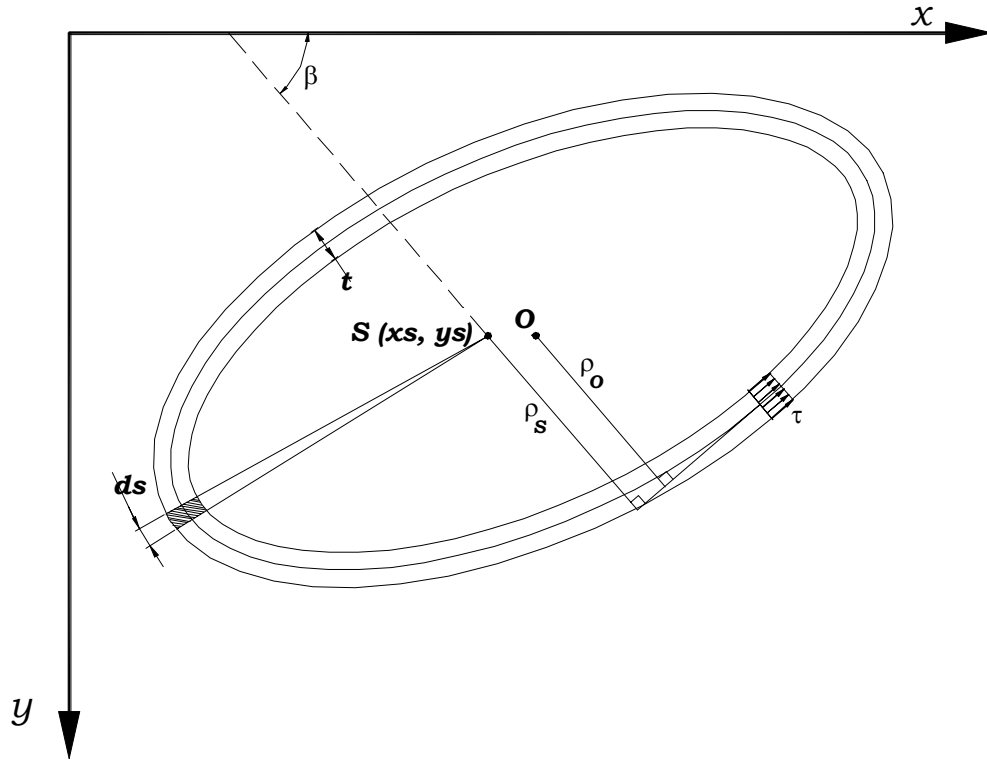


Figure 8.1: A general closed thin-walled cross-section

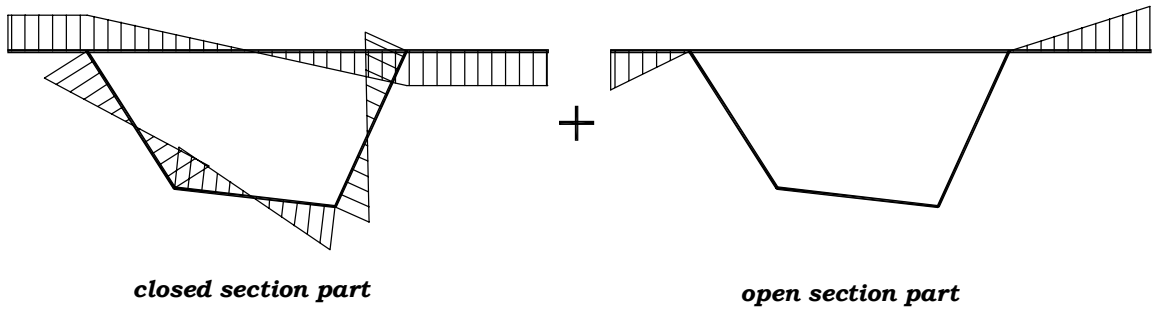


Figure 8.2: w diagrams of closed and open section parts

9 APPENDIX B: RESEARCH DISSEMINATION

9.1 Papers Accepted for Publication

Okeil, A. M. and El-Tawil, S. (Feb. 2002) "Considerations for Opening New Access Holes in Curved Box Girders," Practice Periodical of Structural Design and Construction, ASCE, Vol. 7, No. 1, pp. 26-36.

9.2 Papers Submitted for Publication

Okeil, A. M. and El-Tawil, S. (2002) "Warping Stresses in Curved Box Girder Bridges: A Case Study," submitted for review in the Journal of Bridge Engineering, ASCE.